HGG Advances

ARTICLE

MRBEE: A bias-corrected multivariable Mendelian randomization method

Noah Lorincz-Comi,[1,2] Yihe Yang,[1,2] Gen Li,[1] and Xiaofeng Zhu[1,3,*]

Summary

Mendelian randomization (MR) is an instrumental variable approach used to infer causal relationships between exposures and outcomes, which is becoming increasingly popular because of its ability to handle summary statistics from genome-wide association studies. However, existing MR approaches often suffer the bias from weak instrumental variables, horizontal pleiotropy and sample overlap. We introduce MRBEE (MR using bias-corrected estimating equation), a multivariable MR method capable of simultaneously removing weak instrument and sample overlap bias and identifying horizontal pleiotropy. Our extensive simulations and real data analyses reveal that MRBEE provides nearly unbiased estimates of causal effects, well-controlled type I error rates and higher power than comparably robust methods and is computationally efficient. Our real data analyses result in consistent causal effect estimates and offer valuable guidance for conducting multivariable MR studies, elucidating the roles of pleiotropy, and identifying total 42 horizontal pleiotropic loci missed previously that are associated with myopia, schizophrenia, and coronary artery disease.

Introduction

Mendelian randomization (MR) is an instrumental variable (IV) approach used to infer causal relationships between exposures and outcomes and can apply to summary statistics from genome-wide association studies (GWASs), providing a cost-effective and generalizable alternative to randomized controlled trials.[1] Inverse-variance weighting (IVW)[2] is the fundamental approach to perform MR with GWAS summary statistics, and the validity of which relies heavily on three so-called valid IV assumptions: the genetic IVs are (IV1) strongly associated with the exposures; (IV2) not directly associated with the outcome conditional on the exposures; and (IV3) not associated with any confounders of the exposure-outcome relationships. Violations of the (IV1)–(IV3) assumptions will introduce weak instrument,[3] unbalanced uncorrelated horizontal pleiotropy (UHP),[4] and correlated horizontal pleiotropy (CHP)[5] biases into the casual effect estimation, respectively. As for balanced UHP, which aligns with the instrument strength independent of direct effect (InSIDE) assumption,[4] the causal effect estimation remains unbiased.

From a statistical perspective, both unbalanced UHP and CHP in an MR model exhibit characteristics similar to outliers in traditional regression analyses. Therefore, these issues can be addressed using robust statistical tools. In the literature, MR-PRESSO[6] and IMRP[7] identify and remove horizontal pleiotropic variants through hypothesis tests, while the MR-Lasso[8] and MRcML[9] methods detect horizontal pleiotropy through variable selection tools. On the other hand, approaches like MR-Median[10] and MR-Robust[11] employ robust loss functions to mitigate the horizontally pleiotropic effects. Furthermore, Gaussian mixture models are implemented in methods such as MRMix,[12] MR-Conmix,[13] CAUSE,[5] MRAID,[14] and MR-CUE.[15] These models offer an advantage over traditional robust tools by utilizing fewer degrees of freedom to describe unbalanced UHP and CHP, thereby increasing efficiency when the mixture models are correctly specified.

While univariable MR (UVMR) methods allow some IVs to have horizontally pleiotropic effects, they generally assume that most IVs influence the outcome solely through the mediation of the exposure. However, this assumption can be problematic when traits share more than 50% causal variants. For instance, both systolic and diastolic blood pressure (SBP and DBP)[16] are revealed to share substantial causal variants. When analyzing the causal effect of SBP on cardiovascular disease, it is often challenging to remove the effect through DBP. A more effective way to address this issue is multivariable MR (MVMR), which accounts for the majority of horizontally pleiotropic variants that are shared by multiple exposures.[17] To date, the multivariable versions of IVW,[18] MR-Egger,[19] MR-Median,[10] and MRcML[20] have been developed. As demonstrated by Sanderson et al.,[17] MVMR is reliable in estimating the direct causal effects of one or more exposures.

The issue of weak instrument bias, stemming from the violation of the (IV1) assumption, poses even more challenging to resolve in MVMR than in UVMR. Specifically, it is usually difficult to find a set of IVs that are strongly associated with all exposures under consideration. In contrast, IVs are generally selected if they are associated with at least one exposure.[21] With the growing identification of causal variants for complex traits, the pool of IVs used in MVMR can easily reach the thousands due to this

[1]Department of Population and Quantitative Health Sciences, School of Medicine, Case Western Reserve University, Cleveland, OH, USA
[2]These authors contributed equally
[3]Lead contact
*Correspondence: xxz10@case.edu
https://doi.org/10.1016/j.xhgg.2024.100290.

IV selection procedure, therefore worsen weak instrument bias. Traditional approaches to mitigate this bias involve discarding weak IVs whose F-statistic or conditional F-statistic is less than 10. This threshold is believed to keep the relative bias in causal effect estimates below 10%.[3,22] However, the exclusion of IVs can lead to reduced statistical power and introduce a "winner's curse," thereby compromising the validity of the causal inference.[23]

We propose to resolve the weak instrument bias by using tools in measurement error analysis.[24] Specifically, measurement error bias occurs when explanatory variables are measured with random error, leading to biased estimates of model parameters. Since current MR approaches are performed with GWAS summary statistics that always contain estimation errors, the causal effect estimates inevitably suffer from measurement error bias.[25,26] Therefore, we view a weak instrument as a relatively large measurement error in effect size estimate based on finite sample size and is the primary reason for violating assumption (IV1) in IVW and other MR approaches. Furthermore, unlike traditional measurement error analyses that assume uncorrelated estimation errors in exposures and outcomes, overlapping individuals in exposure and outcome GWAS can result in correlated measurement errors, leading the direction of measurement error bias either toward or away from zero. As we observed in Figure 1, IVW estimates[27] exhibit negative bias with small numbers of overlapping samples and positive bias with large numbers of overlapping samples, respectively.

We develop a computationally efficient MVMR method, MR using bias-corrected estimating equations (MRBEE), to eliminate weak instrument bias while simultaneously accounting for horizontal pleiotropy in the presence of weak IVs or sample overlap. In contrast, existing methods only address weak instrument bias in specific cases such as no sample overlap (debiased IVW)[26] or no horizontal pleiotropy (MRlap).[28] Although the multivariable MRcML methods[20] generally provide unbiased causal estimates, they may be vulnerable to horizontal pleiotropy and computationally intensive. To underscore its practical significance, we apply MRBEE to three datasets, each targeting a unique disease, namely, myopia, schizophrenia (SCZ), and coronary artery disease (CAD), with the aim to unravel the distinct causal exposures associated with each. In addition, we extend the pleiotropy test to a genome-wide pleiotropy test (GWPT) for detecting novel loci. These empirical analyses offer valuable guides for conducting MVMR studies, elucidating the roles of pleiotropy and weak instrument bias, and illustrating how to identify novel loci through pleiotropy tests. The study was approved by the institutional review board (IRB number: STUDY20180592) at Case Western Reserve University.

Results

Overview of method

The detailed MRBEE is described in the material and methods section. Briefly, suppose that there are p exposures having causal effects on an outcome and m genetic variants as IVs. Let $\boldsymbol{\alpha} = (\alpha_1, \ldots, \alpha_m)^T$ be a vector of length m, representing the genetic effect sizes of IVs on the outcome, $\mathbf{B} = (\beta_1, \ldots, \beta_m)^\top$ be an $(m \times p)$ matrix with $\boldsymbol{\beta}_j = (\beta_{j1}, \ldots, \beta_{jp})^\top$ representing the genetic effect sizes of the j th IV on the p exposures, $\boldsymbol{\theta} = (\theta_1, \ldots, \theta_p)^\top$ be a vector of length p representing the causal effects of the p exposures on the outcome, and $\boldsymbol{\gamma} = (\gamma_1, \ldots, \gamma_m)^\top$ be a vector of length m representing horizontal pleiotropy. We model the causal effects of the exposures on the outcome by

$$\alpha_{\mathrm{j}} = \beta_{\mathbf{j}}^\top \theta + \gamma_{\mathrm{j}}.$$

The goal in MR analysis is to estimate the causal effects θ unbiasedly. In the above equation, the true genetic effect sizes $\boldsymbol{\alpha}$ and $\mathbf{B}$ are not observed but can be estimated through the GWAS of exposures and outcome and the pleiotropy effect γ is simply unknown. Let $\widehat{\alpha}_j$ and $\widehat{\beta}_j$ be the effect size estimates of the j th IV from the outcome and exposure GWASs. We have

$$\begin{aligned} \widehat{\alpha}_j &= \alpha_j + w_{\alpha_j}, \\ \widehat{\beta}_j &= \beta_j + \mathbf{w}_{\beta_j}, \end{aligned}$$

where w_{α_j} and $\mathbf{w}_{\beta_j}$ represent the measurement errors because of finite sample sizes of the GWASs.

In general, an MVMR analysis is performed by the following linear regression:

$$\widehat{\alpha}_j = \widehat{\beta}_j^\top \theta + \gamma_j + \varepsilon_j,$$

where ε_j represents the residual. When we standardize $\widehat{\alpha}_j$ and $\widehat{\beta}_j$ by their corresponding standard errors obtained from GWASs, the multivariable IVW (MV-IVW) estimates θ is

$$\widehat{\theta}_{\mathrm{IVW}} = \underset{\theta}{\operatorname{argmin}} \{ \| \widehat{\alpha} - \widehat{\boldsymbol{B}}\theta \|_2^2 \} = (\widehat{\mathbf{B}}^\top \widehat{\mathbf{B}})^{-1} \widehat{\mathbf{B}}^\top \widehat{\alpha},$$

which is equivalent to solve the score equation $\mathbf{S}_{\mathrm{IVW}}(\theta) = \widehat{\mathbf{B}}^\top (\widehat{\mathbf{B}}\theta - \widehat{\alpha}) = 0$. However, the MV-IVW fails to consider the weak IVs and the correlations among w_{α_j} and $\mathbf{w}_{\beta_j}$ induced by sample overlap and assumes pleiotropy $\gamma_j = 0$ for all IVs. Thus, the MV-IVW is biased. To solve this problem, we propose MRBEE by solving the following estimating equation,

$$\mathbf{S}_{\mathrm{BEE}}(\theta) = \mathbf{S}_{\mathrm{IVW}}(\theta) - m\left(\Sigma_{W_\beta W_\beta}\theta - \sigma_{W_\beta w_\alpha}\right) = 0,$$

where $\Sigma_{W_\beta W_\beta}$ and $\sigma_{W_\beta w_\alpha}$ represent the covariance matrix among $\mathbf{w}_{\beta_j}$ and between $\mathbf{w}_{\beta_j}$ and w_{α_j} (material and methods) in the set of the m IVs. The score function in $\mathbf{S}_{\mathrm{BEE}}(\theta)$ adds a corrected term, which corrects the bias because of weak IVs and sample overlap, meanwhile assumes there are no pleiotropic IVs ($\gamma_j = 0$). The solution of the equation $\mathbf{S}_{\mathrm{BEE}}(\theta)$ is

$$\widehat{\theta}_{\mathrm{BEE}} = \left(\widehat{\mathbf{B}}^\top \widehat{\mathbf{B}} - m\Sigma_{W_\beta W_\beta}\right)^{-1} \left(\widehat{\mathbf{B}}^\top \widehat{\alpha} - m\sigma_{W_\beta w_\alpha}\right).$$

With the presence of pleiotropic IVs, we apply an iterative procedure[7] with the pleiotropy test S_{pleio} for multiple

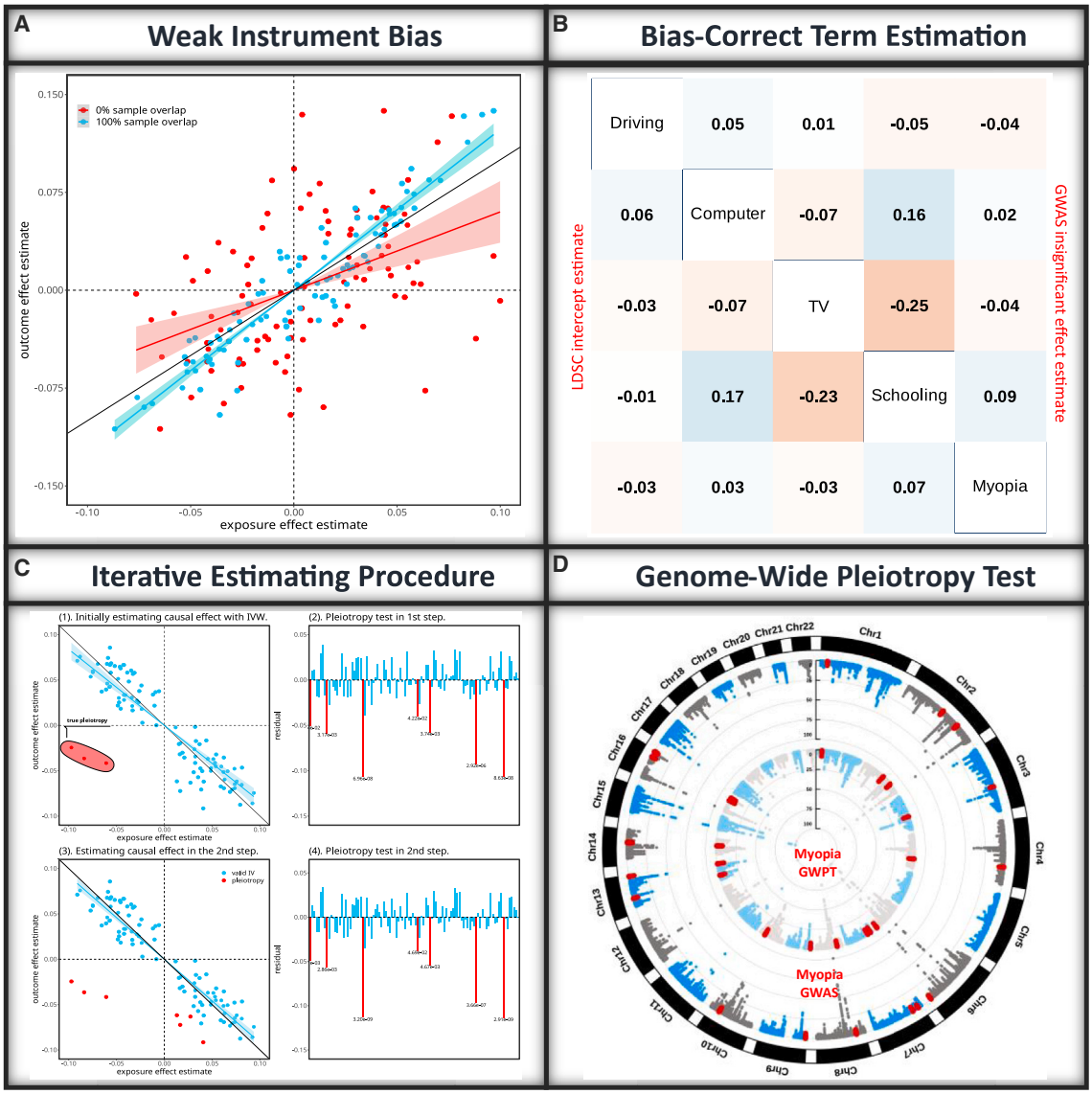

Figure 1. Principle of MRBEE

(A) Traditional MR methods are vulnerable to weak instrument bias arising from the estimation errors in GWAS associations for the exposure(s) and outcome. The direction of the bias is influenced by the degree of sample overlap between the studies where the red and blue points refer to two simulated data with 0% and 100% sample overlap. The shadow regions represent the 95% confidence interval regions.

(B) MRBEE corrects for weak instrument bias using bias-correction terms which are calculated from the matrix of correlations between measurement errors for all exposures and the outcome. In this example with myopia and its four exposures, the numbers in the lower triangle of the table are the correlations estimated using LD score regression and that in the upper triangle of the table are the correlations estimated using non-significant SNPs.

(C) MRBEE uses an iterative estimation procedure, where horizontally pleiotropic IVs are removed at each iteration until convergence. The y axis in panels (2) and (4) reflect the SNP association with the outcome not mediated by the exposures. The numbers under the red vertical lines represent p values.

(D) After estimating causal effects, MRBEE performs genome-wide horizontal pleiotropy testing to find loci associated with the outcome (e.g., myopia) that were not detected in the original GWAS.

exposures and an outcome, which uses the following statistic S_{pleio} for the j th IV,

$$S_{\text{pleio}_j}(\widehat{\theta}) = \frac{\left(\widehat{\alpha}_j - \widehat{\beta}_j^{\top}\widehat{\theta}\right)^2}{\text{var}\left(\widehat{\alpha}_j - \widehat{\beta}_j^{\top}\widehat{\theta}\right)}.$$

Thus, MRBEE estimates the causal effect θ, and identifies pleiotropic IVs with the current estimated causal effect θ iteratively. The entire pipeline from inputting summary statistics, estimating causal effects, and identifying pleiotropic IVs is illustrated in Figure 1. Note that after estimating the causal effect θ, we can further search pleiotropic variants across the entire genome.

Simulation

We compared MRBEE with the multivariable MR of IVW, MR-Egger, MR-Median, MR-Lasso, MRcML-DP, and MRcML-BIC. MRBEE is implemented with the R package

MRBEE and the other methods are implemented through the R package MendelianRandomization.[29] We call IVW, MR-Egger, MR-Median, and MR-Lasso the traditional MVMR methods, as they either do not account for estimation error of effect size or the sample overlap. Our simulation setting was adapted from the ones considered by Lin et al.,[20] but with specific adjustments to better reflect real-world situations. Specifically, we set the heritability of both exposures and confounders at 0.1, introduced moderate genetic correlations among the exposures, and added correlations among random errors of exposure and outcome GWAS cohorts. In our analysis, we consider three scenarios: no pleiotropy, 30% unbalanced UHP, and 30% CHP. All exposures are assumed to come from the same GWAS sample, while the outcome may overlap completely (100% sample overlap), partially (50% and 77% overlap), or be entirely independent (0% sample overlap). In addition, the sample size was set at 50,000, the number of IVs was set at 50, 100, and 200, representing the increasing of weak IVs, the number of exposures was 4, and the causal effect was $\theta = (0, 0.2, -0.2, 0.4)^\top$, which represents no causal effect, and positive, negative, and large causal effects, respectively. Simulation settings are fully presented in supplement 1 and the R code used to generate simulated data is available at the GitHub repository of this paper. The number of simulation replicates was 500, and additional simulations can be found in supplement 1.

Bias of causal effect estimates

Figures 2A, 2D, 2G, and 2J demonstrate that the bias in traditional MVMR methods (IVW, MR-Egger, MR-Median, MR-Lasso) is proportional to the number of IVs used, especially in the absence of horizontal pleiotropy. The direction of this bias is influenced by sample overlap: no overlap results in bias toward the null, while sample overlap leads to bias away from the null. On the contrary, MRBEE, MRcML-BIC, and MRcML-DP are unbiased under these conditions. The unbiasedness for MRcML methods is likely attributed to the fact that the objective function of MRcML methods[20] accounts for the covariance of estimation errors. Our results suggest that incorporating the estimation error covariance matrix mitigates measurement error bias.

Figures 2B, 2E, 2H, and 2K demonstrate that when there was 30% unbalanced UHP, IVW, and MR-Egger generally incurred substantial bias. Moreover, there were inflated standard errors in the causal estimates due to the horizontal pleiotropy. MR-Median and MR-Lasso also incurred substantial bias, but the standard errors of their causal estimates were smaller than that from IVW and MR-Egger. These methods apply robust tools to estimate the causal effects in the presence of horizontal pleiotropy but are not able to remove the bias by weak instrument or sample overlap. MRcML-BIC and MRcML-DP generally provided unbiased causal estimates when there was no sample overlap. When the sample overlap percentage was 100%, both MRcML-BIC and MRcML-DP incurred biases in different directions. The magnitude of this bias was proportional to the number of IVs used. For example, for exposure 1 with true $\theta_1 = 0$, MRcML-BIC and MRcML-DP had bias away from the null; for exposure 3 where $\theta_3 = -0.2$, the two methods had bias toward, and even past, the null. In comparison, MRBEE was unbiased in all scenarios except when there were 200 IVs and 100% overlap. In this case, MRBEE still had a smaller upward bias for exposure 3 with $\theta_3 = -0.2$ than other methods.

Figures 2C, 2F, 2I, and 2L demonstrate that when there was 30% CHP, IVW, and MR-Egger had larger bias and standard errors in their causal estimates than the rest of methods. Both had bias away from the null for exposure 1, and the magnitude of which depended on the number of IVs used. MR-Median and MR-Lasso generally were less biased than IVW and MR-Egger, as they are more robust in handling of CHP IVs. The weak instrument bias of MR-Median and MR-Lasso followed the same bias patterns as no pleiotropy. MRcML-BIC and MRcML-DP were both biased when the sample overlapping percentage was 100% or 0%, potentially due to the instability of algorithm when horizontal pleiotropy is present. MRBEE was unbiased in all cases and generally had standard errors comparable to other methods excluding IVW and MR-Egger. Finally, when the number of IVs increased from 50 to 200, representing the increasing of weak IVs, MRBEE was always performing better than the comparing methods (Figure 2).

Type I error and power

Figures 3A–3C present the type I error rates for all the methods when the true causal effect $\theta_1 = 0$, which corresponds to the first exposure in our simulations. When there was no sample overlap between exposures and the outcome, the type I error was well controlled for MRBEE in all three scenarios, i.e., no pleiotropy, 30% unbalanced UHP, and 30% unbalanced CHP. In comparison, MRcML-DP, MR-Median, MR-Egger, and IVW was generally conservative, while MRcML-BIC and MR-LASSO usually had inflated type I error rates. When 100% overlap between exposures and the outcome, MRBEE still controlled type I error rate well. The rest of the methods either had inflated or extremely conservative type I error rate.

Figures 3D–3L present power for different causal effects in the three scenarios. Overall, MRBEE has comparable power with the best of the other methods but maintains a type I error rate. We specifically compared MRBEE and MRcML-DP, where the latter controlled type I error rate well under all the simulation scenarios. We observed that MRBEE either had similar or better power than MRcML-DP. The power pattern across the seven methods does not align well with the type I error pattern, that is, high type I error rate corresponds to high power and vice visa. We observed that the reason is the bias direction in causal effect estimates as illuminated in Figure 2, i.e., the bias direction could be in opposite to the true causal effect.

Again, when the number of IVs increased from 50 to 200, the performance of type I error and power of MRBEE was either equal well or better than the comparing methods. We further evaluated these approaches in terms

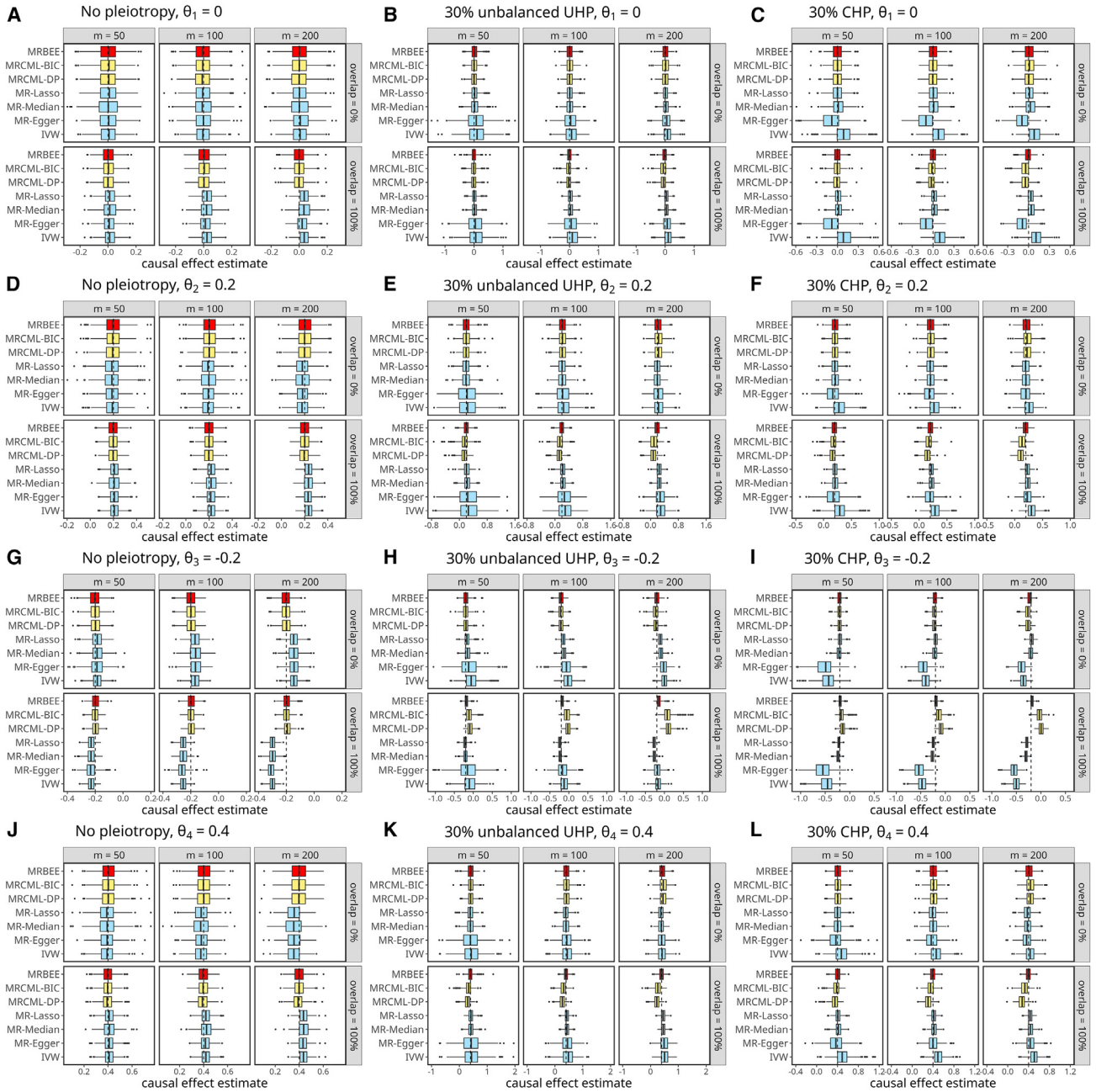

Figure 2. Comparison of the causal effect estimates by the 7 MVMR methods

(A–L) Boxplots display the causal effect estimates from seven methods in the MVMR simulation. The four rows represent the four causal effects θ_j, $j = 1,2,3,4$. Each column corresponds to one of the three pleiotropy scenarios for IVs (i.e., No pleiotropy; 30% unbalanced UHP IVs; 30% CHP IVs). The x axis indicates the value of the causal effect estimate, while the y axis lists the seven methods. The true values of causal effects are denoted by dashed lines. Plots in (A), (D), (G), and (J) when the sample overlap proportion is 0% can be used to infer the magnitude of weak instrument bias since differences between MRBEE and IVW causal estimates in these scenarios are proportional to the degree of weak IV bias. The left and right vertical edges of each box plot represent the 25th and 75th percentiles of causal effect estimate, and the vertical middle line represent the 50th percentile.

of the root-mean-square error (RMSE), standard error (SE) estimation, and coverage frequency of causal effects. MRBEE was again the best among the methods evaluated (Figures S1–S3, and Tables S1–S24 in supplement 1).

We have performed additional simulations in which the overlapping proportion takes values 0, 0.5, 0.77, and 1. In these scenarios MRBEE still performs well. The results are presented in supplement 1.

Computational efficiency

Figure 4 illuminates the computation efficient across seven methods. We observed that MRBEE is computationally as efficient as MR-Median, MR-Lasso, MR-Egger, and MR-IVW. We attribute the computational requirements of MRcML to two potential factors. First, MRcML methods utilize an algorithm similar to the best subset selection to identify the optimal subset of pleiotropic variants. This involves

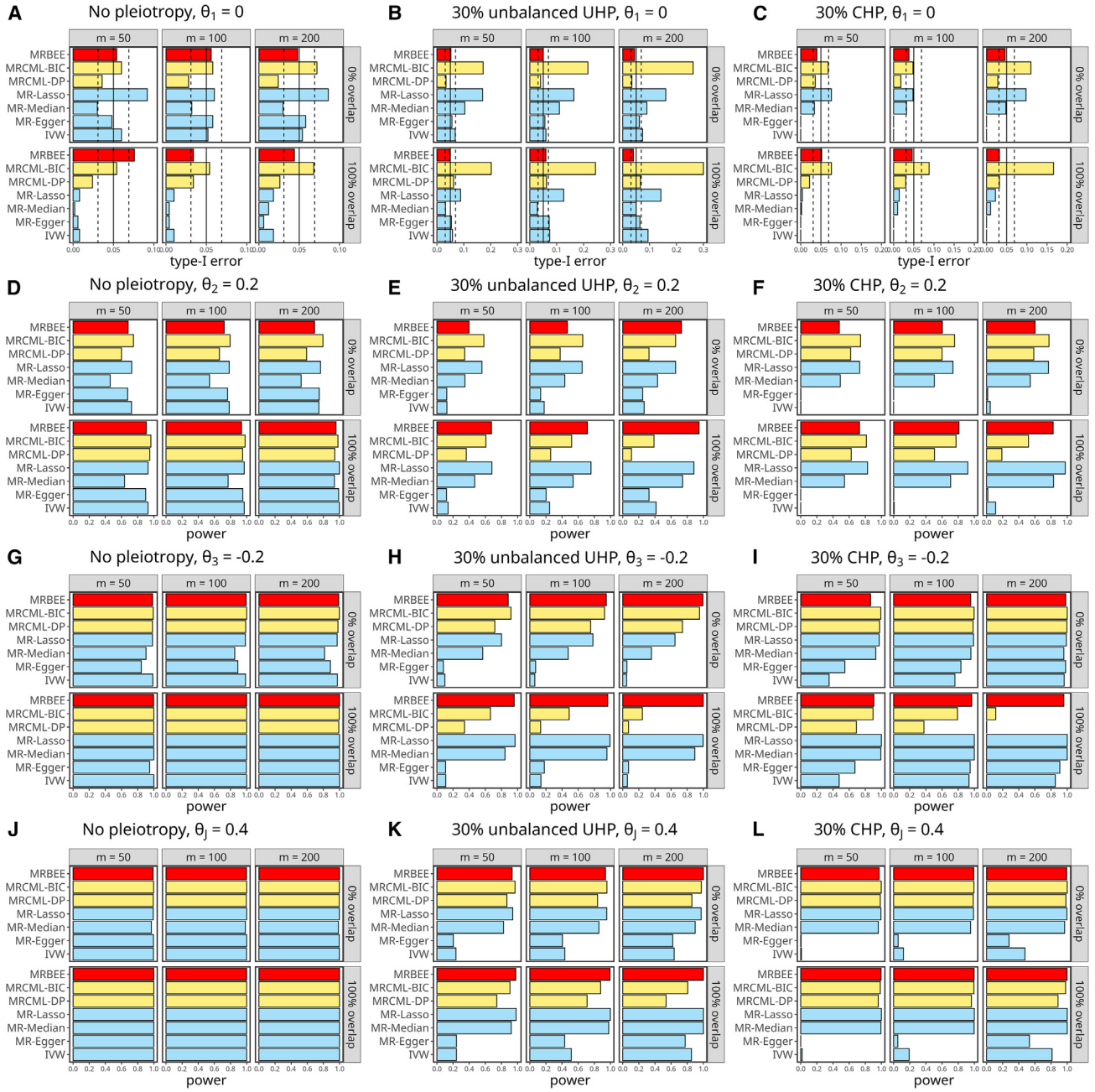

Figure 3. Comparisons of type I error and power of the seven MVMR methods

(A–C) Type I error of the seven methods (MRBEE, MRcML-BIC, MRcML-DP, MR-LASSO, MR-Median, MR-Egger and IVW). (D–L) Power of the seven methods. The three columns corespond to no pleiotropy, 30% unbalanced UHP IVs and 30% CHP IVs, respectively. In each figure, the top and bottom panels represent 0% and 100% sample overlap between exposures and outcome, respectively. Each row represents different causal effects. Simulation settings are described in the simulation section in the main text, supplement 1, and at our GitHub repository. Displayed are bar plots of rejection frequency estimations across 500 simulations for each scenario, which represents the type I error or power depending on the true causal effect is zero or not. The two dotted vertical lines in (A)–(C) represent the 95% confidence interval.

performing MVMR iteratively by considering numbers of pleiotropic variants ranging from 1 to K (defaulting to $m/2$), and determining the optimal number based on the BIC criteria. In contrast, MRBEE automatically detects pleiotropic variants using a hypothesis test, and MR-Lasso utilizes lasso for pleiotropic variant selection, both of which are computationally efficient. Second, MRcML-DP relies on permutations to derive the SE, which further increases computational burden. Conversely, MRBEE uses the sandwich formula to estimate its SE, which appears to be accurate in our simulations (Equation 19 in material and methods).

Real data analysis

Data sources

To demonstrate the MRBEE performance in real data analysis, we analyzed three outcomes, including myopia, SCZ, and

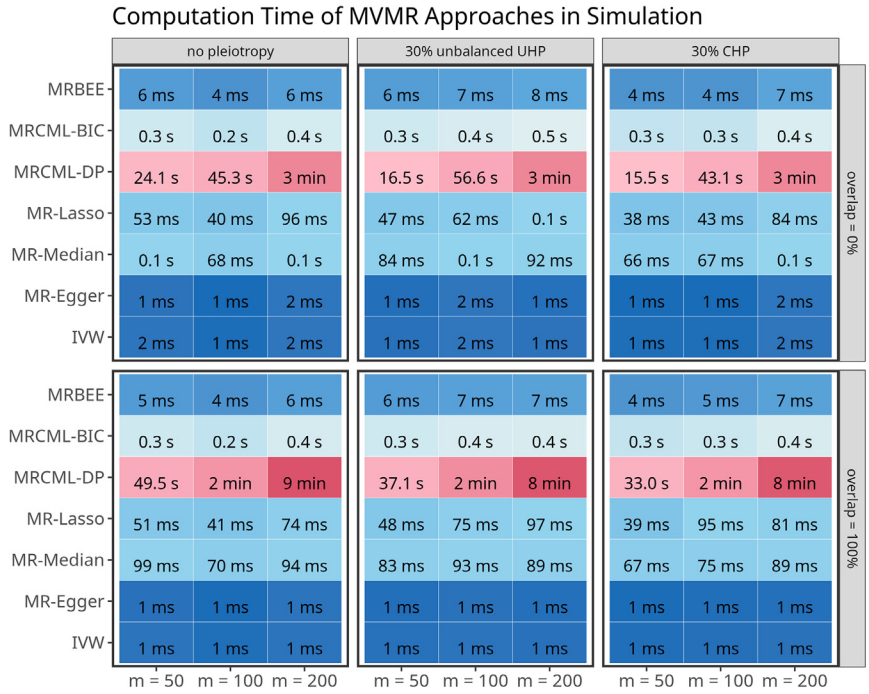

Figure 4. Comparison of computation efficiency of the seven MVMR methods
This figure depicts the average computation time of the seven methods over 500 simulations.

CAD. Myopia is known to be influenced by a combination of genetic and environmental factors, including educational attainment (EDU), near-work activity, and outdoor activities[30] but their direct causality to myopia is not clear. In this MVMR analysis, we considered refractive error, the measure of myopia degree, as the outcome. The exposures include EDU, near-work activity measured by time spent watching TV and playing on the computer (TV and Computer), and outdoor activity measured by time spent driving (Driving).

Attention-deficit/hyperactivity disorder (ADHD), cannabis use disorder (CAN), EDU, intelligence (INT), left-handedness (LH), intelligence (INT), neuroticism (SESA), and sleep duration (SLP) have been reported as risk factors for SCZ. Of these risk factors, CAN arguably has the strongest evidence of causality with respect to SCZ, with studies reporting dose-response[31] and strong temporal[32] relationships for at-risk individuals. The direct causality of the risk factors on SCZ is also not clear.

Many studies have been published to understand the causal effects of risk factors on CAD. However, the findings in these studies have been inconsistent. For instance, Holmes et al. and Lin et al.[20,33] found that HDL-C is not significant, while Zhu et al.,[7] using the GWAS summary data with a much larger sample size (1.3M vs. 90K), found it to be significant. Besides, Wang et al.[21] found that low-density lipoprotein cholesterol (LDL-C) is not significant in European populations, which seems unreasonable. In this data analysis, we investigated the causal relationships of these risk factors on CAD using the GWAS summary data with the largest sample sizes to date. We focus on the same eight factors studied in Lin et al.,[20] i.e., body mass index (BMI), DBP, fasting plasma glucose (FPG), height, HDL-C, LDL-C, triglycerides (TG), and SBP.

Data preprocessing

For UVMR, we applied the C + T procedure with the linkage disequilibrium (LD) parameter $r^2 < 0.01$ in ± 500 Kb window to SNPs with association p value at least as small as 5E−5. We performed this operation for each exposure separately and used the 1000 Genomes project (phase 3) data as the LD reference panel.[34] For MVMR, we initially considered the union set of all exposure-specific IV sets from UVMR, then restricted this set to only include SNPs with a joint χ^2-test p value reaching genome-wide significance and again passing C + T using the same parameters as before. The joint χ^2-test for the exposures is presented in Equation 22 in material and methods and is used to assess the null hypothesis that an SNP is not associated with any exposure. We additionally standardized the GWAS effect size estimates so that their SEs were the inverse of the sample sizes. This procedure leads to comparable causal effect estimates across different exposures. We used false discovery rate (FDR) correction in MRBEE to identify and remove SNPs with evidence of horizontal pleiotropy (see Algorithm 1).

Table 1 summarizes the information of GWAS data in this study. In Table 1, the last three columns present the SNP heritability estimated by the LD score regression (LDSC),[35] the variances explained by the IVs in UVMR, and the variances explained by the IVs in MVMR. It is evident that for the trait with lower heritability and small sample sizes, the UVMR IVs account for about 1% of its SNP heritability, which may reduce power to detect causal effects using UVMR. However, for most traits, IVs in MVMR analyses explain a substantial portion of the variance, which will provide good power to detect causal effects. This is because the standard error of causal estimate(s) is inversely proportional to the variance(s) explained by the IVs. The last column of Table 1 shows the reliability ratios, a measure of IV strength, for exposures used in real data analysis. The estimation errors averagely account for ∼20% variance of the GWAS effect estimates.

Myopia

All the MVMR methods consistently showed that EDU (MRBEE $p = 9.3\text{E}{-21}$) and Driving ($p = 3.8\text{E}{-11}$) are directly causal on myopia, but not TV ($p = 0.136$) or Computer ($p = 0.972$) (Figure 5A). The no direct causal effect of TV or Computer on myopia risk although all exposures were observed to have significant causal effects on myopia in the UVMR

Table 1. Summary of GWAS data used in real data analyses

	Trait	Source	Sample size	Significant IVs	LDSC heritability	UVMR variance[a]	MVMR variance[b]	Reliability ratio[c]
Myopia	Driving	van De Vegte etal. [54]	422K	4	0.0365	0.00034	0.00400	0.705
	Playing computer	Arns et al. [55]	422K	46	0.0719	0.00408	0.01154	0.873
	Watching TV	Rustad et al. [56]	422K	189	0.1321	0.01788	0.02775	0.943
	EDU	Okbay et al. [57]	765K	656	0.1352	0.03954	0.03683	0.976
	Joint 4 test			707				
	Refractive error	Hysi et al. [58]	246K	420	0.2702	0.11079	0.01433	0.838
Schizophrenia	ADHD	Demontis et al. [59]	55K	12	0.0956	0.00279	0.01871	0.832
	CAN	Johnson et al. [60]	384K	5	0.0174	0.00033	0.00272	0.552
	EDU	Okbay et al.[57]	765K	656	0.1222	0.03954	0.03728	0.973
	Intelligence	Neale's Lab	430K	48	0.2326	0.01527	0.06023	0.900
	Left handedness	Cuellar-Partida et al. [61]	205K	4	0.0338	0.00086	0.00533	0.576
	Neuroticism (SESA)	Nagel et al. [62]	450K	42	0.0800	0.00476	0.01056	0.825
	Sleep duration	Dashti et al. [63]	493K	66	0.0649	0.00589	0.00998	0.850
	Joint 7 test			1,227				
	SCZ	Trubetskoy et al.[64]	320K	287	0.3380	0.06378	0.03570	0.855
Coronary artery disease	BMI	Loh et al. [65]	458K	882	0.2076	0.09494	0.10612	0.918
	DBP	Evangelou et al. [66]+MVP	1.00M	942	0.1095	0.06022	0.04525	0.823
	FPG	Neale's Lab	361K	115	0.0848	0.03729	0.05156	0.789
	Height	Loh et al. [65]	458K	2,728	0.6023	0.48986	0.49156	0.981
	HDL-C	Graham et al. [67]	1.32M	1,031	0.1779	0.09207	0.09745	0.965
	LDL-C	Graham et al. [67]	1.32M	754	0.1293	0.08435	0.08713	0.961
	TG	Graham et al. [67]	1.32M	900	0.1251	0.07298	0.08105	0.959
	SBP	Evangelou et al. [66]+MVP	1.00M	895	0.1152	0.05626	0.04550	0.829
	Joint 8 test			4,336				
	CAD	Aragam et al.[68]+MVP	1.45M	343	0.0500	0.01610	0.01712	0.850

[a]Variance explained by the IVs in UVMR analysis.
[b]Variance explained by the IVs in MVMR analysis.
[c]Reliability ratios of exposures in MVMR analysis.

analysis (Figure 5B). The insignificance of both TV and Computer in MVMR analysis suggests their correlations with myopia could be attributed to the confounding with EDU and Driving time. MRBEE provided larger protective causal estimate of driving time than that by IVW (i.e., MRBEE odds ratio [OR] = 0.71 vs. IVW OR = 0.84), likely due to a correction for weak instrument bias given that the driving time variance explained by the IVs was less than 1%. The causal effect of driving time estimated by MRcML-BIC and MRcML-DP was 3–5 times larger in magnitude than those from other methods. (MRcML-BIC OR = 0.38 and MRcML-DP OR = 0.58, respectively). In the iterative pleiotropy test, we detected 31 IVs demonstrating pleiotropy of the exposures and myopia (Figure 5C). Figure 5D compares the computational efficiency of the MR methods. We observed that IVW was the fastest (<0.1 s), followed by MRBEE (0.1 s), MR-Lasso (0.9 s), MR-Median (1.4 s), MRcML-BIC (1 min), and MRcML-DP (107 min), which were consistent with the simulations.

Schizophrenia

All MVMR methods consistently estimated that CAN (MRBEE p = 3.7E−8), EDU (p = 3.6E−15), INT (p = 7.7E−12), and SESA (p = 1.8E−7) have direct causal contributions on schizophrenia (Figure 6A). MRBEE, MR-Lasso, and MR-Median suggested that SLP (p = 3.4E−4) has direct causal contribution on schizophrenia but not MRcML-BIC or MRcML-DP. It is not clear why both MRcML-DP and MRcML-BIC failed to detect this causal contribution given our simulations suggest MRcML-BIC could be more powerful although with inflated type I error. A potential reason could

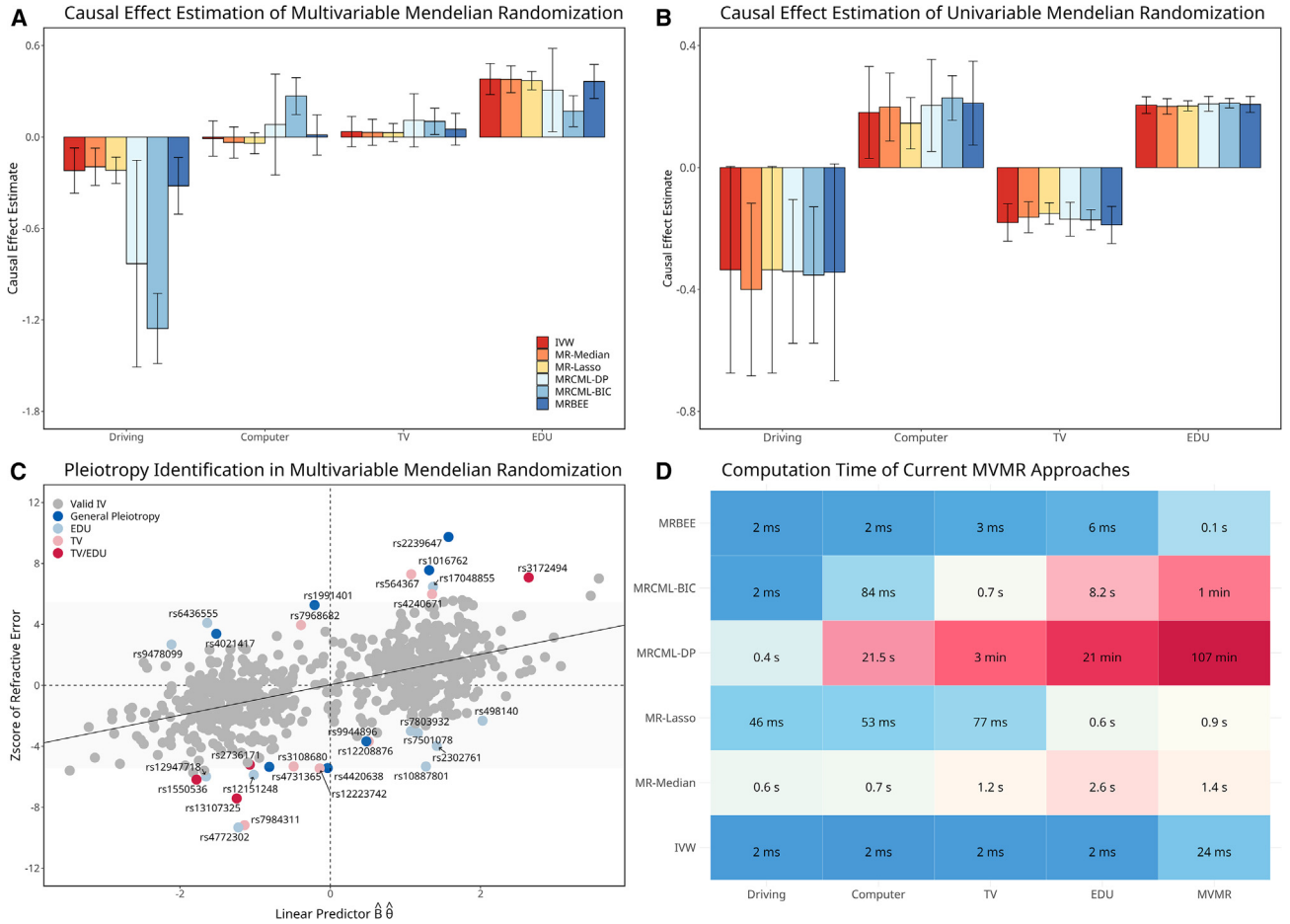

Figure 5. Myopia data analysis

(A) Causal effect estimates by the six MVMR methods. The corresponding 95% confidence interval shown as vertical error bars.

(B) Corresponding causal effect estimates by UVMR approaches. The corresponding 95% confidence interval shown as vertical error bars. The radius of the confidence interval equals $\sqrt{a}\times$ SE, where $a = F^{-1}_{\chi^2}(1 - 0.05/4, 1)$, $F^{-1}_{\chi^2}(x, \mathrm{df})$ is the inverse cumulative distribution function of a χ^2 distribution.

(C) Pleiotropy test where the x axis represents the linear predictor $\widehat{B}\widehat{\theta}_{\mathrm{BEE}}$ and the y axis represents the corresponding standardized association with myopia from GWAS. The annotation of a pleiotropic variant is made if its pleiotropic test p value is $< 5\mathrm{E}{-8}$. Only IVs are present in the figure.

(D) Computation times of the six comparing methods. Columns 1–4 represent computation time for UVMR of four exposures and the last column represents computation time for MVMR.

be the instability of MRcML, which may converge to local maximum. However, this requires additional investigation. MRBEE suggested no direct causal effect of ADHD ($p = 0.510$) or LH ($p = 0.096$), possibly due to the relatively low exposure variance explained by the IV set (i.e., 0.018 for ADHD and 0.005 for LH). We observed relatively larger odds ratios of EDU and CAN for MRBEE than MR-Median, MR-Lasso, and IVW, but less than MRcML-DP and MRcML-BIC. In comparison, UVMR analyses by all methods suggested evidence of total causal effects of CAN (MRBEE $p = 1.6\mathrm{E}{-4}$), INT ($p = 3.2\mathrm{E}{-7}$), SESA ($p = 2.0\mathrm{E}{-10}$), ADHD ($p = 0.017$), and SLP ($p = 1.4\mathrm{E}{-4}$), but not EDU ($p = 0.542$) or LH ($p = 0.716$) (Figure 6B). We did not observe any IVs with evidence of horizontal pleiotropy at the Bonferroni-corrected $p = 0.05$ level (Figure 6C), suggesting that the genetic association of the IVs with SCZ are strictly mediated by the five significant exposures. Again, we observed similar computational efficient for these methods as before (Figure 6D).

Coronary artery disease

Figure 7A presents MVMR causal estimates for the effects of BMI, DBP, SBP, FPG, height, HDL-C, LDL-C, TG, and SBP on CAD. Using MRBEE, we identified the following significant direct causal effects on CAD, including BMI (MRBEE $p = 3.8\mathrm{E}{-39}$), FPG ($p = 6.7\mathrm{E}{-10}$), HDL-C ($p = 8.4\mathrm{E}{-21}$), LDL-C ($p = 1.5\mathrm{E}{-87}$), TG ($p = 1.9\mathrm{E}{-7}$), and SBP ($p = 1.1\mathrm{E}{-25}$). We observed that MRBEE estimates were generally consistent with estimates from IVW, MR-Median, and MR-Lasso. Conversely, MRcML-BIC and MRcML-DP estimates diverged from all other methods for DBP and FPG. For example, MRcML-DP/BIC were the only methods that simultaneously produced significant causal effects for SBP ($p = 1.6\mathrm{E}{-39}$) and DBP ($p = 1.8\mathrm{E}{-45}$) on CAD, two traits that are highly genetically correlated. In

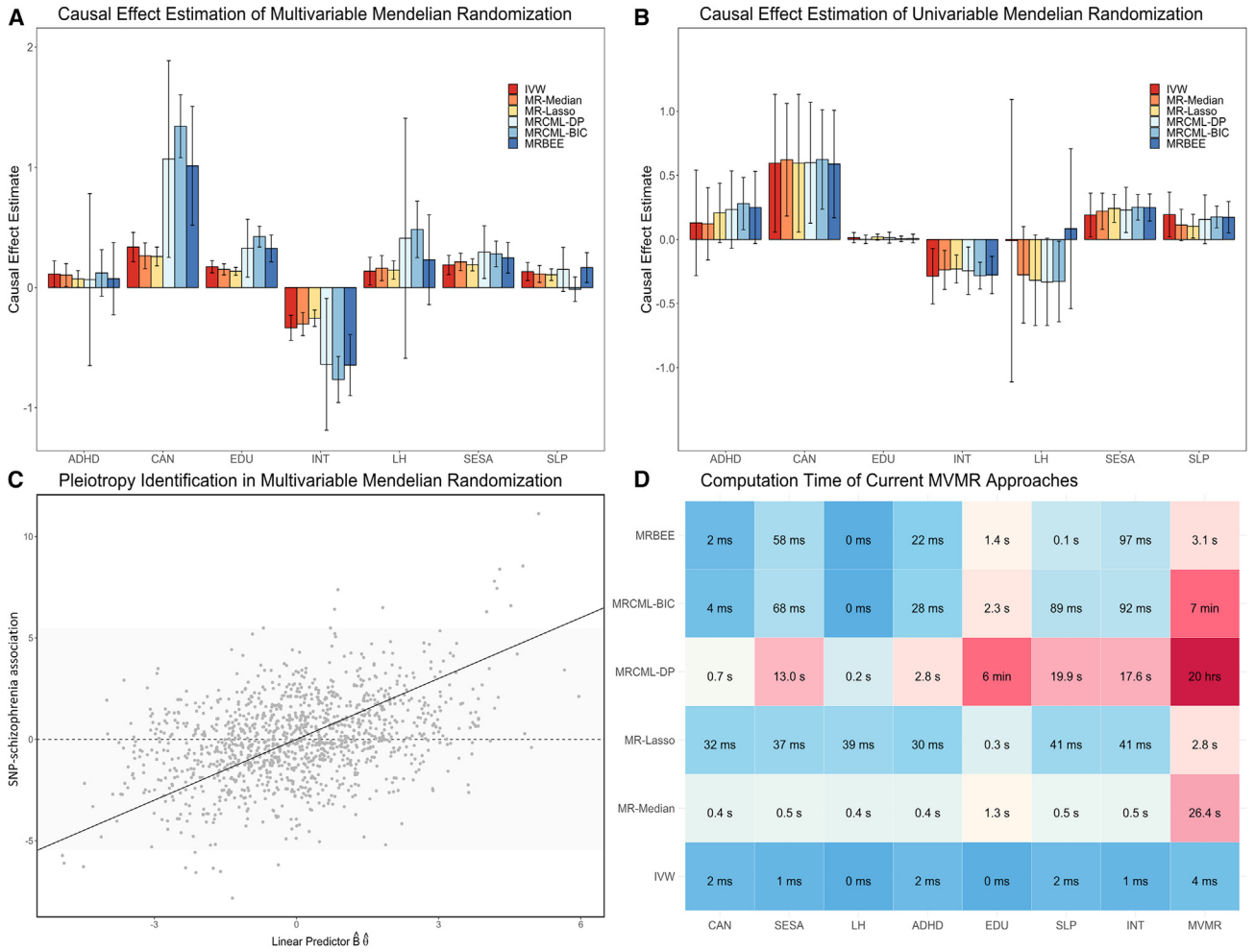

Figure 6. Data analysis of schizophrenia

(A) Causal effect estimates by the six MVMR methods. The corresponding 95% confidence interval shown as vertical error bars.

(B) Causal effect estimates by UVMR approaches. The corresponding 95% confidence interval shown as vertical error bars. The radius of the confidence interval equals $\sqrt{a}\times SE$ where $a = F^{-1}_{\chi^2}(1 - 0.05/7, 1)$.

(C) Pleiotropy test where the x axis represents the linear predictor $\widehat{B}\widehat{\theta}_{\mathrm{BEE}}$ and the y axis represents the standardized association of the IV with SCZ from GWAS.

(D) Computation times of the comparing methods. Columns 1–7 represent computation time for UVMR of seven exposures and the last column represents computation time for MVMR.

comparison, UVMR analyses by all methods consistently suggested that all the exposures have causal contributions on CAD (Figure 7B). We also observed 173 IVs demonstrating horizontal pleiotropy by the horizontal pleiotropy test in MVMR (Figure 7C). Again, our proposed MRBEE is computationally efficient (Figure 7D).

Pleiotropic variants detected by GWPT

GWPT uses the S_{pleio} statistic (Equation 21 in materials and methods) to test whether a genetic variant is associated with the outcome phenotype strictly through the mediation of a select group of exposures. In our GWPT analyses, these groups of exposures are those that were used in each MVMR. This test can be used to find these outcome-associated loci[16] that do not reach the level of genome-wide significance in the original outcome phenotype GWAS but are genome-wide significant in GWPT. In these regions, it is possible that the local genetic correlations between the exposures and outcome are of different sign or magnitude than the genome-wide genetic correlations.[36] To ensure that the loci identified in GWPT were not primarily influenced by other exposures, we excluded any loci that showed even a marginal association with any of the exposures at a genome-wide significance level (i.e., $p < 5E{-}8$). We also compared GWPT with cross-phenotype association analysis (CPASSOC),[37] multi-trait analysis of GWAS (MTAG),[38] which are joint tests of association between all exposures in the outcome.

Table 2 lists the variants detected by GWPT for myopia, SCZ, and CAD but missed in the original GWAS. For comparison, we listed the p values for association from the original outcome GWAS, cross-phenotype tests by CPASSOC and MTAG, and by GWPT, respectively. The GWPT identified 18 genome-wide significant loci for myopia, four for SCZ, and 20 for CAD, respectively. All these loci did not

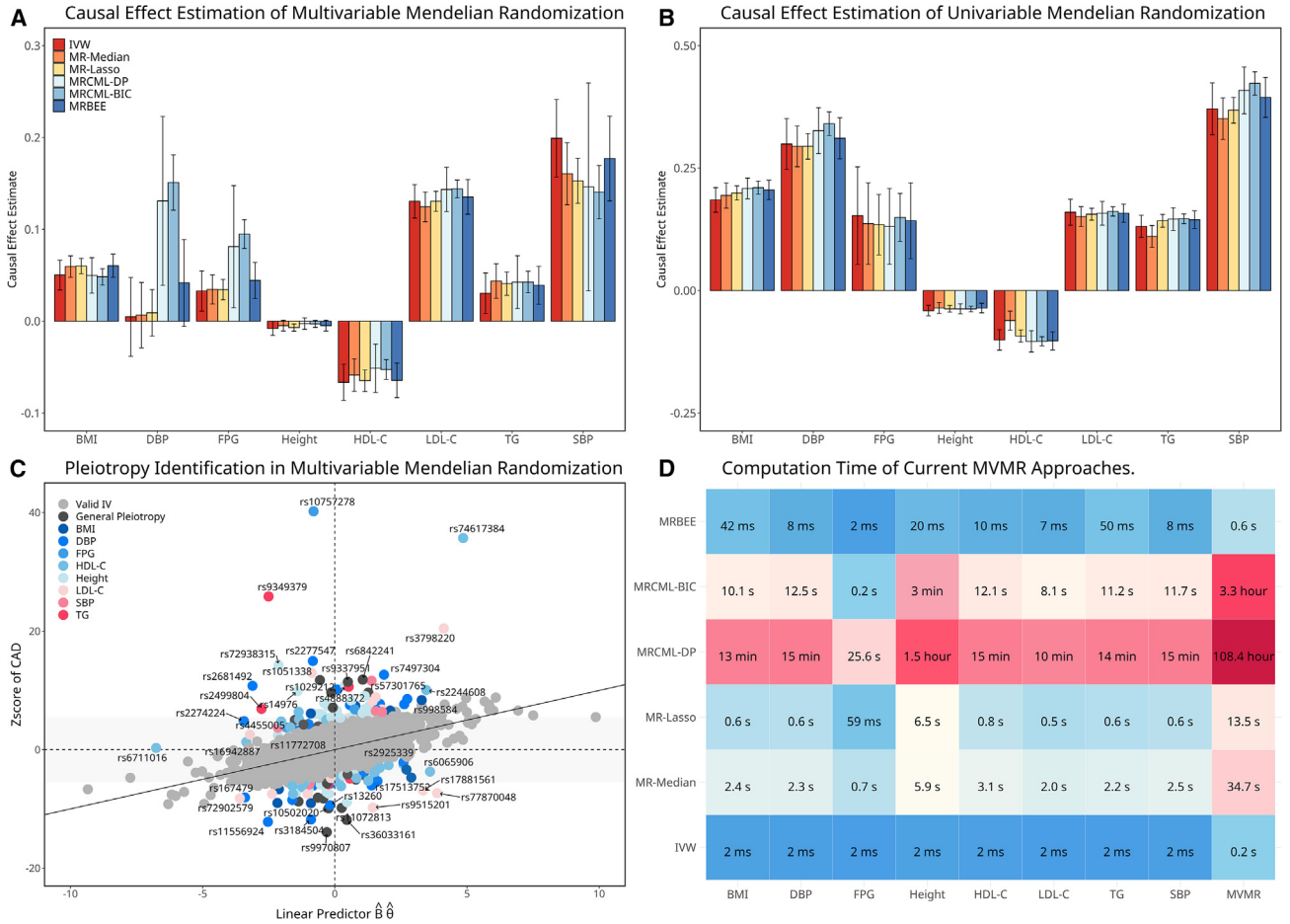

Figure 7. Data analysis of coronary artery disease

(A) Causal effect estimates by the six MVMR methods. The corresponding 95% confidence interval shown as vertical error bars.

(B) Causal effect estimates by UVMR approaches. The corresponding 95% confidence interval shown as vertical error bars. The radius of the confidence interval equals $\sqrt{a}\times$ SE where $a = F_{\chi^2}^{-1}(1 - 0.05/8, 1)$.

(C) Pleiotropy test where the x axis represents the linear predictor $\widehat{B}\widehat{\theta}_{\mathrm{BEE}}$ and the y axis represents the standardized association between the IV and CAD from GWAS. The annotation of this pleiotropic variant is made if it is associated with the most significant exposures with $p < 5\mathrm{E}{-8}$.

(D) Computation times of the comparing methods. Columns 1–8 represent computation time for UVMR of eight exposures and the last column represents computation time for MVMR.

reach genome-wide significance level in the outcome GWASs, suggesting GWPT captures pleiotropic evidence and the standard GWAS does not. We also performed expression quantitative trait loci (eQTL) mapping for the identified loci using functional mapping of GWAS (FUMA GWAS).[39] Each SNP that tagged a locus had marginal evidence of association with the expression of a gene in that locus in at least one tissue, where association p values ranged from 3.3E−310 to 6.7E−5. This suggests that these loci may have functionally relevant consequences in their conferred risk for myopia, SCZ, or CAD.

Discussion

We proposed MRBEE to overcome the weak instrument, pleiotropy and sample overlap bias in MVMR analysis. We pointed out that weak instrument bias is essentially driven by measurement error of GWAS effect estimates, whose scale and bias direction are influenced by the degree of weakness of IVs and the GWAS sample overlap, respectively. An IV is not considered weak when the estimation error is negligible, which can be achieved with a sufficiently large GWAS sample size, no matter how large or small the effect size is. In genetics, Burgess et al.[3] suggested using the F-statistics to define the strength of an IV, whereas we recommend the reliability ratio (material and methods, Equation 11), a commonly used statistic in measurement error analysis. Both metrics are equivalent and will be influenced by the GWAS sample size and the number of IVs, highlighting that the definition of a weak instrument is dynamic. MRBEE removes the measurement error bias by using an unbiased estimating function. Although this estimating function has a long history in the literature of measurement error analysis,[40] it has not been utilized to modify the current MVMR approaches.

Table 2. Loci detection of GWPT and eQTL mapping of leading variant

	SNP information		Association test				eQTL mapping			
	SNP	CHR:BP	GWAS	MTAG	CPASSOC	GWPT	Symbol	Tissue	Database	*p*
Myopia	rs55761633	1:20757820	9.9e−07	3.1e−05	5.6e−07	9.6e−09	CAMK2N1	Muscle Skeletal	GTEx/v8	3.9e−06
	rs2419964	2:124252256	1.3e−07	1.2e−05	2.6e−10	6.0e−10	NA	NA	NA	NA
	rs7602460	2:182261869	4.9e−07	9.2e−06	6.6e−07	3.2e−08	ITGA4	Blood	eQTLgen	2.0e−19
	rs61548163	2:184349492	9.2e−07	1.3e−05	3.3e−06	2.7e−08	NA	NA	NA	NA
	rs6764842	3:123106287	1.6e−06	NA	2.0e−07	3.1e−08	ADCY5	Artery Tibial	GTEx/v8	3.0e−17
	rs9761983	4:138482973	1.5e−07	NA	9.0e−06	4.4e−08	RP11-714L20.1	Cortex	GTEx/v8	2.2e−06
	rs2461726	6:166316838	5.1e−07	1.7e−05	1.2e−06	1.1e−08	SDIM1	Pituitary	GTEx/v7	2.8e−07
	rs12699288	7:11975557	3.8e−06	1.4e−04	3.4e−08	1.4e−08	THSD7A	Nerve Tibial	GTEx/v8	6.7e−05
	rs2970498	7:30478056	1.1e−07	1.8e−06	7.0e−06	3.1e−08	NOD1	Blood	eQTLgen	1.0e−07
	rs1532278	8:27466315	3.4e−07	1.1e−05	9.6e−07	6.7e−09	CLU	Eye	EyeGEx	1.1e−26
	rs7048915	9:4206388	1.0e−07	2.0e−06	6.2e−06	1.3e−08	NA	NA	NA	NA
	rs902997	10:105384262	1.9e−07	9.2e−07	1.2e−08	3.2e−09	USMG5	Blood	eQTLgen	3.0e−37
	rs17065719	13:44925021	4.3e−07	1.1e−05	2.6e−05	3.7e−08	SERP2	Blood	eQTLgen	7.7e−48
	rs1926715	13:111538590	8.6e−08	1.4e−05	2.4e−12	2.0e−09	ANKRD10	Eye	EyeGEx	3.0e−48
	rs7141076	14:67922172	9.2e−08	1.8e−05	5.7e−06	1.7e−08	TMEM229B	Pituitary	GTEx/v8	1.1e−08
	rs12889206	14:68769182	8.8e−08	1.5e−06	1.2e−06	3.9e−08	NA	NA	NA	NA
	rs7198357	16:67884619	2.5e−07	4.2e−06	2.1e−09	4.3e−09	DUS2	Blood	eQTLgen	3.3e−310
	rs35594082	16:84796864	8.5e−07	1.8e−05	1.8e−06	3.1e−08	USP10	Eye	EyeGEx	2.9e−09
Schizophrenia	rs17672204	5:74946518	1.1e−06	8.2e−06	1.9e−06	2.4e−08	COL4A3BP	Muscle Skeletal	GTEx/v8	5.8e−15
	rs79650876	3:187997616	1.7e−07	4.3e−08	4.5e−07	3.2e−08	AC022498.1	Blood	eQTLGen	5.7e−06
	rs2300921	3:185651001	8.0e−06	8.9e−06	4.9e−06	3.2e−08	TRA2B	Breast	GTEx/v8	1.8e−06
	rs7225476	17:78561603	8.2e−07	2.1e−06	7.0e−05	3.3e−08	RPTOR	Blood	eQTLGen	4.0e−89
Coronary artery disease	rs2045886	2:29010517	3.6e−07	4.6e−05	2.7e−21	7.7e−11	PPP1CB	Blood	eQTLGen	3.3e−310
	rs6727524	2:238570309	8.9e−07	6.3e−05	4.4e−09	2.8e−08	LRRFIP1	Blood	eQTLGen	3.4e−76
	rs1868217	3:98445534	2.1e−05	4.5e−04	1.3e−10	3.6e−08	ST3GAL6	Blood	eQTLGen	2.0e−30
	rs73070809	3:186885760	1.1e−07	NA	3.7e−07	1.0e−08	RPL39L	Adipose	GTEx/v8	4.0e−05
	rs12523133	5:86297919	8.5e−08	2.3e−05	3.2e−19	2.5e−10	RP11-72L22.1	Spinal Cord	GTEx/v8	6.6e−08
	rs6899197	5:111250597	8.8e−06	NA	1.2e−20	2.2e−09	EPB41L4A	Esophagus	GTEx/v8	5.0e−05
	rs13202921	6:41687366	3.3e−07	2.9e−06	1.8e−08	3.8e−08	CCDC77	Artery Coronary	GTEx/v7	4.9e−11

(*Continued on next page*)

Table 2. *Continued*

SNP information		Association test				eQTL mapping			
SNP	CHR:BP	GWAS	MTAG	CPASSOC	GWPT	Symbol	Tissue	Database	*p*
rs2073533	7:14029739	1.1e−07	2.6e−05	5.2e−14	3.2e−11	NA	NA	NA	NA
rs7822979	8:106468592	6.0e−08	NA	1.5e−08	1.6e−10	NA	NA	NA	NA
rs4734881	8:106587829	7.8e−08	3.1e−05	5.3e−06	1.3e−10	ZFPM2	Esophagus	GTEx/v8	3.8e−08
rs12375254	8:125054365	3.2e−07	4.0e−06	2.5e−04	1.0e−08	TRMT12	Blood	eQTLGen	4.3e−15
rs12412313	10:134456762	2.4e−06	6.8e−03	2.7e−19	2.3e−10	INPP5A	Blood	eQTLGen	6.6e−13
rs7113595	11:70236819	7.8e−07	2.2e−05	2.7e−08	2.4e−08	PPFIA1	Blood	eQTLGen	5.3e−305
rs7315852	12:417633	3.0e−07	NA	7.7e−19	2.1e−11	CCDC77	Blood	eQTLGen	3.3e−310
rs55893521	15:83955536	2.2e−07	1.7e−04	3.4e−20	2.9e−09	BTBD1	Brain	xQTLServer	3.4e−75
rs12918327	16:30626616	6.8e−06	9.7e−04	2.8e−32	5.2e−10	STX4	Blood	eQTLgen	1.1e−85
rs9958798	18:52769637	4.0e−06	NA	9.9e−10	4.2e−08	RP11-99A1.2	Testis	GTEx/v8	6.3e−08
rs35496634	22:39147235	8.5e−06	1.2e−03	4.6e−17	3.4e−08	SUN2	Blood	eQTLGen	7.0e−79
rs5757949	22:40820151	2.9e−06	9.3e−06	5.2e−15	3.8e−08	MKL1	Eye	EyeGEx	1.6e−07

Our simulations suggested that MRBEE in general leads to equal or less bias of causal effect estimate than the comparing methods when weak IVs, pleiotropy, and sample overlap are present (Figure 2). Similarly, MRBEE also has equal or better type I error control and statistical power than robust comparing methods (Figure 3). MRcML-DP and MRcML-BIC were robust to weak IVs and consistently yield unbiased causal effect estimates under the "no pleiotropy" case. However, in the presence of horizontal pleiotropy, our simulations suggested that MRcML methods may produce local minimizers in some specific scenarios in which horizontal pleiotropy was not completely removed. MRcML employs the best subset selection for detecting pleiotropy and the algorithm's stability and time consumption could be a challenge,[41] as we observed in our simulations. MRBEE uses an iterative pleiotropy test, whose reliability has been validated in MR-PRESSO and IMRP.

In the myopia analysis, our detected causal effects for outdoor activities are consistent with the literature. For example, spending more time outdoors reducing incident myopia was confirmed by a randomized clinical trial.[42] On the other hand, near-work activities such as time spent watching TV or using the computer have not been found to be associated with myopia risk.[43] The potential biological mechanism is that outdoor activities increase the exposure time to natural light, which induces the release of dopamine and thereby inhibits axial elongation, thus suppressing the development of myopia.[30] Moreover, MRBEE yields a relatively large causal estimate for time spent driving, likely correcting for weak instrument bias given the small variation of driving time explained by the IVs. Although MRcML-DP and MRcML-BIC can effectively reduce weak instrument bias in simulations, their estimates for the effects of driving time were 3–5 times larger than those from other methods.

We observed that cannabis use disorder and education have substantially larger causal effects on SCZ than other exposures we examined. For LH, the current GWAS has identified four genome-wide significant IVs together explaining its 0.086% variation. As a result, we did not have sufficient power to confirm their causal effect due to its relatively smaller variance of LH explained by IVs. MRBEE did not identify pleiotropic variants in these data, suggesting that our study may already include most of the direct causal risk factors for SCZ.

Our MVMR analysis seems to suggest that HDL-C is likely a protective factor against CAD but with a weaker effect size than that from UVMR analysis, aligning with recent pharmaceutical trial outcomes.[44] The previously observed negative results[20,33] are likely because they did not utilize the lipid GWAS summary data with the largest available sample sizes. When using the largest GWAS summary statistics of CAD as in this study, all methods including IVW, MRcML-DP, and MRBEE resulted in significant protective causal effect of HDL-C on CAD (Figure 7A). We noted that the estimated equal contributions of DBP and SBP on CAD risk by MRcML-BIC and MRcML-DP,

which is in direct conflict with all other MR methods we tested and the literature.[45] In addition, MRBEE identified 173 pleiotropic IVs, one of which (rs10757278) is strongly associated with CAD ($p < 5E{-}300$) but whose biological mechanism warrants for further investigation.

We introduced the GWPT using the statistic S_{pleio}, which can be applied in UVMR or MVMR to identify specific IVs with evidence of horizontal pleiotropy. When S_{pleio} was applied to the whole genome, we identified genetic loci associated with myopia, SCZ, and CAD that were missed in their original GWAS. These loci also reflect their direct association with the outcomes or through exposures not included in this study. Genes in these loci had genome-wide significant eQTLs across a range of tissues, suggesting that these genes might be functionally relevant in modifying disease risk. For example, we identified the *RPTOR* gene for SCZ, which has previously been found to be associated with BMI[46] and blood pressure.[47] This gene also has significant eQTLs (smallest $p = 4E{-}89$) in blood tissue. This and other examples highlight the potential utility of S_{pleio} in identifying trait-associated loci and functionally relevant genes.

In our theoretical study (supplement 2), we consider the effect size of IVs to follow a normal distribution, representing a genomic random effect model.[48] We observed that increasing the sample size of GWAS often yields more novel loci, hence more IVs with non-zero effects can be used in a corresponding MR analysis. Therefore, in our theoretical investigation, we allow the number of IVs m to increase with the sample size n and examine the outcomes of MRBEE and MV-IVW under different rates of m and n. Our conclusion can be summarized as follows: for scenarios like those in our myopia and CAD data, where GWAS sample sizes for exposures are approximately half a million or more, MRBEE and MV-IVW are equally efficient (supplement 2, Theorem 1.3 (i)). In this case, MRBEE's inference is asymptotically valid, whereas MV-IVW may lead to incorrect inferences. For the SCZ data involving CUD, with GWAS sample sizes in the tens of thousands, MRBEE is less efficient than MV-IVW, but the inference made by MRBEE remains valid (supplement 2, Theorem 1.3 (ii)-(iii)). In these cases, the confidence intervals of MRBEE will be wider than MV-IVW but ensure the 95% coverage frequency. Although MRBEE can remove the weak instrument bias in general, we still recommend including the IVs with the association p values below a significance threshold. The reason is that weak IVs still require to be truly associated with an exposure although their effect sizes can be extremely small. Variants with the association p values above the threshold are likely to be false positive and including false positive IVs will lead to bias for MRBEE because of the violation of assumption (IV1). The purpose of developing MRBEE is to enhance existing methods, making causal effect estimation and inference more robust to weak IVs.

The comparison between MRBEE and MRcML in terms of statistical principle is as follows. MRBEE employs the unbiased estimating function method which constructs its unbiased score function from the score function of the MV-IVW method. In contrast, the MRcML method is a conditional score function method, characterized by first estimating the sufficient statistic containing parameters to be estimated and then estimating the parameter based on this sufficient statistic through an iterative method.[40] Although Stefanski and Carroll[24] demonstrated that the conditional score function possesses statistical efficiency, whether this conclusion can be directly applied to the MRcML method requires further investigation. In contrast, our investigation shows that MRBEE reaches statistical efficiency if $m/n_{min} \to 0$ where n_{min} is the minimum GWAS sample size (supplement 2, Theorem 1.3 (i)). Furthermore, our simulations in Section S1.3 of supplement 1 suggest that MRcML-DP tends to overestimate its SD (i.e., SE > SD), MRcML-BIC underestimates its SD (i.e., SE < SD), and MRBEE estimates its SD well in most cases, suggesting MRBEE can achieve more efficiency than MRcML. The exact reason that MRcML does not estimate SD well warrants further investigation.

MRBEE also has some limitations. MRBEE is ineffective in handling exposures associated with significantly weaker IVs, such as CUD and LH in the SCZ data. This is also a challenge inherited from the field of measurement error analysis. In this case, MRBEE and analogous methods such as MRcML tend to produce causal effect estimates with relatively large SE. MRBEE is effective when the proportion of pleiotropic variants is relatively low (e.g., below 30%). Incorporating a Gaussian mixture model with MRBEE might improve the robustness for scenarios with a high proportion of pleiotropic variants. Finally, MRBEE is designed to handle a fixed number of exposures. Expanding its capability to a high-dimensional MR model is warranted in future research.[49]

Last, it is worth offering guidance on how to perform MVMR analysis from our perspective. First, rather than selecting the optimal number of IVs such that the F-statistics and conditional F-statistics are larger than 10,[3,22] we suggest including all independent IVs that are genome-wide significantly associated with at least one exposure. The main purpose of doing this is to reduce the winner's curse. Our simulations found that all methods, including MRBEE, were affected by the winner's curse, and the only way to alleviate the winner's curse was to include as many causal variants as possible (supplement 1, and Figure S10). Besides, our theory (supplement 2, Theorem 1.2 and 1.3) illustrates that the asymptotic variance of a causal effect estimate is related to the cumulative variance explained by all specified IVs instead of the average variance explained by each IV. Hence, including more IVs in the MR model can reduce the variance of the related causal effect estimate. Second, when performing MVMR analysis, it is not necessary to remove variants that are pleiotropic between the exposures. The reason why Wang et al.[21] found that LDL-C was not significant in European populations is likely caused by this procedure. In contrast, simultaneously including all the relevant exposures and their

IVs is recommended because the multivariable regression can automatically account for the pleiotropic variants shared by the specified exposures. Third, we suggest conducting a GWPT after performing the MR analysis, which represents an effective multi-trait approach for discovering loci with pleiotropy effect, beyond current methods such as CPASSOC and MTAG. In statistical principle, GWPT is likely to identify new loci associated with the outcome if the effect directions of pleiotropy and exposure mediation are opposite in these genome regions.

During the revision of this manuscript, we noted that a recent preprint[53] claimed that MRBEE was biased with extremely large SD and SE for some of simulation scenarios. We observed that the reason was that the authors of the preprint did not perform the standardization for the instrument effects of both exposures and outcome, which was documented in in the MRBEE software. We present the reproduction of Table 1 in the preprint before and after the standardization in Table S25 in supplement 1. The result indicates MRBEE has reasonable SD and SE. We have updated MRBEE software on GitHub and it does not need the standardization now.

Material and methods

MR model

We describe MRBEE with details here. As in the main text, let $\mathbf{g}_i = (g_{i1},\ldots,g_{im})^\top$ be a vector of m independent genetic variants where each variant is standardized with mean zero and variance one, $\mathbf{x}_i = (x_{i1},\ldots,x_{ip})^\top$ be a vector of p exposures, and y_i be an outcome. Consider the following linear structural model:

$$\mathbf{x}_i = \mathbf{B}^\top \mathbf{g}_i + \mathbf{u}_i, \qquad \text{(Equation 1)}$$

$$y_i = \theta^\top \mathbf{x}_i + \gamma^\top \mathbf{g}_i + v_i, \qquad \text{(Equation 2)}$$

where $\mathbf{B} = (\beta_1,\ldots,\beta_m)^\top$ is an $(m \times p)$ matrix of genetic effects on exposures with $\beta_j = (\beta_{j1},\ldots,\beta_{jp})^\top$ being a vector of length p, $\theta = (\theta_1,\ldots,\theta_p)^\top$ is a vector of length p representing the causal effects of the p exposures on the outcome, $\gamma = (\gamma_1,\ldots,\gamma_m)^\top$ is a vector of length m representing horizontal pleiotropy, which may violate the (IV2) or (IV3) conditions, and $\mathbf{u}_i$ and v_i are noise terms. Substituting for $\mathbf{x}_i$ in (2), we obtain the reduced-form model:

$$y_i = \mathbf{g}_i^\top \alpha + \mathbf{u}_i^\top \theta + v_i, \qquad \text{(Equation 3)}$$

where

$$\alpha = \mathbf{B}\boldsymbol{\theta} + \gamma. \qquad \text{(Equation 4)}$$

In practice, $\mathbf{u}_i$ and v_i are usually correlated, and hence traditional linear regression between $\mathbf{x}_i$ and y_i cannot obtain a consistent estimate of θ. In contrast, the genetic variant vector $\mathbf{g}_i$ is assumed to be independent of the noise terms $\mathbf{u}_i$ and v_i because the genotypes of individuals are randomly inherited from their parents and do not change during their lifetime.[50] Hence, $\mathbf{g}_i$ can be used as IVs to remove the confounding effect of $\mathbf{u}_i$ and v_i.

We assume that the genetic effect β_j $(j = 1,\ldots,m)$ is a p-dimensional random vector with zero-mean, covariance matrix $\Sigma_{\beta\beta}$, and cumulative covariance matrix $\Psi_{\beta\beta}$:

$$\Sigma_{\beta\beta} = \mathrm{E}\left(\beta_j\beta_j^\top\right), \Psi_{\beta\beta} = m\Sigma_{\beta\beta}.$$

The covariance matrix $\Sigma_{\beta\beta}$ will vanish as $m \to \infty$, but the cumulative covariance matrix $\Psi_{\beta\beta}$ is still a constant matrix, representing the total genetic covariance contributed from the m IVs. The genetic variant g_{ij} $(i = 1,\ldots,n, j = 1,\ldots,m)$ is standardized so that $\mathrm{E}(g_{ij}) = 0$ and $\mathrm{var}(g_{ij}) = 1$, and all IVs are assumed to be in linkage equilibrium (LE), i.e., $\mathrm{cov}(g_{ij}, g_{ik}) = 0$ for $j \neq k$. Next, the noise terms $\mathbf{u}_i$ and v_j have zero-means and joint covariance matrix:

$$\Sigma_{u\times v} = \mathrm{cov}\left((\mathbf{u}_i^\top, v_j)^\top\right) = \begin{pmatrix} \Sigma_{uu} & \sigma_{uv} \\ \sigma_{uv}^\top & \sigma_{vv} \end{pmatrix}.$$

Thus, the exposure $\mathbf{x}_i$ and outcome y_i have zero-means and joint covariance matrix:

$$\Sigma_{x\times y} = \mathrm{cov}\left(\left(\mathbf{x}_i^\top, y_i\right)^\top\right) = \begin{pmatrix} \Sigma_{xx} & \sigma_{xy} \\ \sigma_{xy}^\top & \sigma_{yy} \end{pmatrix},$$

$\Sigma_{xx} = \Psi_{\beta\beta} + \Sigma_{uu}$, $\sigma_{xy} = \Psi_{\beta\beta}\theta + \Sigma_{uu}\theta + \sigma_{uv}$, and $\sigma_{yy} = \theta^\top\Psi_{\beta\beta}\theta + \theta^\top\Sigma_{uu}\theta + 2\theta^\top\sigma_{uv} + \sigma_{vv}$. Note that $\sigma_{uv} \neq \mathbf{0}$ means the confounders affect both $\mathbf{x}_i$ and y_i.

Bias of multivariable IVW estimate

Since large individual-level data from GWAS are less publicly available, most of the current MR analyses are performed with summary statistics of IVs through the following linear regression:

$$\widehat{\alpha}_j = \widehat{\beta}_j^\top \theta + \gamma_j + \varepsilon_j, \qquad \text{(Equation 5)}$$

where $\widehat{\alpha}_j$ and $\widehat{\beta}_j$ are respectively estimated from the outcome and exposure GWASs, γ_j is the horizontal pleiotropy, ε_j represents the residual of this regression model, and $j = 1,\ldots,m$ referring to the m IVs. MV-IVW, which is the foundation of most existing MR methods, estimates θ by

$$\begin{aligned} \widehat{\theta}_{\mathrm{IVW}} &= \underset{\theta}{\mathrm{argmin}}\{(\widehat{\alpha} - \widehat{\mathbf{B}}\theta)^\top \mathbf{V}^{-1}(\widehat{\alpha} - \widehat{\mathbf{B}}\theta)\} \\ &= \left(\widehat{\mathbf{B}}^\top \mathbf{V}^{-1}\widehat{\mathbf{B}}\right)^{-1}\widehat{\mathbf{B}}^\top \mathbf{V}^{-1}\widehat{\alpha} \end{aligned}, \qquad \text{(Equation 6)}$$

where $\mathbf{V}$ is a diagonal matrix consisting of the variance of estimation errors of $\widehat{\alpha}$. In practice, it is routine to standardize $\widehat{\alpha}_j$ and $\widehat{\beta}_{jk}$ by $\widehat{\alpha}_j/\mathrm{se}(\widehat{\alpha}_j)$ and $\widehat{\beta}_{js}/\mathrm{se}(\widehat{\beta}_{jk})$ to remove the minor allele frequency effect.[16] With this standardization, the MV-IVW estimates θ by

$$\widehat{\theta}_{\mathrm{IVW}} = \underset{\theta}{\mathrm{argmin}}\{\|\widehat{\alpha} - \widehat{\boldsymbol{B}}\theta\|_2^2\} = (\widehat{\mathbf{B}}^\top\widehat{\mathbf{B}})^{-1}\widehat{\mathbf{B}}^\top\widehat{\alpha}. \qquad \text{(Equation 7)}$$

However, the MV-IVW estimate $\widehat{\theta}_{\mathrm{IVW}}$ is biased due to the estimation errors of $\widehat{\alpha}_j$ and $\widehat{\beta}_j$:

$$\widehat{\alpha}_j = \alpha_j + w_{\alpha_j}, \qquad \text{(Equation 8)}$$

$$\widehat{\beta}_j = \beta_j + \mathbf{w}_{\beta_j}. \qquad \text{(Equation 9)}$$

To see this, observe the estimating equation and Hessian matrix of $\widehat{\theta}_{\mathrm{IVW}}$:

$$\mathbf{S}_{\mathrm{IVW}}(\theta) = \widehat{\mathbf{B}}^\top(\widehat{\mathbf{B}}\theta - \widehat{\alpha}), \mathbf{H}_{\mathrm{IVW}} = \widehat{\mathbf{B}}^\top\widehat{\mathbf{B}}.$$

That is, $\mathbf{S}_{\mathrm{IVW}}(\theta)$ is the score function of Equation 7 and $\widehat{\theta}_{\mathrm{IVW}}$ is estimated by solving $\mathbf{S}_{\mathrm{IVW}}(\theta_{\mathrm{IVW}}) = \mathbf{0}$, and $\mathrm{H}_{\mathrm{IVW}}$ is the 2nd derivative matrix of Equation 7. As shown in supplement 2, since $\widehat{\theta}_{\mathrm{IVW}} - \theta = -\mathbf{H}_{\mathrm{IVW}}^{-1}\mathbf{S}_{\mathrm{IVW}}(\theta)$, the bias of $\widehat{\theta}_{\mathrm{IVW}}$ is approximately:

$$\mathrm{E}(\widehat{\theta}_{\mathrm{IVW}} - \theta) \approx -\mathrm{E}(\mathbf{H}_{\mathrm{IVW}})^{-1}\mathrm{E}(\mathbf{S}_{\mathrm{IVW}}(\theta)) = -\left\{\Sigma_{\beta\beta} + \Sigma_{W_\beta W_\beta}\right\}^{-1}\left\{\Sigma_{W_\beta W_\beta}\theta - \sigma_{W_\beta w_\alpha} + \sigma_{\beta\gamma}\right\}, \quad \text{(Equation 10)}$$

where

$$\mathrm{cov}\left(\left(\mathbf{w}_{\beta_j}^{\top}, w_{\alpha_j}\right)^{\top}\right) = \Sigma_{W_\beta \times w_\alpha} = \begin{pmatrix} \Sigma_{W_\beta W_\beta} & \sigma_{W_\beta w_\alpha} \\ \sigma_{W_\beta w_\alpha}^{\top} & \sigma_{w_\alpha w_\alpha} \end{pmatrix}, \mathrm{cov}\left(\beta_j, \gamma_j\right) = \sigma_{\beta\gamma}.$$

Interpretation of weak instrument bias

Here, $\Sigma_{\beta\beta}$ can be regarded as the average information carried by each IV, while $\Sigma_{W_\beta W_\beta}$ can be regarded as the information carried by each estimation error. If $\Sigma_{\beta\beta}$ is not substantially larger than $\Sigma_{W_\beta W_\beta}$, then the weak instrument will inflate the measurement error bias by the multiplier $(\Sigma_{\beta\beta} + \Sigma_{W_\beta W_\beta})^{-1}$. This is the primary reason why violating assumption (IV1) introduces bias into causal effect estimates in IVW and other MR approaches.[26]

The covariance between the estimation errors of SNP-exposure and SNP-outcome associations $\sigma_{W_\beta w_\alpha}$ can be affected by the fraction of overlapping samples of the exposures and outcome GWAS. If the exposures and outcome GWAS are independent of each other, then $\sigma_{W_\beta w_\alpha} = \mathbf{0}$ and hence the measurement error bias always shrinks $\widehat{\theta}_{\mathrm{IVW}}$ toward the null. In contrast, if the exposures GWAS and outcome GWAS are estimated from the same cohorts, $\sigma_{W_\beta w_\alpha}$ usually introduces bias toward the direction of σ_{uv}, reflecting the degree of sample overlap between exposures and outcome. This is the reason why in some empirical studies,[23,27] IVW cannot completely remove the confounding bias if the overlapping sample fraction is large.

If $\sigma_{\beta\gamma} \neq \mathbf{0}$, there is additional pleiotropy bias due to the horizontal pleiotropy that violates the InSIDE assumption. In UVMR, it is challenging to guarantee $\gamma_j = 0$ or $\mathrm{cov}(\gamma_j, \beta_j) = \mathbf{0}$ for all $1 \leq j \leq m$, resulting in a potentially biased IVW estimate. Traditional solutions to horizontal pleiotropy bias require that only a small proportion of IVs exhibit horizontally pleiotropic effects.[5,7,12] However, for complex traits, it is plausible that a large portion of IVs (even possibly $> 50\%$) possess horizontally pleiotropic effects, leading to the failure of UVMR methods. MVMR can balance these pleiotropic effects shared by multiple exposures, significantly reducing the number of IVs with horizontal pleiotropy evidence when conditioned on specified exposures. In other words, it is more likely to guarantee that only few IVs violate the InSIDE assumption $\sigma_{\beta\gamma} = \mathbf{0}$ after accounting for multiple exposures, which can be then detected and removed using the robust tools such as a pleiotropy hypothesis test.

Reliability ratio

In practice, we suggest using the reliability ratio[40]:

$$\omega_k = \frac{\mathrm{var}\left(\beta_{jk}\right)}{\mathrm{var}\left(\widehat{\beta}_{jk}\right)} \quad \text{(Equation 11)}$$

to measure the degree of bias in $\widehat{\theta}_{k,\mathrm{IVW}}$, which can be empirically estimated by

$$\widehat{\omega}_k = \frac{\sum_{j=1}^{m}\left(\widehat{\beta}_{jk}^2 - \mathrm{var}\left(w_{\beta_{jk}}\right)\right)}{\sum_{j=1}^{m}\widehat{\beta}_{jk}^2}. \quad \text{(Equation 12)}$$

$\widehat{\omega}_k$ reflects the proportion of variability in the estimated effects attributable to the underlying true genetic effects. For example, a reliability ratio of 0.6 indicates that 60% of the variance of the estimated effects is attributable to the true effects and the rest is attributable to their estimation errors. From the perspective of measurement error theory, the IVW estimate $\widehat{\theta}_{\mathrm{IVW}}$ converges to $\omega\theta$ in a univariable MR analysis when there is no sample overlap, where ω is equal to $\mathrm{var}(\beta_j)/\mathrm{var}(\widehat{\beta}_j)$.[40] Here ω is less than 1 and is viewed as a shrinkage coefficient for $\widehat{\theta}_{\mathrm{IVW}}$ relative to the true effect θ. We adopt this reliability ratio to much broader contexts, such as multivariable MR and sample overlap. In our real data analysis, we found this reliability ratio works reasonably well although additional investigation is warranted. While the reliability ratio and the F-statistics[3] are similar, the former has a simpler calculation and can more clearly reflect the proportion of weak IV bias than the latter.

MR using bias-corrected estimating equation

We propose MRBEE, which estimates causal effects by solving a new unbiased estimating equation of causal effects. The unbiased estimating equation of θ is

$$\mathbf{S}_{\mathrm{BEE}}(\theta) = \mathbf{S}_{\mathrm{IVW}}(\theta) - m\left(\Sigma_{W_\beta W_\beta}\theta - \sigma_{W_\beta w_\alpha}\right), \quad \text{(Equation 13)}$$

where $\mathbf{S}_{\mathrm{IVW}}(\theta) = -\widehat{\mathbf{B}}^{\top}(\widehat{\alpha} - \widehat{\mathbf{B}}\theta)$. Equation 13 states that the MRBEE estimating function is equal to the IVW estimating equation minus its bias. Unbiasedness of the MRBEE estimating equation implies unbiasedness of the MRBEE estimator. The solution $\widehat{\theta}_{\mathrm{BEE}}$ such that $\mathbf{S}_{\mathrm{BEE}}(\widehat{\theta}_{\mathrm{BEE}}) = \mathbf{0}$ is

$$\widehat{\theta}_{\mathrm{BEE}} = \left(\widehat{\mathbf{B}}^{\top}\widehat{\mathbf{B}} - m\Sigma_{W_\beta W_\beta}\right)^{-1}\left(\widehat{\mathbf{B}}^{\top}\widehat{\alpha} - m\sigma_{W_\beta w_\alpha}\right). \quad \text{(Equation 14)}$$

Note that unlike other optimizations such as generalized linear model in measurement error,[40] the Hessian matrix $\mathbf{H}_{\mathrm{IVW}} = \widehat{\mathbf{B}}^{\top}\widehat{\mathbf{B}}$ does not involve θ and hence $\mathbf{S}_{\mathrm{BEE}}(\theta)$ can be directly obtained from $\mathbf{S}_{\mathrm{IVW}}(\theta)$ without any iterative approximation.

Bias-correction terms estimation

We estimate the bias-correction terms $\Sigma_{W_\beta W_\beta}$ and $\sigma_{W_\beta w_\alpha}$ from the insignificant and independent GWAS summary statistics.[37] Let $\widehat{\alpha}_j^*, \widehat{\beta}_{j1}^*, \ldots, \widehat{\beta}_{jp}^*$ $(j = 1, \ldots, M)$ be M insignificant GWAS effect size estimates of outcome and exposures, where the insignificance means that the p value of the genetic variants are larger than 0.05 for all exposures and outcome, and the independence means that they are not in LD. Because $\widehat{\alpha}_j^*$ and $\widehat{\beta}_{jk}^*$ follow the same distributions of w_{α_j} and $w_{\beta_{jk}}$, $\Sigma_{W_\beta \times w_\alpha}$ can be estimated by

$$\widehat{\Sigma}_{W_\beta \times w_\alpha} = \frac{1}{M}\sum_{j=1}^{M}\left(\widehat{\beta}_{j1}^*, \ldots, \widehat{\beta}_{jp}^*, \widehat{\alpha}_j^*\right)^{\top}\left(\widehat{\beta}_{j1}^*, \ldots, \widehat{\beta}_{jp}^*, \widehat{\alpha}_j^*\right). \quad \text{(Equation 15)}$$

Here, $\widehat{\Sigma}_{W_\beta W_\beta}$ is the first $(p \times p)$ sub-matrix of $\widehat{\Sigma}_{W_\beta \times w_\alpha}$ and $\widehat{\sigma}_{W_\beta w_\alpha}$ consists of the first p elements of the last column of $\widehat{\Sigma}_{W_\beta \times w_\alpha}$. The intercept provided by LDSC[35] is also a consistent estimate of $\mathrm{cov}(w_{\alpha_j}, w_{\beta_{jk}})$. Each of these two estimators may be used by MRBEE and experience with real data suggests that they generally produce similar results. LDSC requires specification of an LD reference panel that is from an ancestrally similar population to that under study in MR. Differences in genetic architecture between the LD reference panel and the MR study population could introduce bias. Use of Equation 15 does not require an LD reference panel and so will not be biased for this reason. Additionally, use of Equation 15 is computationally simpler.

Algorithm 1. Pseudo-code of MRBEE + pleiotropy test

1. Input: Initial estimates $\widehat{\theta}^{(0)}$, Bias-correction terms $\widehat{\Sigma}_{W_\beta W_\beta}$ and $\widehat{\sigma}_{W_\beta W_\alpha}$, S_{pleio}, FDR q-value threshold κ, Tolerance ϵ, Full set of m^* IVs
2. Output: Causal effect estimates $\widehat{\theta}_{\text{BEE}}$, Set of m non-UHP/CHP IVs $\mathcal{F}_\Theta$
3. Pseudo-code:
Initialize $\mathcal{F}_\Theta^{(0)} = \{j : j = 1, ..., m^*\}$
While $\|\widehat{\theta}^{(t+1)} - \widehat{\theta}^{(t)}\|_2 > \epsilon$
1. Calculate $S_{\text{pleio}_j}^{(t)}(\widehat{\theta}^{(t)})$ for all $j = 1, ..., m^*$,
2. Update $\mathcal{F}_\Theta^{(t+1)} = \{j : S_{\text{pleio}_j}^{(t)}(\widehat{\theta}^{(t)}) < F_{\chi_1^2}^{-1}(1-\kappa)\}$,
3. Update $\widehat{\theta}^{(t+1)}$ using Equation 14 and IVs in $\mathcal{F}_\Theta^{(t+1)}$
End While

SE estimation

The covariance matrix of $\widehat{\theta}_{\text{BEE}}$ is yielded through the sandwich formula:

$$\text{cov}(\widehat{\theta}_{\text{BEE}}) := \Sigma_{\text{BEE}}(\theta) = \text{F}_{\text{BEE}}^{-1}\text{V}_{\text{BEE}}(\theta)\text{F}_{\text{BEE}}^{-1}, \quad \text{(Equation 16)}$$

where the outer matrix F_{BEE} is the Fisher information matrix, i.e., the expectation of the Hessian matrix of $\mathbf{S}_{\text{BEE}}(\theta)$, and the inner matrix $\text{V}_{\text{BEE}}(\theta)$ is the covariance matrix of $\mathbf{S}_{\text{BEE}}(\theta)$. A consistent estimate of $\Sigma_{\text{BEE}}(\theta)$ is

$$\widehat{\Sigma}_{\text{BEE}}(\theta) = \widehat{\text{F}}_{\text{BEE}}^{-1}\widehat{\text{V}}_{\text{BEE}}(\widehat{\theta}_{\text{BEE}})\widehat{\text{F}}_{\text{BEE}}^{-1}, \quad \text{(Equation 17)}$$

where $\widehat{\text{F}}_{\text{BEE}} = \widehat{\mathbf{B}}^\top\widehat{\mathbf{B}} - \widehat{\Sigma}_{W_\beta W_\beta}$, $\widehat{\text{V}}_{\text{BEE}}(\widehat{\theta}_{\text{BEE}}) = \sum_{j=1}^m \widehat{\mathbf{S}}_j(\widehat{\theta}_{\text{BEE}})\widehat{\mathbf{S}}_j(\widehat{\theta}_{\text{BEE}})^\top$, and $\widehat{\mathbf{S}}_j(\widehat{\theta}_{\text{BEE}}) = -(\widehat{\alpha}_j - \widehat{\theta}_{\text{BEE}}^\top\widehat{\beta}_j)\widehat{\beta}_j - \widehat{\Sigma}_{W_\beta W_\beta}\widehat{\theta}_{\text{BEE}} + \widehat{\sigma}_{W_\beta W_\alpha}$.

When the number of IVs m is small, the standard sandwich formula has been observed to underestimate the SE.[51] We apply the MD correction[52] to solve this problem. Consider the so-called hat matrix:

$$\mathbf{H} = \widehat{\mathbf{B}}\left(\widehat{\mathbf{B}}^\top\widehat{\mathbf{B}} - m\widehat{\Sigma}_{W_\beta W_\beta}\right)^{-1}\widehat{\mathbf{B}}^\top$$

and H_{jj} is its j th diagonal entries. The MD correction adjusts the inner matrix as

$$\widehat{\text{V}}_{\text{BEE}}^{\text{MD}}(\widehat{\theta}_{\text{BEE}}) = \sum_{j=1}^m (1 - H_{jj})^{-2}\widehat{\mathbf{S}}_j(\widehat{\theta}_{\text{BEE}})\widehat{\mathbf{S}}_j(\widehat{\theta}_{\text{BEE}})^\top. \quad \text{(Equation 18)}$$

Their theory shows that

$$\text{E}\left(\widehat{\mathbf{S}}_j(\widehat{\theta}_{\text{BEE}})\widehat{\mathbf{S}}_j(\widehat{\theta}_{\text{BEE}})^\top\right) \approx (1 - H_{jj})^2\text{V}_{\text{BEE}}(\theta),$$

and hence it can obtain a more reliable covariance matrix by adjusting $(1 - H_{jj})^{-2}$ when estimating $\text{V}_{\text{BEE}}(\theta)$ with the moment method. When there is horizontal pleiotropy, we adjust Equation 18 as

$$\widehat{\text{V}}_{\text{BEE}}^{\text{MD}}(\widehat{\theta}_{\text{BEE}}) = \frac{m + m_{pleiotropy}}{m}\sum_{j=1}^m (1 - H_{jj})^{-2}\widehat{\mathbf{S}}_j(\widehat{\theta}_{\text{BEE}})\widehat{\mathbf{S}}_j(\widehat{\theta}_{\text{BEE}})^\top, \quad \text{(Equation 19)}$$

where m is number of valid IVs and $m_{pleiotropy}$ is the number of detected pleiotropies. Section S1.3 of supplement 1 compares the estimated and true standard errors of causal effect estimates for MRBEE and other MVMR estimators. These results demonstrate that the MD correction described above controls the Type I error rate well. It is also worth noting that the standard errors of the MRBEE causal estimates will generally become smaller as the degree of weak instrument bias becomes smaller.

Horizontal pleiotropy detection

We illustrate how to remove specific IVs with evidence of UHP or CHP effects with the pleiotropy test S_{pleio} which tests the same null hypothesis for each SNP as MR-PRESSO and IMRP. The null hypothesis for the j th IV not having any horizontally pleiotropic effects on the outcome is

$$\mathbf{H_{0j}} : \gamma_j = 0 \; v.s. \; \mathbf{H_{1j}} : \gamma_j \neq 0. \quad \text{(Equation 20)}$$

The statistic S_{pleio} for the j th IV is defined as

$$S_{\text{pleio}_j}(\widehat{\theta}) = \frac{\left(\widehat{\alpha}_j - \widehat{\beta}_j^\top\widehat{\theta}\right)^2}{\text{var}\left(\widehat{\alpha}_j - \widehat{\beta}_j^\top\widehat{\theta}\right)}, \quad \text{(Equation 21)}$$

which follows a χ_1^2 distribution under $\mathbf{H_{0j}}$. The only assumption here is that $\widehat{\alpha}_j - \widehat{\beta}_j^\top\widehat{\theta}$ is asymptotically normal distributed. In fact, this test examines whether the outcome effect can be explained by the mediation effects through all exposures. In practice, we estimate $\text{var}(\widehat{\alpha}_j - \widehat{\beta}_j^\top\widehat{\theta})$ using the delta method:

$$\widehat{\text{var}}\left(\widehat{\alpha}_j - \widehat{\beta}_j^\top\widehat{\theta}\right) = \sigma_{w_\alpha}^2 + \widehat{\theta}^\top\widehat{\Sigma}_{W_\beta W_\beta}\widehat{\theta} + \widehat{\beta}_j^\top\widehat{\Sigma}_{\text{BEE}}\widehat{\beta}_j - 2\widehat{\theta}^\top\widehat{\sigma}_{W_\beta w_\alpha}.$$

Other methods such as empirical variance and robust variance estimates of the residual can also be used here. We calculate S_{pleio} for all candidate IVs and remove IVs with large S_{pleio} values in an iterative manner. Algorithm 1 uses an FDR Q-value threshold to exclude IVs showing potential pleiotropy evidence. We suggest a threshold Q-value <0.05 in general. Additional simulation results presented in Section S2.5 of supplement 1 show that FDR correction generally performs well.

GWPT

Since S_{pleio} tests a very general null hypothesis, we can also calculate S_{pleio} for all SNPs across the genome after obtaining the causal effect estimates of p exposures on the outcome. Results from these tests can be used to (1) find novel loci associated with the MR outcome and (2) draw inferences about pathways of genetic association with the MR outcome. Specifically, when an SNP has a negative effect on the exposure $\boldsymbol{\beta_j}$ and a positive pleiotropic effect on the outcome γ_j, and simultaneously the causal effect $\boldsymbol{\theta}$ is positive, then the total effect of this variant on the outcome α_j is canceled and hence cannot be detected in the outcome GWAS. In contrast, the pleiotropy test directly tests the effect γ_j and therefore can detect novel loci. For example, Zhu et al.[16] successfully detected many blood pressure loci missed previously by using this

GWPT with IMRP as the estimator of the causal effect. The results indicated that most detected pleiotropic variants influenced SBP and DBP in opposite directions, providing support for the principle of the GWPT.

Joint χ^2-test for IVs selection

We applied the joint χ^2-test to select a set of IVs that are strongly associated with multiple exposures. Let $\boldsymbol{\beta}_j = (\beta_{j1}, \ldots, \beta_{jp})^\top$ be the p-length vector of standardized associations between the jth SNP and the p exposures. We performed the following hypothesis test:

$$\mathbf{H}_{0j} : \beta_{j1} = \cdots = \beta_{jp} = 0, \ v.s. \ \mathbf{H}_{1j} : \beta_{j1} \neq 0, \text{or} \cdots \text{or} \ \beta_{jp} \neq 0. \quad \text{(Equation 22)}$$

The test statistic is

$$t_j = \widehat{\beta}_j^\top \widehat{\Sigma}_{W_\beta W_\beta}^{-1} \widehat{\beta}_j, \quad \text{(Equation 23)}$$

which follows a χ_p^2 distribution when the null hypothesis holds, where $\widehat{\Sigma}_{W_\beta W_\beta}$ is the estimated matrix of covariances between estimation errors. We only considered variants as IVs if they are genome-wide significant in the joint χ^2-test.

Estimation of variance explained by instrument variables

Assume that we intend to estimate the SNP heritability of a trait Y using a set of m IVs in the m-length vector $\mathbf{g} = (G_1, \ldots, G_m)^\top$ with corresponding associations with Y in the vector $\beta = (\beta_1, \ldots, \beta_m)^\top$. If the variance of Y is 1 and $E(G_j) = 0$, we can estimate the variance in Y explained by the m IVs using the following equation:

$$R^2 = \sum_{j=1}^{m} 2\widehat{\beta}_j^2 p_j\left(1 - p_j\right) \quad \text{(Equation 24)}$$

where p_j is the minor allele frequency of G_j. We used Equation 24 to produce the heritability estimates in Table 1.

Asymptotic results

We assume that both total number of IVs m and the minimum sample size among the exposure and outcome GWAS $n_{\min}$ can approach infinity, while the number of exposures p and the p-dimensional causal effect vector θ are fixed and bounded. Our goal is to identify the scenarios when MV-IVW outperforms MRBEE, when they perform equally well, and when MRBEE outperforms MV-IVW in terms of unbiased estimation of causal effects and the asymptotic validity of causal inference. We demonstrate the related theorems and the related regularity conditions and lemmas in supplement 2.

Data and code availability

The data referenced in this study can be accessed through the GWAS Catalog (https://www.ebi.ac.uk/gwas/home), with the corresponding GWAS summary data available for download in the "data availability" section of the respective papers. Some of the GWAS summary data are exclusive of the Million Veteran Program (MVP) summary results, which are available through dbGAP under the accession number phs001672.v3.p1.

The MRBEE R package generated during this study is available at https://github.com/noahlorinczcomi/MRBEE. Simulation codes generated during this study are available at https://github.com/harryyiheyang/MRBEE.Simulation.

Supplemental information

Supplemental information can be found online at https://doi.org/10.1016/j.xhgg.2024.100290.

Acknowledgments

This work was supported by grant HG011052 and HG011052-03S1 (to X.Z.) from the National Human Genome Research Institute (NHGRI), USA. N.L.-C. was partially supported by grant T32 HL007567 from the National Heart, Lung, and Blood Institute (NHLBI).

Declaration of interests

The authors declare no competing interests.

Received: November 17, 2023
Accepted: April 1, 2024

References

1. Sanderson, E., Glymour, M.M., Holmes, M.V., Kang, H., Morrison, J., Munafò, M.R., Palmer, T., Schooling, C.M., Wallace, C., Zhao, Q., and Davey Smith, G. (2022). Mendelian Randomization. Nat. Rev. Methods Primers *2*, 6–21.
2. Burgess, S., Butterworth, A., and Thompson, S.G. (2013). Mendelian Randomization Analysis with Multiple Genetic Variants Using Summarized Data. Genet. Epidemiol. *37*, 658–665.
3. Burgess, S., Thompson, S.G.; and CRP CHD Genetics Collaboration (2011). Avoiding Bias from Weak Instruments in Mendelian Randomization Studies. Int. J. Epidemiol. *40*, 755–764.
4. Bowden, J., Davey Smith, G., and Burgess, S. (2015). Mendelian Randomization with Invalid Instruments: Effect Estimation and Bias Detection Through Egger Regression. Int. J. Epidemiol. *44*, 512–525.
5. Morrison, J., Knoblauch, N., Marcus, J.H., Stephens, M., and He, X. (2020). Mendelian Randomization Accounting for Correlated and Uncorrelated Pleiotropic Effects Using Genome-Wide Summary Statistics. Nat. Genet. *52*, 740–747.
6. Verbanck, M., Chen, C.-Y., Neale, B., and Do, R. (2018). Detection of Widespread Horizontal Pleiotropy in Causal Relationships Inferred from Mendelian Randomization Between Complex Traits and Diseases. Nat. Genet. *50*, 693–698.
7. Zhu, X., Li, X., Xu, R., and Wang, T. (2021). An Iterative Approach to Detect Pleiotropy and Perform Mendelian Randomization Analysis Using GWAS Summary Statistics. Bioinformatics *37*, 1390–1400.
8. Kang, H., Zhang, A., Cai, T.T., and Small, D.S. (2016). Instrumental Variables Estimation with Some Invalid Instruments and Its Application to Mendelian Randomization. J. Am. Stat. Assoc. *111*, 132–144.
9. Xue, H., Shen, X., and Pan, W. (2021). Constrained Maximum Likelihood-Based Mendelian Randomization Robust to Both Correlated and Uncorrelated Pleiotropic Effects. Am. J. Hum. Genet. *108*, 1251–1269.
10. Bowden, J., Davey Smith, G., Haycock, P.C., and Burgess, S. (2016). Consistent Estimation in Mendelian Randomization

with Some Invalid Instruments Using a Weighted Median Estimator. Genet. Epidemiol. *40*, 304–314.
11. Rees, J.M.B., Wood, A.M., Dudbridge, F., and Burgess, S. (2019). Robust Methods in Mendelian Randomization via Penalization of Heterogeneous Causal Estimates. PLoS One *14*, e0222362.
12. Qi, G., and Chatterjee, N. (2019). Mendelian Randomization Analysis Using Mixture Models for Robust and Efficient Estimation of Causal Effects. Nat. Commun. *10*, 1941.
13. Burgess, S., Foley, C.N., Allara, E., Staley, J.R., and Howson, J.M.M. (2020). A Robust and Efficient Method for Mendelian Randomization with Hundreds of Genetic Variants. Nat. Commun. *11*, 376.
14. Yuan, Z., Liu, L., Guo, P., Yan, R., Xue, F., and Zhou, X. (2022). Likelihood-Based Mendelian Randomization Analysis with Automated Instrument Selection and Horizontal Pleiotropic Modeling. Sci. Adv. *8*, eabl5744.
15. Cheng, Q., Zhang, X., Chen, L.S., and Liu, J. (2022). Mendelian Randomization Accounting for Complex Correlated Horizontal Pleiotropy While Elucidating Shared Genetic Etiology. Nat. Commun. *13*, 6490.
16. Zhu, X., Zhu, L., Wang, H., Cooper, R.S., and Chakravarti, A. (2022). Genome-Wide Pleiotropy Analysis Identifies Novel Blood Pressure Variants and Improves Its Polygenic Risk Scores. Genet. Epidemiol. *46*, 105–121.
17. Sanderson, E., Davey Smith, G., Windmeijer, F., and Bowden, J. (2019). An Examination of Multivariable Mendelian Randomization in the Single-Sample and Two-Sample Summary Data Settings. Int. J. Epidemiol. *48*, 713–727.
18. Burgess, S., and Thompson, S.G. (2015). Multivariable Mendelian Randomization: The Use of Pleiotropic Genetic Variants to Estimate Causal Effects. Am. J. Epidemiol. *181*, 251–260.
19. Rees, J.M.B., Wood, A.M., and Burgess, S. (2017). Extending the MR-Egger Method for Multivariable Mendelian Randomization to Correct for Both Measured and Unmeasured Pleiotropy. Stat. Med. *36*, 4705–4718.
20. Lin, Z., Xue, H., and Pan, W. (2023). Robust Multivariable Mendelian Randomization Based on Constrained Maximum Likelihood. Am. J. Hum. Genet. *110*, 592–605.
21. Wang, K., Shi, X., Zhu, Z., Hao, X., Chen, L., Cheng, S., Foo, R.S.Y., and Wang, C. (2022). Mendelian Randomization Analysis of 37 Clinical Factors and Coronary Artery Disease in East Asian and European Populations. Genome Med. *14*, 63.
22. Sanderson, E., Spiller, W., and Bowden, J. (2021). Testing and Correcting for Weak and Pleiotropic Instruments in Two-Sample Multivariable Mendelian Randomization. Stat. Med. *40*, 5434–5452.
23. Sadreev, I.I., Elsworth, B.L., Mitchell, R.E., Paternoster, L., Sanderson, E., Davies, N.M., Millard, L.A.C., Davey Smith, G., Haycock, P.C., Bowden, J., et al. (2021). Navigating sample overlap, winner's curse and weak instrument bias in mendelian randomization studies using the UK Biobank. Preprint at medRxiv. https://doi.org/10.1101/2021.06.28.21259622.
24. Carroll, R.J., Ruppert, D., Stefanski, L.A., and Crainiceanu, C.M. (2006). Measurement Error in Nonlinear Models: A Modern Perspective. Chapman (Hall/CRC).
25. VanderWeele, T.J., Tchetgen Tchetgen, E.J., Cornelis, M., and Kraft, P. (2014). Methodological Challenges in Mendelian Randomization. Epidemiology *25*, 427–435.
26. Ye, T., Shao, J., and Kang, H. (2021). Debiased Inverse-Variance Weighted Estimator in Two-Sample Summary-Data Mendelian Randomization. Ann. Stat. *49*, 2079–2100.
27. Burgess, S., Davies, N.M., and Thompson, S.G. (2016). Bias Due to Participant Overlap in Two-Sample Mendelian Randomization. Genet. Epidemiol. *40*, 597–608.
28. Mounier, N., and Kutalik, Z. (2023). Bias Correction for Inverse Variance Weighting Mendelian Randomization. Genet. Epidemiol. *47*, 314–333.
29. Yavorska, O.O., and Burgess, S. (2017). MendelianRandomization: An r Package for Performing Mendelian Randomization Analyses Using Summarized Data. Int. J. Epidemiol. *46*, 1734–1739.
30. Morgan, I.G., French, A.N., Ashby, R.S., Guo, X., Ding, X., He, M., and Rose, K.A. (2018). The Epidemics of Myopia: Aetiology and Prevention. Prog. Retin. Eye Res. *62*, 134–149.
31. Marconi, A., Di Forti, M., Lewis, C.M., Murray, R.M., and Vassos, E. (2016). Meta-Analysis of the Association Between the Level of Cannabis Use and Risk of Psychosis. Schizophr. Bull. *42*, 1262–1269.
32. Corcoran, C.M., Kimhy, D., Stanford, A., Khan, S., Walsh, J., Thompson, J., Schobel, S., Harkavy-Friedman, J., Goetz, R., Colibazzi, T., et al. (2008). Temporal Association of Cannabis Use with Symptoms in Individuals at Clinical High Risk for Psychosis. Schizophr. Res. *106*, 286–293.
33. Holmes, M.V., Asselbergs, F.W., Palmer, T.M., Drenos, F., Lanktree, M.B., Nelson, C.P., Dale, C.E., Padmanabhan, S., Finan, C., Swerdlow, D.I., et al. (2015). Mendelian Randomization of Blood Lipids for Coronary Heart Disease. Eur. Heart J. *36*, 539–550.
34. 1000 Genomes Project Consortium, Auton, A., Brooks, L.D., Durbin, R.M., Garrison, E.P., Kang, H.M., Korbel, J.O., Marchini, J.L., McCarthy, S., McVean, G.A., and Abecasis, G.R. (2015). A Global Reference for Human Genetic Variation. Nature *526*, 68–74.
35. Bulik-Sullivan, B.K., Neale, B.M., Loh, P.-R., Finucane, H.K., Ripke, S., Yang, J., Schizophrenia Working Group of the Psychiatric Genomics Consortium, Patterson, N., Daly, M.J., and Price, A.L. (2015). LD Score Regression Distinguishes Confounding from Polygenicity in Genome-Wide Association Studies. Nat. Genet. *47*, 291–295.
36. Smith, C.J., Sinnott-Armstrong, N., Cichońska, A., Julkunen, H., Fauman, E.B., Würtz, P., and Pritchard, J.K. (2022). Integrative Analysis of Metabolite GWAS Illuminates the Molecular Basis of Pleiotropy and Genetic Correlation. Elife *11*, e79348.
37. Zhu, X., Feng, T., Tayo, B.O., Liang, J., Young, J.H., Franceschini, N., Smith, J.A., Yanek, L.R., Sun, Y.V., Edwards, T.L., et al. (2015). Meta-Analysis of Correlated Traits via Summary Statistics from GWASs with an Application in Hypertension. Am. J. Hum. Genet. *96*, 21–36.
38. Turley, P., Walters, R.K., Maghzian, O., Okbay, A., Lee, J.J., Fontana, M.A., Nguyen-Viet, T.A., Wedow, R., Zacher, M., Furlotte, N.A., et al. (2018). Multi-Trait Analysis of Genome-Wide Association Summary Statistics Using MTAG. Nat. Genet. *50*, 229–237.
39. Watanabe, K., Taskesen, E., Van Bochoven, A., and Posthuma, D. (2017). Functional Mapping and Annotation of Genetic Associations with FUMA. Nat. Commun. *8*, 1826.
40. Yi, G.Y. (2017). Statistical Analysis with Measurement Error or Misclassification: Strategy, Method and Application (Springer).

41. Breiman, L. (1996). Heuristics of instability and stabilization in model selection. Ann. Statist. *24*, 2350–2383.
42. He, M., Xiang, F., Zeng, Y., Mai, J., Chen, Q., Zhang, J., Smith, W., Rose, K., and Morgan, I.G. (2015). Effect of Time Spent Outdoors at School on the Development of Myopia Among Children in China: A Randomized Clinical Trial. JAMA *314*, 1142–1148.
43. Lin, Z., Vasudevan, B., Jhanji, V., Mao, G.Y., Gao, T.Y., Wang, F.H., Rong, S.S., Ciuffreda, K.J., and Liang, Y.B. (2014). Near Work, Outdoor Activity, and Their Association with Refractive Error. Optom. Vis. Sci. *91* (4), 376–382.
44. The HPS3/TIMI55–REVEAL Collaborative Group (2017). Effects of Anacetrapib in Patients with Atherosclerotic Vascular Disease. N. Engl. J. Med. *377*, 1217–1227.
45. Chobanian, A.V., Bakris, G.L., Black, H.R., Cushman, W.C., Green, L.A., Izzo, J.L., Jr, W Jones, D., Materson, B.J., Oparil, S., Wright, J.T., Jr., et al. (2004). The seventh report of the joint national committee on prevention, detection, evaluation, and treatment of high blood pressure. Hypertension *42*, 1206–1252.
46. Locke, A.E., Kahali, B., Berndt, S.I., Justice, A.E., Pers, T.H., Day, F.R., Powell, C., Vedantam, S., Buchkovich, M.L., Yang, J., et al. (2015). Genetic studies of body mass index yield new insights for obesity biology. Nature *518*, 197–206.
47. Takeuchi, F., Akiyama, M., Matoba, N., Katsuya, T., Nakatochi, M., Tabara, Y., Narita, A., Saw, W.Y., Moon, S., Spracklen, C.N., et al. (2018). Interethnic analyses of blood pressure loci in populations of East Asian and European descent. Nat. Commun. *9*, 5052.
48. Yang, J., Benyamin, B., McEvoy, B.P., Gordon, S., Henders, A.K., Nyholt, D.R., Madden, P.A., Heath, A.C., Martin, N.G., Montgomery, G.W., et al. (2010). Common SNPs Explain a Large Proportion of the Heritability for Human Height. Nat. Genet. *42*, 565–569.
49. Zuber, V., Colijn, J.M., Klaver, C., and Burgess, S. (2020). Selecting likely causal risk factors from high-throughput experiments using multivariable Mendelian randomization. Nat. Commun. *11*, *29*.
50. Lawlor, D.A., Harbord, R.M., Sterne, J.A.C., Timpson, N., and Davey Smith, G. (2008). Mendelian Randomization: Using Genes as Instruments for Making Causal Inferences in Epidemiology. Stat. Med. *27*, 1133–1163.
51. Wang, M., Kong, L., Li, Z., and Zhang, L. (2016). Covariance Estimators for Generalized Estimating Equations (GEE) in Longitudinal Analysis with Small Samples. Stat. Med. *35*, 5318–5319.
52. Mancl, L.A., and DeRouen, T.A. (2001). A Covariance Estimator for GEE with Improved Small-Sample Properties. Biometrics *57*, 126–134.
53. Wu, Y., Kang, H., and Ye, T. (2024). Debiased Multivariable Mendelian Randomization. Preprint at arXiv. https://doi.org/10.48550/arXiv.2402.00307.
54. van De Vegte, Y.J., Said, M.A., Rienstra, M., van Der Harst, P., and Verweij, N. (2020). Genome-wide association studies and Mendelian randomization analyses for leisure sedentary behaviours. Nature Commun. *11*, 1770. https://doi.org/10.1038/s41467-020-15553-w.
55. Arns, A., Wahl, T., Wolff, C., Vafeidis, A.T., Haigh, I.D., Woodworth, P., Niehüser, S., and Jensen, J. (2020). Non-linear interaction modulates global extreme sea levels, coastal flood exposure, and impacts. Nature Commun. *11*, 1918. https://doi.org/10.1038/s41467-020-15752-5.
56. Rustad, E.H., Yellapantula, V., Leongamornlert, D., Bolli, N., Ledergor, G., Nadeu, F., Angelopoulos, N., Dawson, K.J., Mitchell, T.J., Osborne, R.J., et al. (2020). Timing the initiation of multiple myeloma. Nature Commun. *11*, 1917. https://doi.org/10.1038/s41467-020-15740-9.
57. Okbay, A., Wu, Y., Wang, N., Jayashankar, H., Bennett, M., Nehzati, S.M., Sidorenko, J., Kweon, H., Goldman, G., Gjorgjieva, T., et al. (2022). Polygenic prediction of educational attainment within and between families from genome-wide association analyses in 3 million individuals. Nature Genet. *54*, 437–449. https://doi.org/10.1038/s41588-022-01016-z.
58. Hysi, P.G., Choquet, H., Khawaja, A.P., Wojciechowski, R., Tedja, M.S., Yin, J., Simcoe, M.J., Patasova, K., Mahroo, O.A., Thai, K.K., et al. (2020). Meta-analysis of 542,934 subjects of European ancestry identifies new genes and mechanisms predisposing to refractive error and myopia. Nature genetics *52*, 401–407. https://doi.org/10.1038/s41588-020-0599-0.
59. Demontis, D., Walters, R.K., Martin, J., Mattheisen, M., Als, T.D., Agerbo, E., Baldursson, G., Belliveau, R., Bybjerg-Grauholm, J., Bækvad-Hansen, M., et al. (2019). Discovery of the first genome-wide significant risk loci for attention deficit/hyperactivity disorder. Nature Genet. *51*, 63–75. https://doi.org/10.1038/s41588-018-0269-7.
60. Johnson, E.C., Demontis, D., Thorgeirsson, T.E., Walters, R.K., Polimanti, R., Hatoum, A.S., Sanchez-Roige, S., Paul, S.E., Wendt, F.R., Clarke, T.K., et al. (2020). A large-scale genome-wide association study meta-analysis of cannabis use disorder. The Lancet Psychiatry *7*, 1032–1045.
61. Cuellar-Partida, G., Tung, J.Y., Eriksson, N., Albrecht, E., Aliev, F., Andreassen, O.A., Barroso, I., Beckmann, J.S., Boks, M.P., Boomsma, D.I., et al. (2021). Genome-wide association study identifies 48 common genetic variants associated with handedness. Nature Human Behav. *5*, 59–70. https://doi.org/10.1038/s41562-020-00956-y.
62. Nagel, M., Jansen, P.R., Stringer, S., Watanabe, K., De Leeuw, C.A., Bryois, J., Savage, J.E., Hammerschlag, A.R., Skene, N.G., and Muñoz-Manchado, A.B. (2018). Meta-analysis of genome-wide association studies for neuroticism in 449,484 individuals identifies novel genetic loci and pathways. Nature Genet. *50*, 920–927. https://doi.org/10.1038/s41588-018-0151-7.
63. Dashti, H.S., Jones, S.E., Wood, A.R., Lane, J.M., Van Hees, V.T., Wang, H., Rhodes, J.A., Song, Y., Patel, K., Anderson, S.G., et al. (2019). Genome-wide association study identifies genetic loci for self-reported habitual sleep duration supported by accelerometer-derived estimates. Nature Commun. *10*, 1100.
64. Trubetskoy, V., Pardiñas, A.F., Qi, T., Panagiotaropoulou, G., Awasthi, S., Bigdeli, T.B., Bryois, J., Chen, C.Y., Dennison, C.A., Hall, L.S., et al. (2022). Mapping genomic loci implicates genes and synaptic biology in schizophrenia. Nature *604*, 502–508.
65. Loh, P.R., Kichaev, G., Gazal, S., Schoech, A.P., and Price, A.L. (2018). Mixed-model association for biobank-scale datasets. Nature Genet. *50*, 906–908. https://doi.org/10.1038/s41588-018-0144-6.
66. Evangelou, E., Warren, H.R., Mosen-Ansorena, D., Mifsud, B., Pazoki, R., Gao, H., Ntritsos, G., Dimou, N., Cabrera, C.P., Karaman, I., et al. (2018). Genetic analysis of over 1 million people identifies 535 new loci associated with blood pressure traits. Nature Genet. *50*, 1412–1425. https://doi.org/10.1038/s41588-018-0205-x.

67. Graham, S.E., Clarke, S.L., Wu, K.H.H., Kanoni, S., Zajac, G.J., Ramdas, S., Surakka, I., Ntalla, I., Vedantam, S., Winkler, T.W., et al. (2021). The power of genetic diversity in genome-wide association studies of lipids. Nature *600*, 675–679. https://doi.org/10.1038/s41586-021-04064-3.

68. Aragam, K.G., Jiang, T., Goel, A., Kanoni, S., Wolford, B.N., Atri, D.S., Weeks, E.M., Wang, M., Hindy, G., Zhou, W., et al. (2022). Discovery and systematic characterization of risk variants and genes for coronary artery disease in over a million participants. Nature Genet. *54*, 1803–1815. https://doi.org/10.1038/s41588-022-01233-6.

HGGA, Volume *5*

Supplemental information

MRBEE: A bias-corrected multivariable Mendelian randomization method

Noah Lorincz-Comi, Yihe Yang, Gen Li, and Xiaofeng Zhu

Supplementary material 1 of MRBEE: simulation and data analysis

Noah Lorincz-Comi, Yihe Yang, Gen Li, Xiaofeng Zhu

Contents

1 Supplemental Multivariable Simulations

1.1 Simulation settings for MVMR analysis in the main body

We consider the following statistical model which has the same representation as Lin (2023):

$$\boldsymbol{U} = \mathbf{G}\boldsymbol{\gamma}_U + \boldsymbol{e}_U, \tag{1}$$

$$\boldsymbol{X}_k = \mathbf{G}\boldsymbol{\gamma}_{X_k} + 0.25\boldsymbol{U} + \boldsymbol{e}_{X_j}, \quad j = 1, ..., 4 \tag{2}$$

$$\boldsymbol{Y} = \sum_{k=1}^{4} \theta_j \boldsymbol{X}_k + \mathbf{G}\boldsymbol{\alpha} + \boldsymbol{U} + \boldsymbol{e}_Y. \tag{3}$$

To make $\gamma_{X_1}, ..., \gamma_{X_4}$ to have correlation, we generate it from the Gaussian-Uniform copula model:

$$\begin{pmatrix} z_{j1} \\ z_{j2} \\ z_{j3} \\ z_{j4} \end{pmatrix} \sim \mathcal{N}\left(\begin{pmatrix} 0 \\ 0 \\ 0 \\ 0 \end{pmatrix}, \begin{pmatrix} 1 & 0.5 & -0.5 & 0.5 \\ 0.5 & 1 & -0.5 & 0.5 \\ -0.5 & -0.5 & 1 & -0.5 \\ 0.5 & 0.5 & -0.5 & 1 \end{pmatrix} \right), \tag{4}$$

$$\gamma_{X_k,j} = \Phi(z_{jk}) \times 0.22, \tag{5}$$

where $\Phi(\cdot)$ is the CDF of standard normal distribution. In this simulation, we consider the compound symmetric structure with a correlation $\text{cor}(z_{jk}, z_{js}) = 0.5$ for all $k \neq s$. As for $\boldsymbol{\gamma}_u$, each element γ_{uj} are independently generated from

$$\gamma^*_{uj} \sim 0.3\text{Unif}(0, 0.1) + 0.7\delta \tag{6}$$

where δ is a point mass at zero. As for α, each element α_j are independently generated from

$$\alpha_j \sim 0.3\mathcal{N}(0.1, 0.2^2) + 0.7\delta \tag{7}$$

where δ is a point mass at zero. The next part is fixing the heritability, which is achieved by

$$\sigma_e^2 = \frac{\text{var}(\mathbf{G}\boldsymbol{\gamma}_{X_k})}{h^2} - 1, \tag{8}$$

where $h^2 = 0.1$ in this simulation. Finally, the random error is generated from

$$\begin{pmatrix} \boldsymbol{e}_U \\ \boldsymbol{e}_{X_1} \\ \boldsymbol{e}_{X_2} \\ \boldsymbol{e}_{X_3} \\ \boldsymbol{e}_{X_4} \\ \boldsymbol{e}_Y \end{pmatrix} \sim \mathcal{N}\left(\begin{pmatrix} 0 \\ 0 \\ 0 \\ 0 \\ 0 \\ 0 \end{pmatrix}, \sigma_e^2 \begin{pmatrix} 1 & 0.5 & 0.5 & -0.5 & 0.5 & 0.5 \\ 0.5 & 1 & 0.5 & -0.5 & 0.5 & 0.5 \\ 0.5 & 0.5 & 1 & -0.5 & 0.5 & 0.5 \\ -0.5 & -0.5 & -0.5 & 1 & -0.5 & -0.5 \\ 0.5 & 0.5 & 0.5 & -0.5 & 1 & 0.6 \\ 0.5 & 0.5 & 0.5 & -0.5 & 0.5 & 1 \end{pmatrix} \right) \tag{9}$$

In Lin (2023), they did not consider the correlations among $\{\gamma_{X_k}\}$ and the error terms, and did not fix the heritability. These are two major adjustments me made.

1.2 Root Mean Square Error

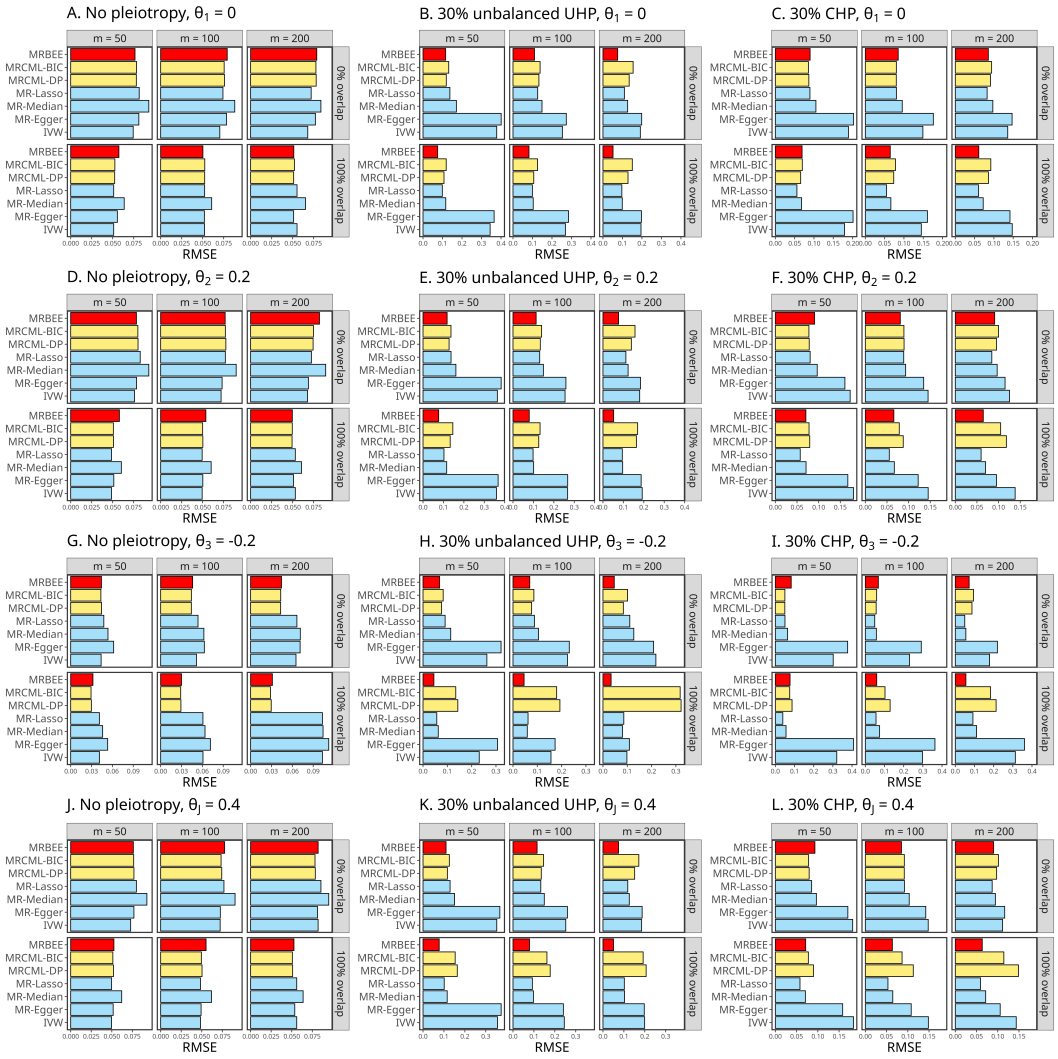

Figure S1: Barplot of the square-root of mean square error (RMSE). Panel A - L displays the barplots of the values of RMSE from seven methods in the MVMR simulation. The four rows represent the four causal effects θ_j, $j = 1, 2, 3, 4$. Each column corresponds to one of the three scenarios. The x-axis indicates the value of RMSE, while the y-axis lists the seven methods.

1.3 Standard Error Evaluation

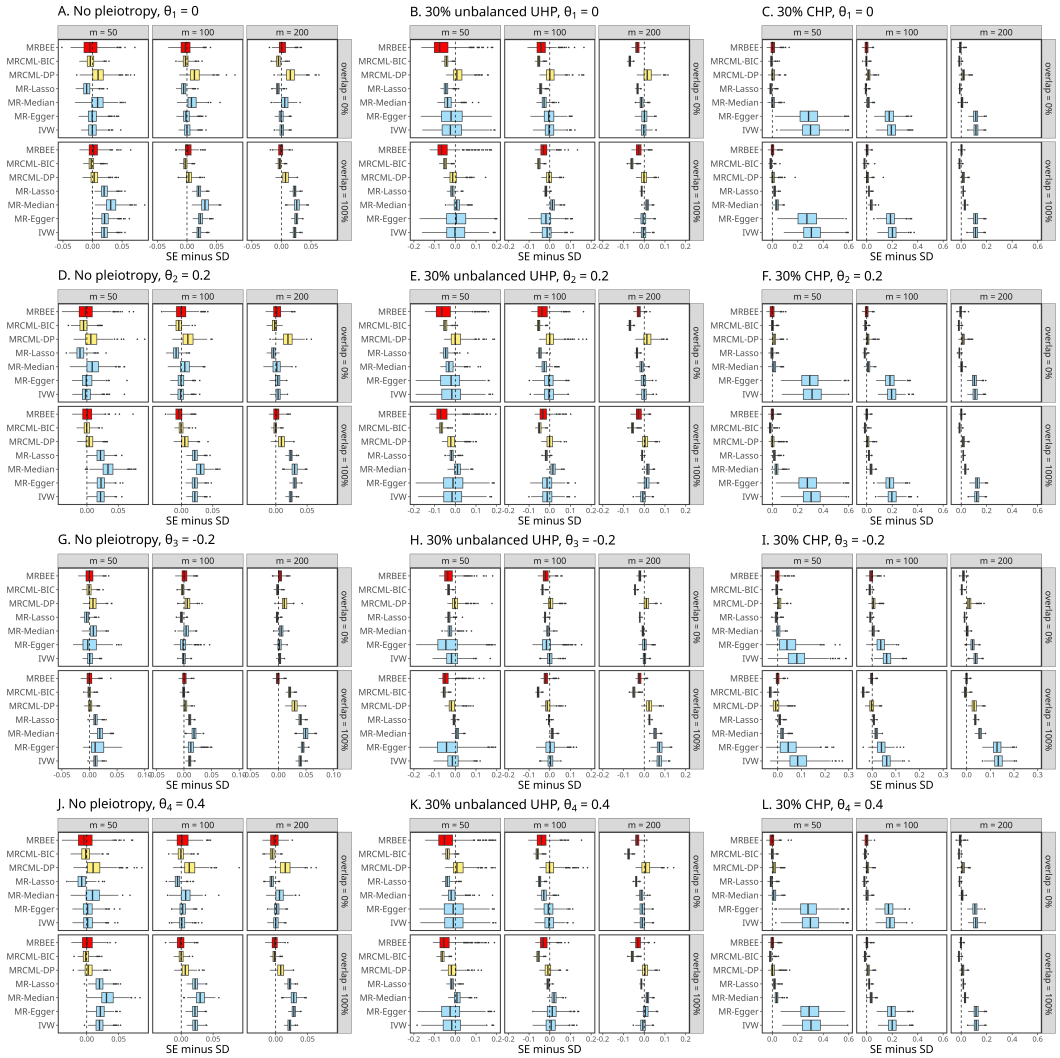

Figure S2: Boxplot of SE minus SD. Panel A - L displays the boxplots of the values of SE minus SD from seven methods in the MVMR simulation. The four rows represent the four causal effects θ_j, $j = 1, 2, 3, 4$. Each column corresponds to one of the three scenarios. The x-axis indicates the value of SE minus SD, while the y-axis lists the seven methods. If SE is correctly estimated, the mean of SE minus SD should be close to zero, which is indicated by a dashed line.

1.4 Coverage Frequency

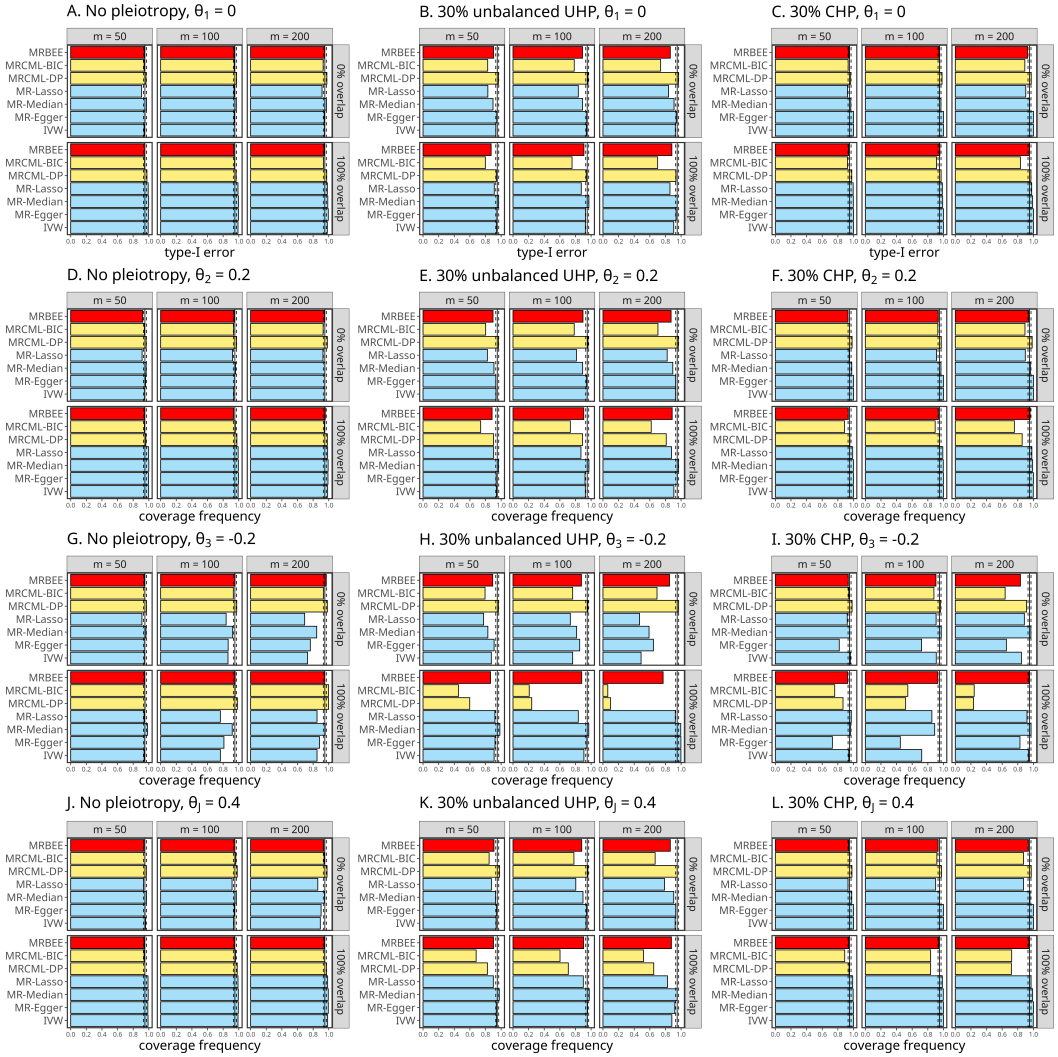

Figure S3: Boxplot of the coverage frequency. Panel A - L displays the boxplots of the values of coverage frequency from seven methods in the MVMR simulation. The four rows represent the four causal effects θ_j, $j = 1, 2, 3, 4$. Each column corresponds to one of the three scenarios. The x-axis indicates the coverage frequency, while the y-axis lists the seven methods. If SE is correctly estimated, the mean of coverage frequency should be around 95

1.5 Summary Table

Table S1. 0% sample overlap, theta1=0, number of IVs = 50

Scenario	Method	Bias	SD	SE	CovFreq	RJF
no pleiotropy	IVW	0.003	0.074	0.075	0.940	0.060
	MR-Egger	0.003	0.081	0.082	0.952	0.048
	MR-Median	0.001	0.093	0.102	0.970	0.030
	MR-Lasso	0.006	0.081	0.072	0.908	0.092
	MRCML-DP	0.002	0.078	0.089	0.964	0.036
	MRCML-BIC	0.003	0.078	0.075	0.940	0.060
	MRBEE	0.008	0.081	0.079	0.942	0.058
30% unbalanced UHP	IVW	0.096	0.366	0.351	0.932	0.068
	MR-Egger	0.058	0.397	0.381	0.944	0.056
	MR-Median	0.031	0.169	0.135	0.896	0.104
	MR-Lasso	0.021	0.136	0.093	0.830	0.170
	MRCML-DP	0.005	0.119	0.134	0.966	0.034
	MRCML-BIC	0.008	0.132	0.089	0.828	0.172
	MRBEE	0.004	0.204	0.146	0.904	0.096
30% CHP	IVW	0.094	0.165	0.479	1.000	0.000
	MR-Egger	-0.097	0.178	0.471	1.000	0.000
	MR-Median	0.011	0.105	0.112	0.966	0.034
	MR-Lasso	0.000	0.090	0.080	0.924	0.076
	MRCML-DP	-0.001	0.087	0.095	0.964	0.036
	MRCML-BIC	0.000	0.086	0.080	0.932	0.068
	MRBEE	0.005	0.080	0.087	0.940	0.060

Table S2. 100% sample overlap, theta1=0, number of IVs = 50

Scenario	Method	Bias	SD	SE	CovFreq	RJF
no pleiotropy	IVW	0.012	0.050	0.070	0.992	0.008
	MR-Egger	0.008	0.055	0.077	0.994	0.006
	MR-Median	0.012	0.063	0.095	0.998	0.002
	MR-Lasso	0.012	0.050	0.070	0.992	0.008
	MRCML-DP	0.002	0.052	0.056	0.976	0.024
	MRCML-BIC	0.003	0.053	0.051	0.946	0.054
	MRBEE	-0.002	0.051	0.054	0.950	0.050
30% unbalanced UHP	IVW	0.071	0.337	0.342	0.942	0.058
	MR-Egger	0.037	0.363	0.372	0.946	0.054
	MR-Median	0.020	0.115	0.124	0.968	0.032
	MR-Lasso	0.012	0.098	0.085	0.912	0.088
	MRCML-DP	-0.012	0.107	0.099	0.938	0.062
	MRCML-BIC	-0.013	0.118	0.069	0.798	0.202
	MRBEE	-0.004	0.152	0.100	0.872	0.128
30% CHP	IVW	0.099	0.150	0.470	1.000	0.000
	MR-Egger	-0.100	0.175	0.459	1.000	0.000
	MR-Median	0.016	0.066	0.103	0.998	0.002
	MR-Lasso	0.008	0.055	0.074	0.996	0.004
	MRCML-DP	-0.011	0.065	0.073	0.978	0.022
	MRCML-BIC	-0.005	0.070	0.059	0.924	0.076
	MRBEE	-0.005	0.057	0.061	0.938	0.062

Table S3. 0% sample overlap, theta2=0.2, number of IVs = 50

Scenario	Method	Bias	SD	SE	CovFreq	RJF
no pleiotropy	IVW	-0.011	0.075	0.075	0.946	0.724
	MR-Egger	-0.012	0.078	0.079	0.958	0.676
	MR-Median	-0.014	0.092	0.102	0.966	0.460
	MR-Lasso	-0.013	0.082	0.072	0.914	0.726
	MRCML-DP	-0.006	0.080	0.088	0.966	0.600
	MRCML-BIC	-0.006	0.080	0.075	0.944	0.748
	MRBEE	-0.005	0.078	0.077	0.922	0.718
30% unbalanced UHP	IVW	0.043	0.362	0.348	0.934	0.124
	MR-Egger	0.013	0.383	0.362	0.932	0.122
	MR-Median	-0.002	0.161	0.135	0.908	0.348
	MR-Lasso	-0.004	0.137	0.092	0.824	0.558
	MRCML-DP	-0.002	0.128	0.135	0.966	0.344
	MRCML-BIC	-0.001	0.137	0.089	0.802	0.582
	MRBEE	0.022	0.193	0.145	0.896	0.432
30% CHP	IVW	0.084	0.151	0.476	1.000	0.002
	MR-Egger	-0.036	0.157	0.462	1.000	0.002
	MR-Median	0.009	0.096	0.111	0.978	0.490
	MR-Lasso	0.002	0.080	0.079	0.946	0.730
	MRCML-DP	0.006	0.078	0.094	0.982	0.618
	MRCML-BIC	0.005	0.077	0.080	0.950	0.742
	MRBEE	0.005	0.087	0.088	0.930	0.660

Table S4. 100% sample overlap, theta2=0.2, number of IVs = 50

Scenario	Method	Bias	SD	SE	CovFreq	RJF
no pleiotropy	IVW	0.008	0.048	0.070	0.998	0.928
	MR-Egger	0.008	0.051	0.074	0.996	0.900
	MR-Median	0.006	0.060	0.094	1.000	0.638
	MR-Lasso	0.008	0.048	0.070	0.998	0.928
	MRCML-DP	-0.004	0.051	0.055	0.962	0.950
	MRCML-BIC	-0.002	0.051	0.051	0.944	0.964
	MRBEE	0.000	0.053	0.054	0.946	0.940
30% unbalanced UHP	IVW	0.069	0.353	0.342	0.940	0.138
	MR-Egger	0.044	0.365	0.357	0.936	0.118
	MR-Median	0.023	0.114	0.125	0.966	0.468
	MR-Lasso	0.010	0.102	0.085	0.904	0.682
	MRCML-DP	-0.063	0.118	0.101	0.902	0.364
	MRCML-BIC	-0.050	0.137	0.070	0.738	0.608
	MRBEE	-0.001	0.157	0.101	0.884	0.632
30% CHP	IVW	0.098	0.152	0.472	1.000	0.000
	MR-Egger	-0.026	0.166	0.454	1.000	0.000
	MR-Median	0.010	0.070	0.105	1.000	0.542
	MR-Lasso	0.003	0.057	0.075	0.990	0.828
	MRCML-DP	-0.039	0.069	0.075	0.954	0.626
	MRCML-BIC	-0.025	0.074	0.059	0.886	0.814
	MRBEE	-0.001	0.058	0.061	0.934	0.892

Table S5. 0% sample overlap, theta3=-0.2, number of IVs = 50

Scenario	Method	Bias	SD	SE	CovFreq	RJF
no pleiotropy	IVW	0.014	0.041	0.043	0.946	0.988
	MR-Egger	0.012	0.061	0.062	0.948	0.846
	MR-Median	0.014	0.052	0.059	0.964	0.904
	MR-Lasso	0.014	0.046	0.041	0.912	0.984
	MRCML-DP	0.002	0.044	0.051	0.970	0.984
	MRCML-BIC	-0.001	0.043	0.043	0.950	0.994
	MRBEE	0.001	0.044	0.044	0.942	0.990
30% unbalanced UHP	IVW	0.152	0.215	0.199	0.874	0.098
	MR-Egger	0.086	0.310	0.281	0.910	0.080
	MR-Median	0.054	0.101	0.076	0.830	0.568
	MR-Lasso	0.038	0.083	0.053	0.776	0.800
	MRCML-DP	0.005	0.076	0.077	0.966	0.718
	MRCML-BIC	0.000	0.083	0.051	0.794	0.918
	MRBEE	0.014	0.109	0.081	0.892	0.678
30% CHP	IVW	-0.249	0.171	0.254	0.960	0.352
	MR-Egger	-0.317	0.204	0.248	0.818	0.546
	MR-Median	-0.019	0.061	0.063	0.952	0.930
	MR-Lasso	0.001	0.050	0.045	0.920	0.972
	MRCML-DP	-0.008	0.049	0.055	0.982	0.978
	MRCML-BIC	-0.011	0.049	0.045	0.940	0.992
	MRBEE	-0.013	0.051	0.050	0.934	0.982

Table S6. 100% sample overlap, theta3=-0.2, number of IVs = 50

Scenario	Method	Bias	SD	SE	CovFreq	RJF
no pleiotropy	IVW	-0.030	0.029	0.040	0.940	1.000
	MR-Egger	-0.031	0.043	0.058	0.948	0.948
	MR-Median	-0.030	0.035	0.054	0.984	1.000
	MR-Lasso	-0.030	0.029	0.040	0.940	1.000
	MRCML-DP	0.002	0.030	0.031	0.952	1.000
	MRCML-BIC	-0.001	0.029	0.029	0.948	1.000
	MRBEE	0.004	0.030	0.031	0.946	0.998
30% unbalanced UHP	IVW	0.109	0.204	0.194	0.910	0.110
	MR-Egger	0.062	0.300	0.274	0.922	0.108
	MR-Median	-0.007	0.062	0.071	0.984	0.844
	MR-Lasso	-0.016	0.054	0.048	0.920	0.968
	MRCML-DP	0.117	0.082	0.067	0.598	0.342
	MRCML-BIC	0.097	0.094	0.041	0.454	0.664
	MRBEE	0.029	0.098	0.056	0.864	0.830
30% CHP	IVW	-0.276	0.162	0.250	0.940	0.476
	MR-Egger	-0.357	0.197	0.243	0.730	0.672
	MR-Median	-0.039	0.039	0.058	0.964	0.992
	MR-Lasso	-0.021	0.033	0.042	0.972	1.000
	MRCML-DP	0.064	0.060	0.055	0.866	0.690
	MRCML-BIC	0.039	0.064	0.034	0.760	0.896
	MRBEE	0.003	0.035	0.034	0.926	0.998

Table S7. 0% sample overlap, theta4=0.4, number of IVs = 50

Scenario	Method	Bias	SD	SE	CovFreq	RJF
no pleiotropy	IVW	-0.008	0.073	0.075	0.958	0.996
	MR-Egger	-0.009	0.076	0.079	0.952	0.996
	MR-Median	-0.004	0.093	0.103	0.970	0.970
	MR-Lasso	-0.008	0.080	0.072	0.932	0.994
	MRCML-DP	0.004	0.077	0.089	0.968	0.994
	MRCML-BIC	0.003	0.077	0.076	0.950	0.998
	MRBEE	-0.003	0.080	0.079	0.938	0.994
30% unbalanced UHP	IVW	0.021	0.352	0.349	0.936	0.236
	MR-Egger	-0.006	0.368	0.365	0.942	0.204
	MR-Median	-0.005	0.151	0.136	0.928	0.826
	MR-Lasso	-0.014	0.129	0.092	0.876	0.940
	MRCML-DP	0.004	0.117	0.136	0.980	0.868
	MRCML-BIC	0.006	0.126	0.089	0.846	0.968
	MRBEE	0.011	0.182	0.145	0.908	0.794
30% CHP	IVW	0.082	0.163	0.474	1.000	0.008
	MR-Egger	-0.035	0.167	0.460	1.000	0.004
	MR-Median	0.002	0.097	0.111	0.978	0.962
	MR-Lasso	-0.001	0.085	0.079	0.930	0.994
	MRCML-DP	0.005	0.079	0.095	0.980	0.986
	MRCML-BIC	0.006	0.078	0.079	0.952	0.998
	MRBEE	0.000	0.088	0.087	0.938	0.978

Table S8. 100% sample overlap, theta4=0.4, number of IVs = 50

Scenario	Method	Bias	SD	SE	CovFreq	RJF
no pleiotropy	IVW	0.010	0.049	0.069	0.990	1.000
	MR-Egger	0.009	0.051	0.073	0.988	1.000
	MR-Median	0.011	0.061	0.094	0.992	1.000
	MR-Lasso	0.010	0.049	0.069	0.990	1.000
	MRCML-DP	-0.004	0.052	0.055	0.950	1.000
	MRCML-BIC	-0.001	0.051	0.050	0.940	1.000
	MRBEE	-0.002	0.052	0.053	0.940	1.000
30% unbalanced UHP	IVW	0.046	0.354	0.341	0.942	0.242
	MR-Egger	0.026	0.373	0.354	0.938	0.242
	MR-Median	0.013	0.115	0.126	0.976	0.922
	MR-Lasso	0.014	0.101	0.085	0.900	0.982
	MRCML-DP	-0.113	0.119	0.105	0.824	0.742
	MRCML-BIC	-0.079	0.132	0.070	0.680	0.906
	MRBEE	-0.001	0.142	0.099	0.902	0.900
30% CHP	IVW	0.097	0.157	0.473	1.000	0.018
	MR-Egger	-0.029	0.156	0.455	1.000	0.000
	MR-Median	0.015	0.069	0.104	0.996	0.994
	MR-Lasso	0.011	0.057	0.075	0.990	1.000
	MRCML-DP	-0.052	0.073	0.080	0.944	0.962
	MRCML-BIC	-0.024	0.074	0.060	0.888	0.986
	MRBEE	0.000	0.059	0.060	0.938	0.998

Table S9. 0% sample overlap, theta1=0, number of IVs = 100

Scenario	Method	Bias	SD	SE	CovFreq	RJF
no pleiotropy	IVW	-0.003	0.070	0.071	0.948	0.052
	MR-Egger	0.001	0.078	0.078	0.942	0.058
	MR-Median	-0.005	0.088	0.097	0.968	0.032
	MR-Lasso	-0.003	0.074	0.069	0.940	0.060
	MRCML-DP	-0.006	0.076	0.090	0.972	0.028
	MRCML-BIC	-0.004	0.076	0.074	0.942	0.058
	MRBEE	-0.003	0.079	0.077	0.940	0.060
30% unbalanced UHP	IVW	0.061	0.246	0.246	0.940	0.060
	MR-Egger	0.032	0.272	0.270	0.944	0.056
	MR-Median	0.012	0.148	0.122	0.890	0.110
	MR-Lasso	0.007	0.127	0.083	0.836	0.164
	MRCML-DP	0.005	0.133	0.139	0.960	0.040
	MRCML-BIC	0.013	0.139	0.086	0.784	0.216
	MRBEE	0.009	0.175	0.135	0.890	0.110
30% CHP	IVW	0.082	0.125	0.322	1.000	0.000
	MR-Egger	-0.104	0.143	0.323	1.000	0.000
	MR-Median	0.013	0.095	0.107	0.968	0.032
	MR-Lasso	0.007	0.080	0.074	0.952	0.048
	MRCML-DP	0.000	0.080	0.097	0.982	0.018
	MRCML-BIC	0.003	0.080	0.078	0.952	0.048
	MRBEE	0.017	0.086	0.085	0.944	0.056

Table S10. 100% sample overlap, theta1=0, number of IVs = 100

Scenario	Method	Bias	SD	SE	CovFreq	RJF
no pleiotropy	IVW	0.022	0.047	0.067	0.990	0.010
	MR-Egger	0.012	0.051	0.074	0.996	0.004
	MR-Median	0.019	0.058	0.088	0.996	0.004
	MR-Lasso	0.023	0.047	0.067	0.990	0.010
	MRCML-DP	0.001	0.052	0.056	0.966	0.034
	MRCML-BIC	0.004	0.052	0.050	0.946	0.054
	MRBEE	-0.002	0.050	0.052	0.938	0.062
30% unbalanced UHP	IVW	0.088	0.254	0.241	0.926	0.074
	MR-Egger	0.044	0.282	0.264	0.928	0.072
	MR-Median	0.032	0.099	0.113	0.972	0.028
	MR-Lasso	0.024	0.097	0.078	0.874	0.126
	MRCML-DP	-0.032	0.102	0.099	0.938	0.062
	MRCML-BIC	-0.033	0.122	0.070	0.756	0.244
	MRBEE	0.000	0.117	0.091	0.908	0.092
30% CHP	IVW	0.097	0.108	0.311	1.000	0.000
	MR-Egger	-0.105	0.122	0.310	1.000	0.000
	MR-Median	0.022	0.062	0.098	0.990	0.010
	MR-Lasso	0.016	0.053	0.071	0.986	0.014
	MRCML-DP	-0.026	0.069	0.076	0.970	0.030
	MRCML-BIC	-0.020	0.076	0.059	0.912	0.088
	MRBEE	0.000	0.054	0.058	0.954	0.046

Table S11. 0% sample overlap, theta2=0.2, number of IVs = 100

Scenario	Method	Bias	SD	SE	CovFreq	RJF
no pleiotropy	IVW	-0.008	0.072	0.071	0.936	0.784
	MR-Egger	-0.006	0.073	0.073	0.948	0.764
	MR-Median	-0.006	0.090	0.096	0.958	0.540
	MR-Lasso	-0.009	0.077	0.069	0.920	0.784
	MRCML-DP	0.001	0.078	0.089	0.972	0.662
	MRCML-BIC	0.003	0.077	0.073	0.934	0.794
	MRBEE	-0.001	0.077	0.077	0.940	0.734
30% unbalanced UHP	IVW	0.049	0.250	0.248	0.950	0.178
	MR-Egger	0.028	0.258	0.254	0.942	0.134
	MR-Median	0.012	0.149	0.123	0.892	0.434
	MR-Lasso	0.007	0.131	0.084	0.812	0.648
	MRCML-DP	0.016	0.133	0.137	0.960	0.376
	MRCML-BIC	0.018	0.139	0.086	0.784	0.656
	MRBEE	0.031	0.166	0.135	0.896	0.436
30% CHP	IVW	0.073	0.125	0.323	1.000	0.000
	MR-Egger	-0.022	0.133	0.316	1.000	0.000
	MR-Median	0.007	0.093	0.107	0.968	0.504
	MR-Lasso	0.000	0.089	0.074	0.912	0.736
	MRCML-DP	0.010	0.089	0.097	0.972	0.600
	MRCML-BIC	0.012	0.088	0.078	0.928	0.756
	MRBEE	0.005	0.084	0.084	0.934	0.686

Table S12. 100% sample overlap, theta2=0.2, number of IVs = 100

Scenario	Method	Bias	SD	SE	CovFreq	RJF
no pleiotropy	IVW	0.019	0.046	0.068	0.992	0.970
	MR-Egger	0.016	0.048	0.069	0.996	0.952
	MR-Median	0.018	0.057	0.088	0.994	0.770
	MR-Lasso	0.019	0.046	0.068	0.992	0.970
	MRCML-DP	-0.002	0.050	0.056	0.976	0.950
	MRCML-BIC	0.000	0.050	0.050	0.956	0.980
	MRBEE	-0.001	0.056	0.052	0.934	0.950
30% unbalanced UHP	IVW	0.088	0.253	0.242	0.926	0.244
	MR-Egger	0.065	0.260	0.248	0.922	0.202
	MR-Median	0.031	0.096	0.113	0.972	0.536
	MR-Lasso	0.023	0.096	0.079	0.870	0.758
	MRCML-DP	-0.079	0.098	0.099	0.890	0.258
	MRCML-BIC	-0.059	0.119	0.070	0.734	0.518
	MRBEE	0.007	0.120	0.090	0.906	0.662
30% CHP	IVW	0.092	0.112	0.312	1.000	0.006
	MR-Egger	-0.008	0.122	0.303	1.000	0.002
	MR-Median	0.022	0.063	0.097	0.998	0.706
	MR-Lasso	0.016	0.053	0.071	0.992	0.920
	MRCML-DP	-0.054	0.069	0.077	0.950	0.506
	MRCML-BIC	-0.030	0.073	0.059	0.894	0.774
	MRBEE	0.000	0.057	0.057	0.936	0.928

Table S13. 0% sample overlap, theta3=-0.2, number of IVs = 100

Scenario	Method	Bias	SD	SE	CovFreq	RJF
no pleiotropy	IVW	0.032	0.040	0.040	0.862	0.986
	MR-Egger	0.035	0.052	0.051	0.864	0.890
	MR-Median	0.034	0.052	0.056	0.922	0.852
	MR-Lasso	0.032	0.043	0.039	0.838	0.984
	MRCML-DP	0.003	0.044	0.051	0.974	0.988
	MRCML-BIC	0.002	0.044	0.042	0.930	1.000
	MRBEE	-0.002	0.043	0.045	0.952	0.994
30% unbalanced UHP	IVW	0.174	0.141	0.141	0.764	0.062
	MR-Egger	0.132	0.190	0.179	0.854	0.072
	MR-Median	0.070	0.078	0.070	0.814	0.476
	MR-Lasso	0.054	0.070	0.048	0.734	0.782
	MRCML-DP	-0.011	0.076	0.081	0.958	0.754
	MRCML-BIC	-0.016	0.085	0.050	0.764	0.926
	MRBEE	0.024	0.095	0.076	0.876	0.646
30% CHP	IVW	-0.203	0.109	0.172	0.908	0.760
	MR-Egger	-0.260	0.133	0.170	0.720	0.834
	MR-Median	-0.016	0.055	0.060	0.972	0.958
	MR-Lasso	0.004	0.049	0.041	0.906	0.990
	MRCML-DP	-0.024	0.051	0.058	0.964	0.984
	MRCML-BIC	-0.024	0.054	0.044	0.878	0.998
	MRBEE	-0.028	0.056	0.052	0.904	0.990

Table S14. 100% sample overlap, theta3=-0.2, number of IVs = 100

Scenario	Method	Bias	SD	SE	CovFreq	RJF
no pleiotropy	IVW	-0.054	0.028	0.038	0.764	1.000
	MR-Egger	-0.062	0.036	0.049	0.810	0.996
	MR-Median	-0.054	0.034	0.052	0.916	1.000
	MR-Lasso	-0.054	0.028	0.038	0.764	1.000
	MRCML-DP	0.004	0.029	0.031	0.982	1.000
	MRCML-BIC	0.000	0.029	0.028	0.954	1.000
	MRBEE	0.006	0.030	0.031	0.954	1.000
30% unbalanced UHP	IVW	0.081	0.134	0.136	0.908	0.138
	MR-Egger	0.034	0.170	0.173	0.946	0.180
	MR-Median	-0.027	0.052	0.065	0.970	0.956
	MR-Lasso	-0.039	0.049	0.044	0.836	0.994
	MRCML-DP	0.177	0.077	0.068	0.240	0.134
	MRCML-BIC	0.151	0.097	0.041	0.208	0.488
	MRBEE	0.029	0.069	0.052	0.880	0.828
30% CHP	IVW	-0.278	0.109	0.169	0.722	0.934
	MR-Egger	-0.340	0.127	0.166	0.448	0.948
	MR-Median	-0.063	0.039	0.056	0.888	1.000
	MR-Lasso	-0.045	0.033	0.040	0.852	1.000
	MRCML-DP	0.115	0.059	0.058	0.516	0.376
	MRCML-BIC	0.073	0.072	0.034	0.544	0.792
	MRBEE	0.006	0.036	0.034	0.928	0.996

Table S15. 0% sample overlap, theta4=0.4, number of IVs = 100

Scenario	Method	Bias	SD	SE	CovFreq	RJF
no pleiotropy	IVW	-0.021	0.069	0.071	0.934	0.998
	MR-Egger	-0.019	0.070	0.073	0.942	1.000
	MR-Median	-0.023	0.088	0.095	0.968	0.984
	MR-Lasso	-0.021	0.074	0.068	0.914	1.000
	MRCML-DP	0.001	0.074	0.088	0.980	0.996
	MRCML-BIC	0.000	0.074	0.073	0.962	1.000
	MRBEE	0.005	0.075	0.078	0.950	0.998
30% unbalanced UHP	IVW	0.039	0.250	0.248	0.936	0.434
	MR-Egger	0.021	0.260	0.255	0.942	0.404
	MR-Median	-0.003	0.150	0.123	0.896	0.856
	MR-Lasso	-0.014	0.132	0.084	0.804	0.954
	MRCML-DP	0.015	0.135	0.138	0.958	0.840
	MRCML-BIC	0.014	0.146	0.086	0.780	0.956
	MRBEE	0.017	0.172	0.136	0.880	0.814
30% CHP	IVW	0.063	0.134	0.321	1.000	0.122
	MR-Egger	-0.030	0.139	0.314	1.000	0.056
	MR-Median	0.001	0.103	0.107	0.950	0.954
	MR-Lasso	-0.009	0.092	0.074	0.900	0.990
	MRCML-DP	0.014	0.091	0.097	0.974	0.986
	MRCML-BIC	0.013	0.091	0.078	0.916	0.996
	MRBEE	0.007	0.086	0.085	0.932	0.998

Table S16. 100% sample overlap, theta4=0.4, number of IVs = 100

Scenario	Method	Bias	SD	SE	CovFreq	RJF
no pleiotropy	IVW	0.018	0.045	0.067	0.990	1.000
	MR-Egger	0.014	0.047	0.069	0.994	1.000
	MR-Median	0.022	0.058	0.088	0.994	1.000
	MR-Lasso	0.018	0.045	0.067	0.990	1.000
	MRCML-DP	-0.008	0.050	0.056	0.980	1.000
	MRCML-BIC	-0.003	0.049	0.049	0.958	1.000
	MRBEE	-0.002	0.053	0.052	0.946	1.000
30% unbalanced UHP	IVW	0.067	0.236	0.243	0.952	0.514
	MR-Egger	0.044	0.237	0.249	0.954	0.432
	MR-Median	0.031	0.093	0.114	0.976	0.978
	MR-Lasso	0.031	0.087	0.079	0.900	0.998
	MRCML-DP	-0.140	0.109	0.102	0.708	0.710
	MRCML-BIC	-0.103	0.126	0.071	0.602	0.878
	MRBEE	-0.009	0.118	0.091	0.904	0.944
30% CHP	IVW	0.100	0.109	0.311	1.000	0.192
	MR-Egger	-0.002	0.108	0.303	1.000	0.052
	MR-Median	0.019	0.062	0.097	0.998	0.998
	MR-Lasso	0.015	0.051	0.071	0.986	1.000
	MRCML-DP	-0.090	0.068	0.080	0.836	0.964
	MRCML-BIC	-0.047	0.073	0.059	0.836	0.996
	MRBEE	-0.007	0.055	0.057	0.938	1.000

Table S17. 0% sample overlap, theta1=0, number of IVs = 200

Scenario	Method	Bias	SD	SE	CovFreq	RJF
no pleiotropy	IVW	0.005	0.068	0.069	0.946	0.054
	MR-Egger	0.010	0.076	0.076	0.942	0.058
	MR-Median	0.003	0.084	0.090	0.970	0.030
	MR-Lasso	0.005	0.072	0.066	0.914	0.086
	MRCML-DP	-0.002	0.078	0.094	0.976	0.024
	MRCML-BIC	0.003	0.078	0.073	0.928	0.072
	MRBEE	0.002	0.076	0.078	0.948	0.052
30% unbalanced UHP	IVW	0.070	0.179	0.176	0.926	0.074
	MR-Egger	0.043	0.194	0.195	0.938	0.062
	MR-Median	0.027	0.124	0.111	0.910	0.090
	MR-Lasso	0.013	0.109	0.078	0.840	0.160
	MRCML-DP	0.005	0.135	0.153	0.966	0.034
	MRCML-BIC	0.010	0.154	0.085	0.738	0.262
	MRBEE	0.010	0.140	0.107	0.862	0.138
30% CHP	IVW	0.085	0.106	0.222	1.000	0.000
	MR-Egger	-0.092	0.115	0.229	1.000	0.000
	MR-Median	0.027	0.094	0.100	0.952	0.048
	MR-Lasso	0.015	0.081	0.070	0.902	0.098
	MRCML-DP	0.009	0.091	0.107	0.972	0.028
	MRCML-BIC	0.014	0.093	0.079	0.890	0.110
	MRBEE	0.003	0.089	0.083	0.926	0.074

Table S18. 100% sample overlap, theta1=0, number of IVs = 200

Scenario	Method	Bias	SD	SE	CovFreq	RJF
no pleiotropy	IVW	0.036	0.042	0.065	0.982	0.018
	MR-Egger	0.022	0.046	0.072	0.994	0.006
	MR-Median	0.036	0.055	0.081	0.988	0.012
	MR-Lasso	0.036	0.042	0.065	0.982	0.018
	MRCML-DP	-0.003	0.051	0.058	0.974	0.026
	MRCML-BIC	-0.001	0.052	0.049	0.932	0.068
	MRBEE	-0.001	0.051	0.053	0.940	0.060
30% unbalanced UHP	IVW	0.098	0.169	0.165	0.906	0.094
	MR-Egger	0.064	0.187	0.183	0.936	0.064
	MR-Median	0.047	0.087	0.101	0.950	0.050
	MR-Lasso	0.046	0.085	0.073	0.858	0.142
	MRCML-DP	-0.064	0.112	0.112	0.934	0.066
	MRCML-BIC	-0.067	0.135	0.076	0.700	0.300
	MRBEE	-0.001	0.120	0.095	0.882	0.118
30% CHP	IVW	0.108	0.100	0.213	1.000	0.000
	MR-Egger	-0.096	0.104	0.218	1.000	0.000
	MR-Median	0.036	0.063	0.091	0.990	0.010
	MR-Lasso	0.030	0.052	0.068	0.978	0.022
	MRCML-DP	-0.050	0.070	0.087	0.968	0.032
	MRCML-BIC	-0.049	0.078	0.065	0.834	0.166
	MRBEE	0.000	0.057	0.059	0.948	0.052

Table S19. 0% sample overlap, theta2=0.2, number of IVs = 200

Scenario	Method	Bias	SD	SE	CovFreq	RJF
no pleiotropy	IVW	-0.020	0.065	0.069	0.950	0.744
	MR-Egger	-0.018	0.067	0.070	0.950	0.748
	MR-Median	-0.018	0.088	0.089	0.950	0.524
	MR-Lasso	-0.019	0.070	0.066	0.926	0.764
	MRCML-DP	0.001	0.074	0.094	0.982	0.592
	MRCML-BIC	0.002	0.075	0.073	0.928	0.794
	MRBEE	0.000	0.076	0.078	0.946	0.742
30% unbalanced UHP	IVW	0.037	0.176	0.176	0.930	0.266
	MR-Egger	0.027	0.182	0.179	0.930	0.248
	MR-Median	-0.005	0.123	0.111	0.894	0.432
	MR-Lasso	-0.005	0.112	0.077	0.822	0.656
	MRCML-DP	0.030	0.136	0.152	0.964	0.326
	MRCML-BIC	0.034	0.153	0.085	0.704	0.656
	MRBEE	0.005	0.133	0.108	0.872	0.462
30% CHP	IVW	0.056	0.112	0.222	1.000	0.046
	MR-Egger	-0.008	0.115	0.220	1.000	0.014
	MR-Median	0.002	0.097	0.101	0.964	0.542
	MR-Lasso	-0.002	0.084	0.070	0.896	0.768
	MRCML-DP	0.024	0.092	0.108	0.984	0.586
	MRCML-BIC	0.026	0.097	0.079	0.892	0.774
	MRBEE	0.015	0.087	0.083	0.938	0.740

Table S20. 100% sample overlap, theta2=0.2, number of IVs = 200

Scenario	Method	Bias	SD	SE	CovFreq	RJF
no pleiotropy	IVW	0.034	0.041	0.065	0.986	0.998
	MR-Egger	0.030	0.041	0.072	0.990	0.988
	MR-Median	0.033	0.051	0.081	0.992	0.936
	MR-Lasso	0.034	0.041	0.065	0.986	0.998
	MRCML-DP	-0.005	0.049	0.058	0.982	0.940
	MRCML-BIC	0.000	0.050	0.049	0.944	0.980
	MRBEE	0.000	0.052	0.053	0.956	0.956
30% unbalanced UHP	IVW	0.087	0.172	0.165	0.908	0.414
	MR-Egger	0.075	0.171	0.183	0.952	0.326
	MR-Median	0.049	0.084	0.101	0.966	0.742
	MR-Lasso	0.045	0.083	0.073	0.878	0.882
	MRCML-DP	-0.125	0.107	0.112	0.810	0.108
	MRCML-BIC	-0.108	0.132	0.076	0.618	0.388
	MRBEE	-0.005	0.121	0.096	0.886	0.534
30% CHP	IVW	0.104	0.091	0.213	0.998	0.112
	MR-Egger	0.028	0.091	0.218	1.000	0.016
	MR-Median	0.037	0.059	0.091	0.990	0.830
	MR-Lasso	0.029	0.052	0.068	0.980	0.976
	MRCML-DP	-0.095	0.070	0.087	0.856	0.190
	MRCML-BIC	-0.071	0.077	0.065	0.756	0.520
	MRBEE	-0.003	0.058	0.060	0.958	0.916

Table S21. 0% sample overlap, theta3=-0.2, number of IVs = 200

Scenario	Method	Bias	SD	SE	CovFreq	RJF
no pleiotropy	IVW	0.054	0.036	0.039	0.728	0.972
	MR-Egger	0.057	0.043	0.045	0.764	0.886
	MR-Median	0.053	0.048	0.053	0.846	0.814
	MR-Lasso	0.054	0.040	0.037	0.692	0.970
	MRCML-DP	0.000	0.043	0.055	0.982	0.980
	MRCML-BIC	-0.003	0.043	0.042	0.932	0.998
	MRBEE	0.001	0.042	0.045	0.968	0.994
30% unbalanced UHP	IVW	0.195	0.098	0.099	0.488	0.048
	MR-Egger	0.175	0.113	0.115	0.646	0.052
	MR-Median	0.106	0.070	0.063	0.590	0.356
	MR-Lasso	0.090	0.065	0.044	0.468	0.648
	MRCML-DP	-0.028	0.079	0.091	0.968	0.740
	MRCML-BIC	-0.039	0.093	0.049	0.692	0.952
	MRBEE	-0.020	0.083	0.062	0.852	0.890
30% CHP	IVW	-0.159	0.082	0.120	0.846	0.962
	MR-Egger	-0.199	0.094	0.119	0.654	0.980
	MR-Median	-0.008	0.055	0.057	0.968	0.958
	MR-Lasso	0.013	0.048	0.039	0.884	0.990
	MRCML-DP	-0.066	0.057	0.069	0.912	0.996
	MRCML-BIC	-0.069	0.065	0.044	0.638	1.000
	MRBEE	-0.027	0.062	0.049	0.834	0.978

Table S22. 100% sample overlap, theta3=-0.2, number of IVs = 200

Scenario	Method	Bias	SD	SE	CovFreq	RJF
no pleiotropy	IVW	-0.100	0.025	0.065	0.850	1.000
	MR-Egger	-0.109	0.028	0.072	0.882	1.000
	MR-Median	-0.099	0.032	0.081	0.954	1.000
	MR-Lasso	-0.100	0.025	0.065	0.850	1.000
	MRCML-DP	0.007	0.029	0.058	0.998	0.990
	MRCML-BIC	0.001	0.029	0.049	0.998	0.996
	MRBEE	0.006	0.033	0.032	0.948	1.000
30% unbalanced UHP	IVW	0.033	0.093	0.165	0.998	0.058
	MR-Egger	0.010	0.108	0.183	0.998	0.072
	MR-Median	-0.064	0.049	0.101	0.996	0.894
	MR-Lasso	-0.071	0.048	0.073	0.926	0.996
	MRCML-DP	0.309	0.087	0.112	0.096	0.072
	MRCML-BIC	0.292	0.125	0.076	0.062	0.244
	MRBEE	0.063	0.079	0.057	0.770	0.658
30% CHP	IVW	-0.303	0.079	0.213	0.938	0.852
	MR-Egger	-0.350	0.088	0.218	0.828	0.908
	MR-Median	-0.105	0.035	0.091	0.970	1.000
	MR-Lasso	-0.087	0.031	0.068	0.918	1.000
	MRCML-DP	0.206	0.054	0.087	0.234	0.002
	MRCML-BIC	0.170	0.070	0.065	0.242	0.114
	MRBEE	0.009	0.037	0.037	0.944	0.996

Table S23. 0% sample overlap, theta4=0.4, number of IVs = 200

Scenario	Method	Bias	SD	SE	CovFreq	RJF
no pleiotropy	IVW	-0.046	0.068	0.069	0.892	0.998
	MR-Egger	-0.045	0.068	0.070	0.902	0.996
	MR-Median	-0.045	0.084	0.090	0.946	0.986
	MR-Lasso	-0.046	0.072	0.066	0.860	0.998
	MRCML-DP	-0.006	0.078	0.094	0.978	0.996
	MRCML-BIC	-0.004	0.078	0.073	0.940	0.998
	MRBEE	-0.003	0.080	0.078	0.936	1.000
30% unbalanced UHP	IVW	0.011	0.185	0.176	0.924	0.638
	MR-Egger	0.002	0.188	0.178	0.932	0.620
	MR-Median	-0.018	0.125	0.111	0.906	0.898
	MR-Lasso	-0.025	0.116	0.077	0.788	0.972
	MRCML-DP	0.053	0.142	0.152	0.950	0.858
	MRCML-BIC	0.062	0.160	0.085	0.668	0.974
	MRBEE	0.008	0.141	0.107	0.862	0.912
30% CHP	IVW	0.029	0.108	0.222	1.000	0.476
	MR-Egger	-0.033	0.112	0.219	1.000	0.278
	MR-Median	-0.020	0.092	0.100	0.956	0.968
	MR-Lasso	-0.027	0.083	0.070	0.874	0.996
	MRCML-DP	0.032	0.092	0.108	0.972	0.984
	MRCML-BIC	0.035	0.096	0.079	0.874	1.000
	MRBEE	0.012	0.091	0.083	0.936	0.998

Table S24. 100% sample overlap, theta4=0.4, number of IVs = 200

Scenario	Method	Bias	SD	SE	CovFreq	RJF
no pleiotropy	IVW	0.036	0.043	0.065	0.986	1.000
	MR-Egger	0.032	0.043	0.072	0.994	1.000
	MR-Median	0.037	0.052	0.081	0.994	1.000
	MR-Lasso	0.036	0.043	0.065	0.986	1.000
	MRCML-DP	-0.010	0.050	0.058	0.972	1.000
	MRCML-BIC	0.000	0.051	0.049	0.948	1.000
	MRBEE	-0.003	0.055	0.053	0.942	1.000
30% unbalanced UHP	IVW	0.102	0.171	0.165	0.882	0.852
	MR-Egger	0.090	0.176	0.183	0.920	0.774
	MR-Median	0.058	0.086	0.101	0.950	1.000
	MR-Lasso	0.054	0.087	0.073	0.826	1.000
	MRCML-DP	-0.177	0.107	0.112	0.650	0.538
	MRCML-BIC	-0.139	0.133	0.076	0.520	0.806
	MRBEE	0.012	0.125	0.096	0.876	0.952
30% CHP	IVW	0.108	0.095	0.213	0.998	0.812
	MR-Egger	0.034	0.100	0.218	1.000	0.532
	MR-Median	0.037	0.061	0.091	0.990	1.000
	MR-Lasso	0.030	0.051	0.068	0.970	1.000
	MRCML-DP	-0.129	0.074	0.087	0.718	0.886
	MRCML-BIC	-0.080	0.082	0.065	0.722	0.980
	MRBEE	-0.005	0.061	0.060	0.944	1.000

1.6 Replication of Lin et al

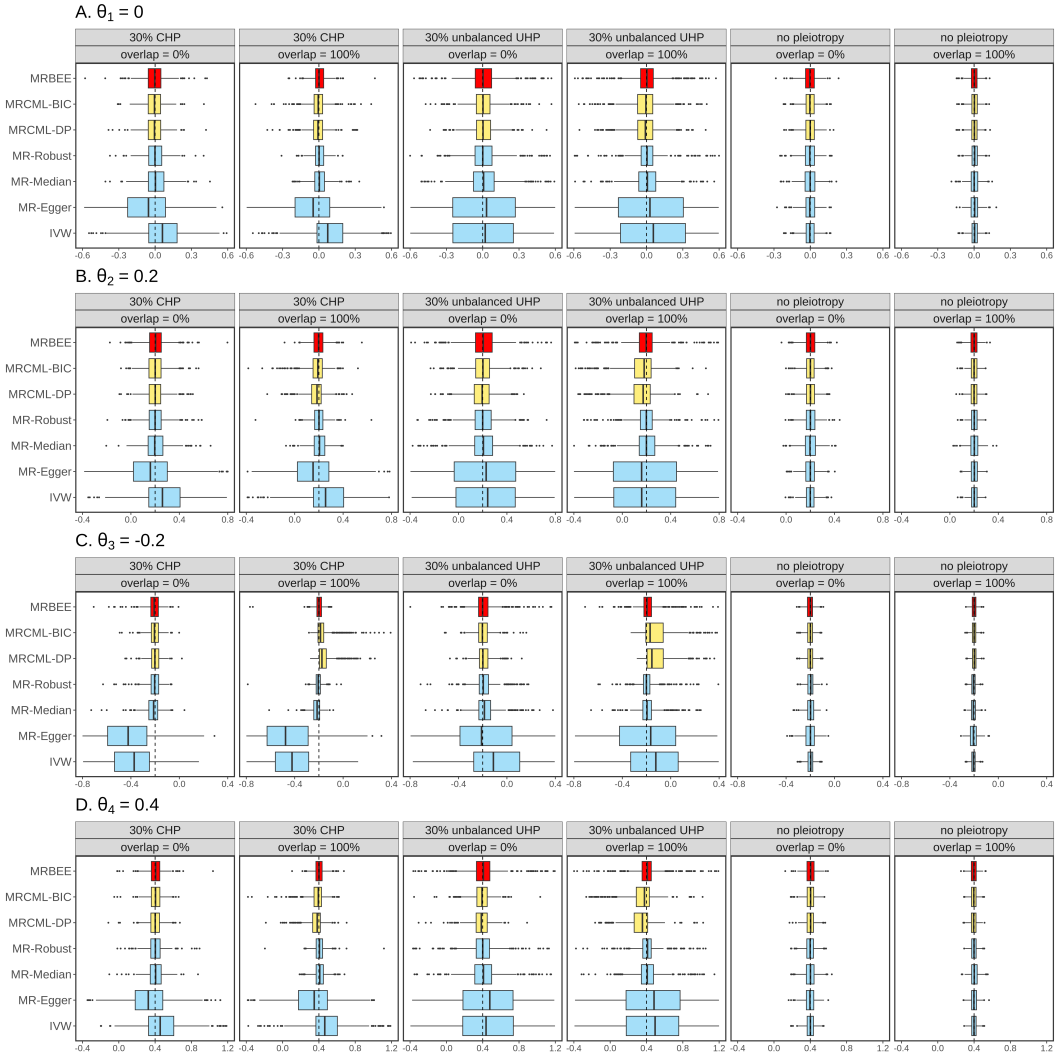

Figure S4: Estimation results of Lin et al. Panel A - L displays the boxplots of causal effect estimates from seven methods in the MVMR simulation. The four rows represent the four causal effects θ_j, $j = 1, 2, 3, 4$. Each column corresponds to one of the three scenarios. The x-axis indicates the value of the causal effect estimate, while the y-axis lists the seven methods. The true values of causal effects are denoted by dashed lines.

1.7 Replication of Wu et al

Table S25. Replication of the Table 1 in Wu et al. MRBEE represents the estimates with effect size standardization. MRBEE.Understandarized represents the estimates without effect size standardization. (see highlighted in yellow, the results were based on 500 replications).

		beta01=-0.5				beta02=-0.7				beta03=-0.3			
lambda/sqrt p	Estimator	Est	SD	SE	CP	EST	SD	SE	CP	EST	SD	SE	CP
35.6	IVW	-0.4011	0.0257	0.0265	0.0460	-0.6529	0.0200	0.0216	0.4020	0.3821	0.0274	0.0295	0.2200
	Egger	-0.4266	0.0353	0.0370	0.4920	-0.6526	0.0200	0.0208	0.3560	0.3847	0.0278	0.0305	0.2140
	Median	-0.4049	0.0350	0.0418	0.3600	-0.6474	0.0277	0.0358	0.7560	0.3797	0.0393	0.0446	0.6060
	GRAPPLE	-0.4957	0.0337	0.0346	0.9520	-0.6974	0.0243	0.0253	0.9600	0.3042	0.0367	0.0391	0.9680
	MRBEE	-0.5074	0.0393	0.0408	0.9740	-0.7024	0.0263	0.0272	0.9520	0.2941	0.0411	0.0447	0.9680
	MRBEE Unstandarized	-0.5581	0.0620	7.6143	1.0000	-0.7126	0.0424	3.0688	1.0000	0.2544	0.0629	7.0391	1.0000
	dIVW	-0.5049	0.0391	0.0390	0.9700	-0.7018	0.0261	0.0271	0.9640	0.2963	0.0411	0.0426	0.9720
	adIVW	-0.5049	0.0391	0.0390	0.9700	-0.7018	0.0261	0.0271	0.9640	0.2963	0.0411	0.0426	0.9720
11	IVW	-0.2890	0.0350	0.0359	0.0000	-0.5850	0.0290	0.0317	0.0520	0.4528	0.0401	0.0400	0.0380
	Egger	-0.3230	0.0529	0.0558	0.1200	-0.5861	0.0294	0.0326	0.0600	0.4544	0.0404	0.0442	0.0480
	Median	-0.2933	0.0504	0.0570	0.0440	-0.5733	0.0423	0.0569	0.3580	0.4474	0.0575	0.0596	0.3300
	GRAPPLE	-0.4828	0.0708	0.0694	0.9180	-0.6936	0.0437	0.0464	0.9560	0.3173	0.0793	0.0793	0.9480
	MRBEE	-0.5217	0.0996	0.1096	0.9560	-0.7090	0.0535	0.0597	0.9640	0.2829	0.1053	0.1161	0.9720
	MRBEE Unstandarized	-0.9042	2.6129	34.9001	1.0000	-0.8177	0.7338	10.6841	1.0000	-0.0506	2.5668	32.0195	1.0000
	dIVW	-0.5131	0.0973	0.0974	0.9320	-0.7055	0.0521	0.0560	0.9540	0.2903	0.1023	0.1036	0.9520
	adIVW	-0.5016	0.0798	0.0900	0.9320	-0.7012	0.0483	0.0545	0.9540	0.2974	0.0869	0.0949	0.9520
7.4	IVW	-0.2507	0.0396	0.0389	0.0000	-0.5502	0.0334	0.0359	0.0220	0.4571	0.0450	0.0436	0.0700
	Egger	-0.2806	0.0590	0.0623	0.0660	-0.5510	0.0334	0.0374	0.0300	0.4582	0.0451	0.0489	0.0840
	Median	-0.2616	0.0566	0.0597	0.0200	-0.5268	0.0515	0.0615	0.1640	0.4463	0.0645	0.0631	0.3640
	GRAPPLE	-0.4808	0.0927	0.0902	0.9380	-0.6889	0.0571	0.0582	0.9360	0.3128	0.1049	0.1036	0.9460
	MRBEE	-0.5566	0.1843	0.2033	0.9780	-0.7208	0.0837	0.0945	0.9600	0.2420	0.1965	0.2132	0.9760
	MRBEE Unstandarized	2.1489	80.3074	5037.7991	1.0000	0.2806	24.8002	1530.8156	1.0000	2.2589	64.7862	4079.5503	1.0000
	dIVW	-0.5442	0.1782	0.1613	0.9640	-0.7167	0.0810	0.0832	0.9580	0.2536	0.1899	0.1702	0.9520
	adIVW	-0.4895	0.0899	0.1136	0.9600	-0.6940	0.0586	0.0707	0.9560	0.2875	0.1075	0.1164	0.9440

1.8 Bias-correction terms: Correlation matrix estimation from insignificant GWAS statistics

We investigate the estimation error of $\hat{\mathbf{R}}_{W_\beta \times w_\alpha}$, i.e., the correlation version of covariance matrix $\hat{\mathbf{\Sigma}}_{W_\beta \times w_\alpha}$. We first examine if increasing M results in a decreasing estimation error. Besides, we consider studying the Frobenius norm rather than the ℓ_2 norm, as $||\mathbf{A}||_2 \leq ||\mathbf{A}||_{\mathrm{F}}$ and the calculation of the Frobenius norm is much less costly than the ℓ_2 norm. In comparison, we also consider the correlation matrix estimate directly yielded by the individual data, whose convergence rate is roughly $O(\min(\sqrt{n_1}, \sqrt{n_0}))$. The number of replications is 1000.

For this purpose, we set $M = 250, 500, \ldots, 2000$, $n_1 = n_0 = 2000, 20000$, and $n_o/n_0 = 0.5$. Figure S5 shows the investigation, from which we witness: (1), as M increases, the Frobenius norm of $\hat{\mathbf{R}}_{W_\beta \times w_\alpha}$ is reduced; (2) directly estimating $\hat{\mathbf{R}}_{W_\beta \times w_\alpha}$ from the individual data is always more precise than indirectly estimating it from insignificant GWAS statistics. In addition, although the estimation error of $\hat{\mathbf{R}}_{W_\beta \times w_\alpha}$ only depends on M, low sample sizes will introduce finite-sample bias into the estimation.

We then study if increasing n_1 and n_0 will influence the estimation error of $\hat{\mathbf{R}}_{W_\beta \times w_\alpha}$. For this purpose, we set $M = 250, 500, 1000$ and let n_1 and n_0 increase from 5000 to 40000 with a lag 5000. The number of replications is 1000. Figure S6 exhibits the results, from which we observe: increasing n_1 and n_0 cannot reduce estimation error of $\hat{\mathbf{R}}_{W_\beta \times w_\alpha}$. These results confirm our theory: the estimation error of $\hat{\mathbf{R}}_{W_\beta \times w_\alpha}$ only depends on M.

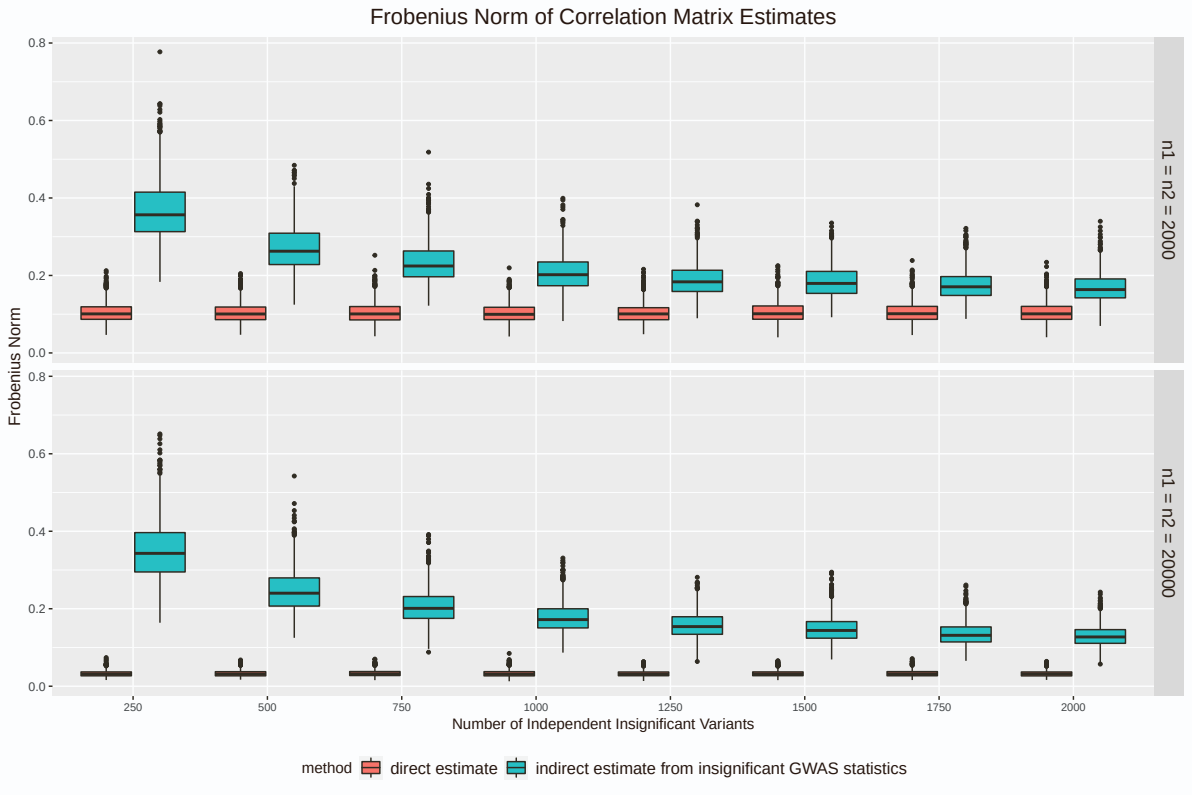

Figure S5: The Frobenius norms of correlation matrix esimates when M increases.

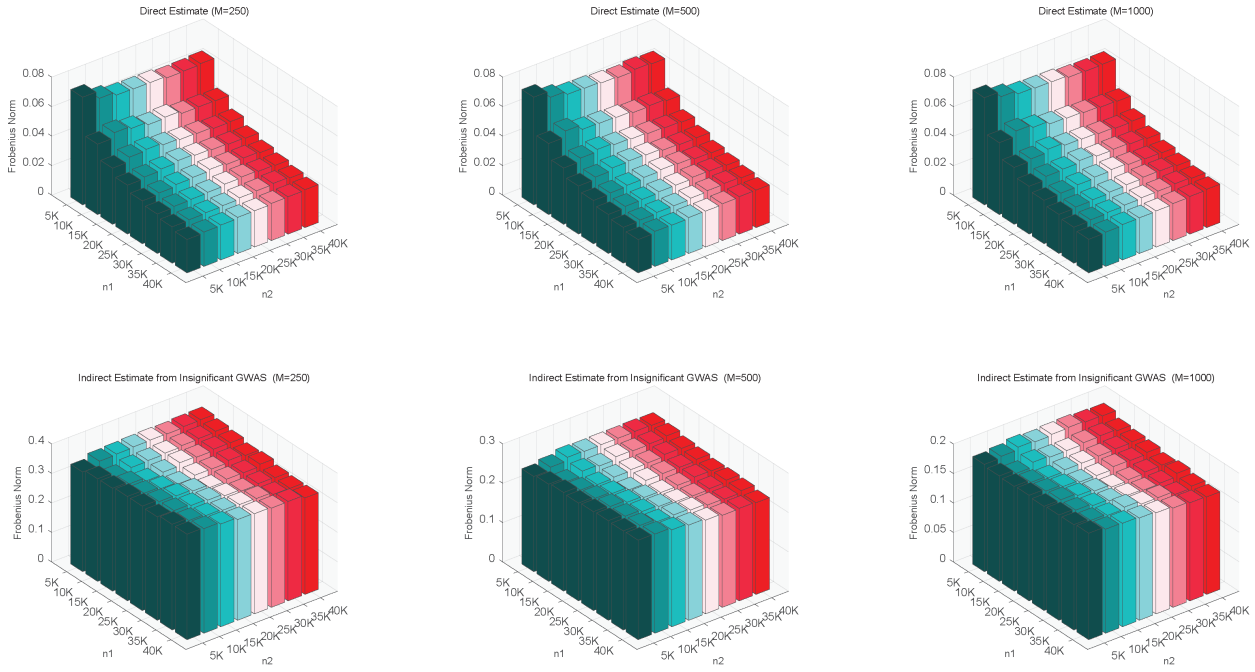

Figure S6: The Frobenius norms of correlation matrix estimates when n_0 and n_1 increase.

2 Supplemental Univariable Simulations

2.1 Overlapping Fraction

We briefly introduce the simulation settings for UVMR. First, we generate a binomial variable from $\text{Binom}(2, b_j)$ where $b_j \sim \text{Unif}(0.05, 0.5)$ and standardize it as g_{ij}, the direct effect β_j from $\mathcal{N}(0, 1/m)$, and u_i, v_i from a normal distribution with correlation coefficient 0.5. The variances of u_i and v_i are chosen such that the IV-heritabilities are $\sigma_{\beta\beta}/\sigma_{xx} = 0.3$ and $\theta^2 \times (\sigma_{\beta\beta}/\sigma_{yy}) = 0.15$, respectively. We specify the causal effect $\theta = 0.3/\sqrt{2}$. We compare MRBEE with IVW, DIVW, MR-RAPS, MR-Egger, MR-Lasso, MR-Median, IMRP, MR-Conmix, and MR-MiX, where most are implemented by using the R package `MendelianRandomization`. We fix $n_0 = n_1 = 20000$, specify n_{01} according to the overlapping fraction, and assume no UHP or CHP. The so-called overlapping fraction is n_{01}/n_0, where the special fraction such that $\text{E}(S_{\text{IVW}}(\theta)) = 0$ is $n_{01}/n_0 \approx 0.77$. The number of independent replications is 1000.

First, we study the influences of overlapping fraction n_{01}/n_0 and the number of IVs m, with the results displayed in Fig.S7. It is easy to see that only MRBEE is able to yield an unbiased estimate of θ in all cases. For a special overlapping fraction $n_{01}/n_0 \approx 0.77$, all approaches become unbiased except MR-RAPS and DIVW. These two methods perform badly because are based on no sample overlap assumption, which in turn add extra biases to the estimates as long as sample overlap exists. The SEs of causal effect estimates for all methods increases as the overlapping fraction decreases but remains unchanged by the increase of m, confirming that the convergence rates of causal estimates are mainly determined by $n_{\min}$.

As for the SE estimation, we display the boxplot of $\hat{\text{se}}(\hat{\theta}) - \text{se}(\hat{\theta})$ where $\text{se}(\hat{\theta})$ is approximated by the empirical SE calculated from the independent replications. It is evident that the SE estimates produced by all approaches have reduced variances as m grows. However, only MRBEE and DIVW can provide consistent SE estimates, confirming the accuracy of their SE formulas. MR-ConMix is extremely likely to underestimate the standard error, while MR-Egger, MR-Lasso, MR-Median, and MR-Mix constantly overestimate it. IVW underestimates the SE when the fraction is large and overestimates it when the fraction is small. In contrast, MR-RAPS seems to overestimate the SE unless the overlapping fraction is 0%.

The coverage frequency refers to the frequency that the confidence interval covers the true causal effect among simulations. Here, this confidence interval is constructed by doubling $\hat{\text{se}}(\hat{\theta})$, meaning that the coverage frequency corresponding to neither an inflated type-I error nor an inflated type-II error should be 0.95. We observed that only MRBEE enjoys a coverage frequency around 0.95. When $m = 250$, MR-Egger, MR-Lasso, and MR-Median suffer from inflated type-II errors, likely because these methods cannot estimate the SE properly. These approaches also result in inflated type-I errors caused by weak instrument bias as m increases. Additionally, because MR-Mix overestimates the SE, it consistently exhibits a substantially inflated type-II error. Furthermore, IMRP and MR-ConMix consistently have inflated type I errors because they frequently underestimate the SE.

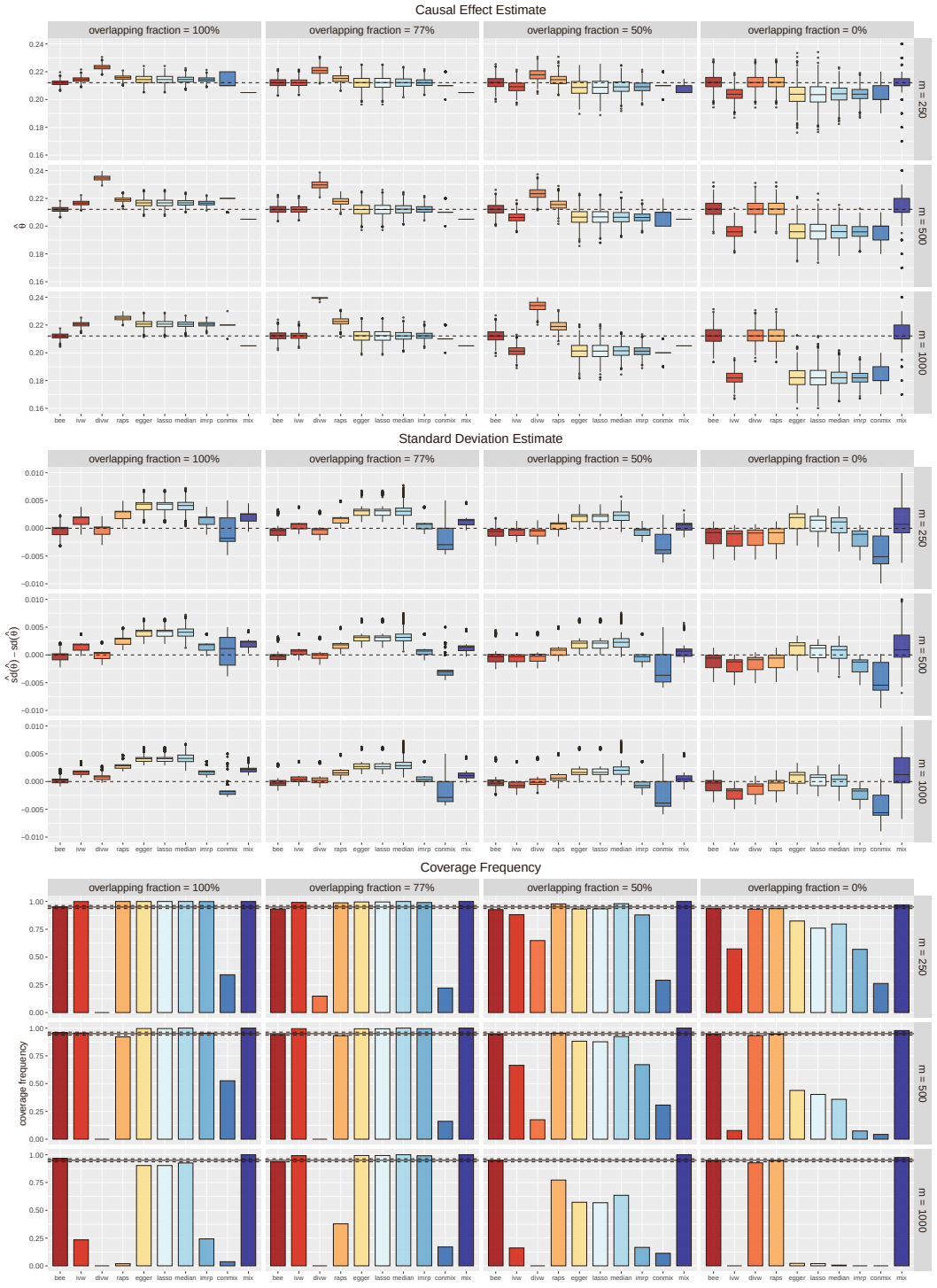

Figure S7: Investigation of UVMR approaches for univariable MR with sample sizes $n_0 = n_1 = 20000$, in terms of overlapping fraction and number of instrumental variants.

2.2 Sample size

In this section, we examine the influence of sample sizes. Here, we fix the number of variants $m = 500$ and consider $n_0 = n_1 = 20K$; $n_0 = 40K, n_1 = 20K$; $n_0 = 20K, n_1 = 40K$; and $n_0 = n_1 = 40K$ four cases. Recall that the overlapping fraction is defined as n_{01}/n_0, and 100%, 77%,50%, and 0% four cases will be studied. Other setting remains the same as the one shown in section 4.1 in the main paper.

Figure S8 displays the results of this examination. Preliminary, it illustrates neither increasing n_0 nor increasing n_1 along is able to make the causal effect estimate more accuracy. Besides, increasing the sample sizes of the exposure GWAS and the outcome GWAS has different impacts: the former decreases the measurement error bias, while the latter reduces the variance of all causal effect estimates. The reason is that the estimation error of $\hat{\alpha}_j$ will not cause estimation bias, in contrast, it is indeed the random error term of the multivariate MR model. Furthermore, only the MR-BEE is able to produce unbiased causal effect estimate and reliable SE estimate in all cases.

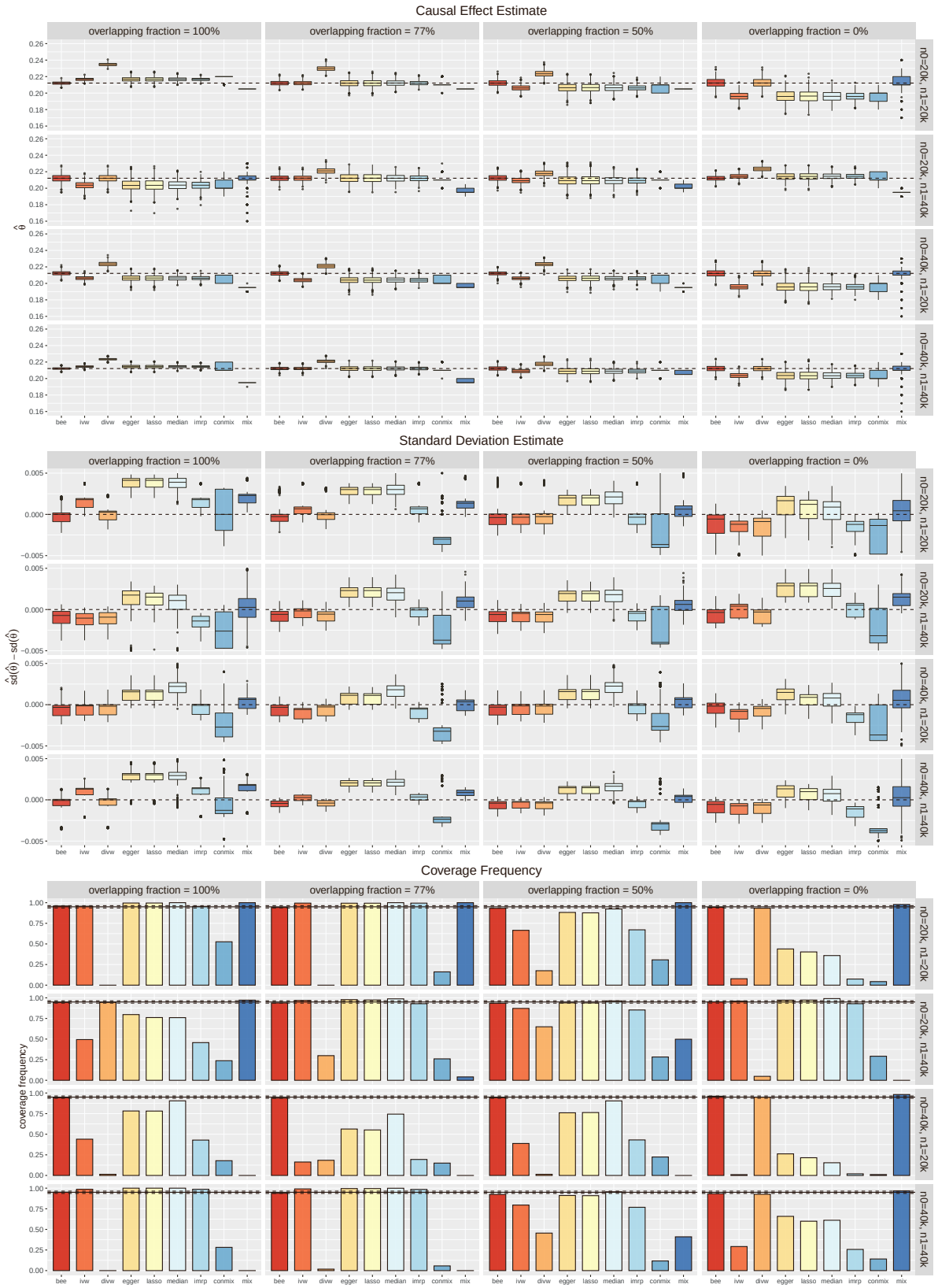

Figure S8: The investigation of univariate MR in terms of sample sizes.

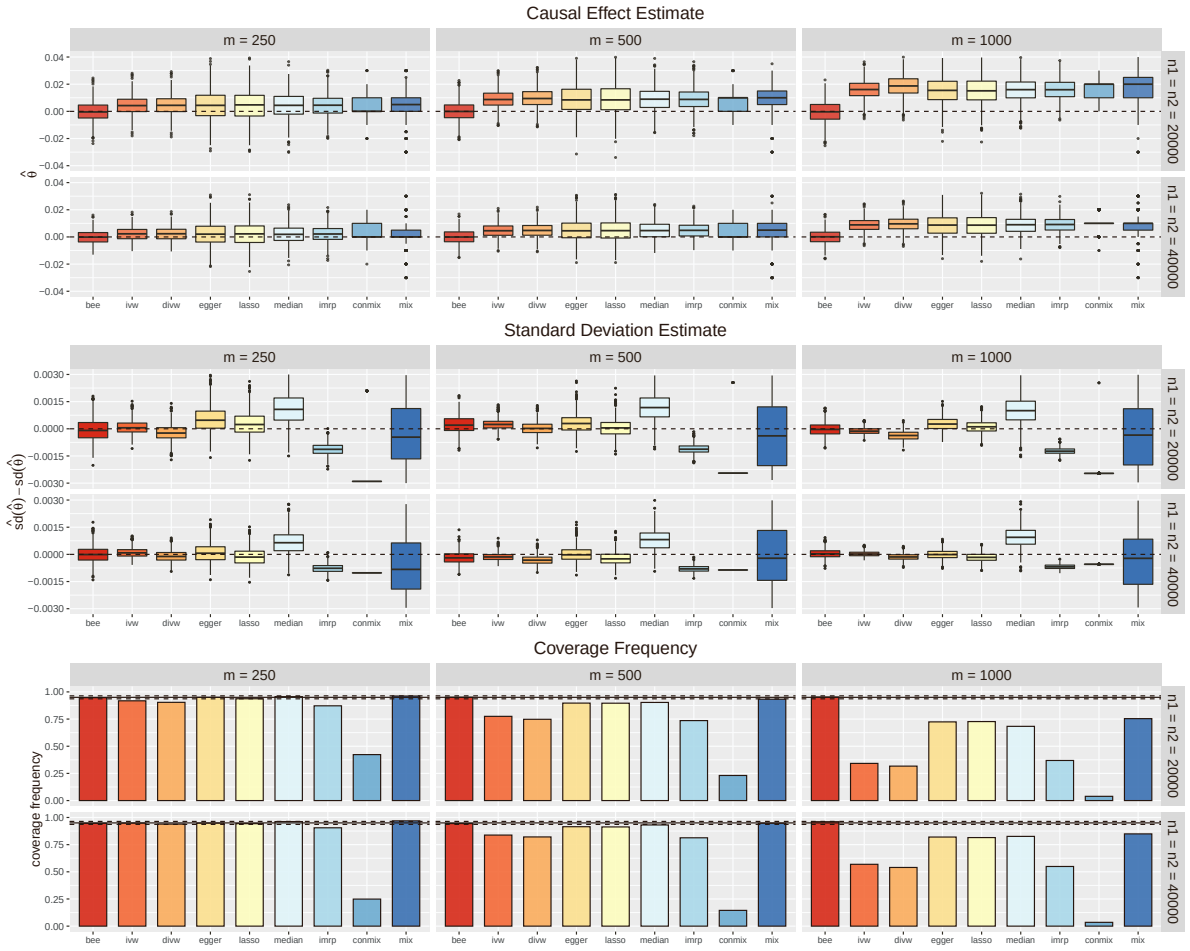

Figure S9: The investigation of univariate MR in terms of type-I error.

2.3 Type-I error

Now we turn to examine whether MRBEE and existing approaches produce inflated type-I error rates when UHP is present. Note that the UHP γ_{u_j} must exist otherwise the IV-heritability of outcome will be zero when $\theta = 0$. We independently generate γ_{u_j} from the same distribution as β_j. The simulation settings are: IV-heritability of exposure = 0.3, IV-heritability of outcome = 0.15, $n_{01}/n_0 = 0.5$, and the number of replications is 1000.

Figure S9 exhibits the results, from which some phenomena are consistently observed; e.g., increasing n_1 and n_0 simultaneously reduces the variances of all causal estimates, while increasing m increases weak instrument bias. Since $\theta = 0$ implies that only the confounder bias ($n_{01}/n_0\sigma_{uv}$) exists, all the weak instrument biases are upward. (The correlation coefficient between u_i and v_i is 0.5.) In addition, all the existing approaches incur inflated type-I errors as m rises. The result suggests that the weak instrument bias is likely to explain some significant causal relationships observed in the literature. However, using MRBEE can produce reliable causal inferences..

2.4 Winner's curse

In this section, we examine the impact winner's curse. We use the exactly same setting as the one in section 4.1. To simulate the winner's curse, we only use the variants with absolute t-statistics (i.e., $|\hat{\beta}/\text{se}(\hat{\beta})|$) larger than 1 or 2.

Figure S10 displays the results of this examination. It shows the winner's curse will not introduce a significant bias into MR-BEE as long as the overlapping fraction is not zero. As for other MR approaches that suffer from biases, we observed that the winner's curse will indeed slightly reduce the biases but inflate the variances. We believe that only selecting the significant variants will reduce the weak instrument bias somehow, because the weak instrument bias is determined by the ratio of signal-by-noise, i.e.,

$$\frac{\psi_{\beta\beta}}{m} \text{ v.s. } \sigma_{W_\beta W_\beta}, \tag{10}$$

where $\psi_{\beta\beta} = \sum_{j=1}^{m} \text{var}(\beta_j)$. If $\psi_{\beta\beta}/m$ is significantly larger than $\sigma_{W_\beta W_\beta}$, the bias of the IVW estimate should disappear due to the structure of "weak instrument bias x estimation error bias".

In addition, as the overlapping fraction decreases, the MR-BEE also encounters small bias especially when this fraction is zero. The reason for this problem is

$$\frac{1}{m}\sum_{j=1}^{m} \beta_j \omega_{\beta_j} \to 0, \quad \frac{1}{|\mathcal{W}|}\sum_{j\in\mathcal{W}} \beta_j \omega_{\beta_j} \not\to 0, \tag{11}$$

where $\mathcal{W}$ is the set of all "winners". In this case, extra selection bias arises but MR-BEE fails to account for it. Fortunately, such a bias is usually modest and it seems only existing when the overlapping fraction is 0. Increasing the sample size to identify more causal variants is one of the practical ways to resolve the winner's curse in this case.

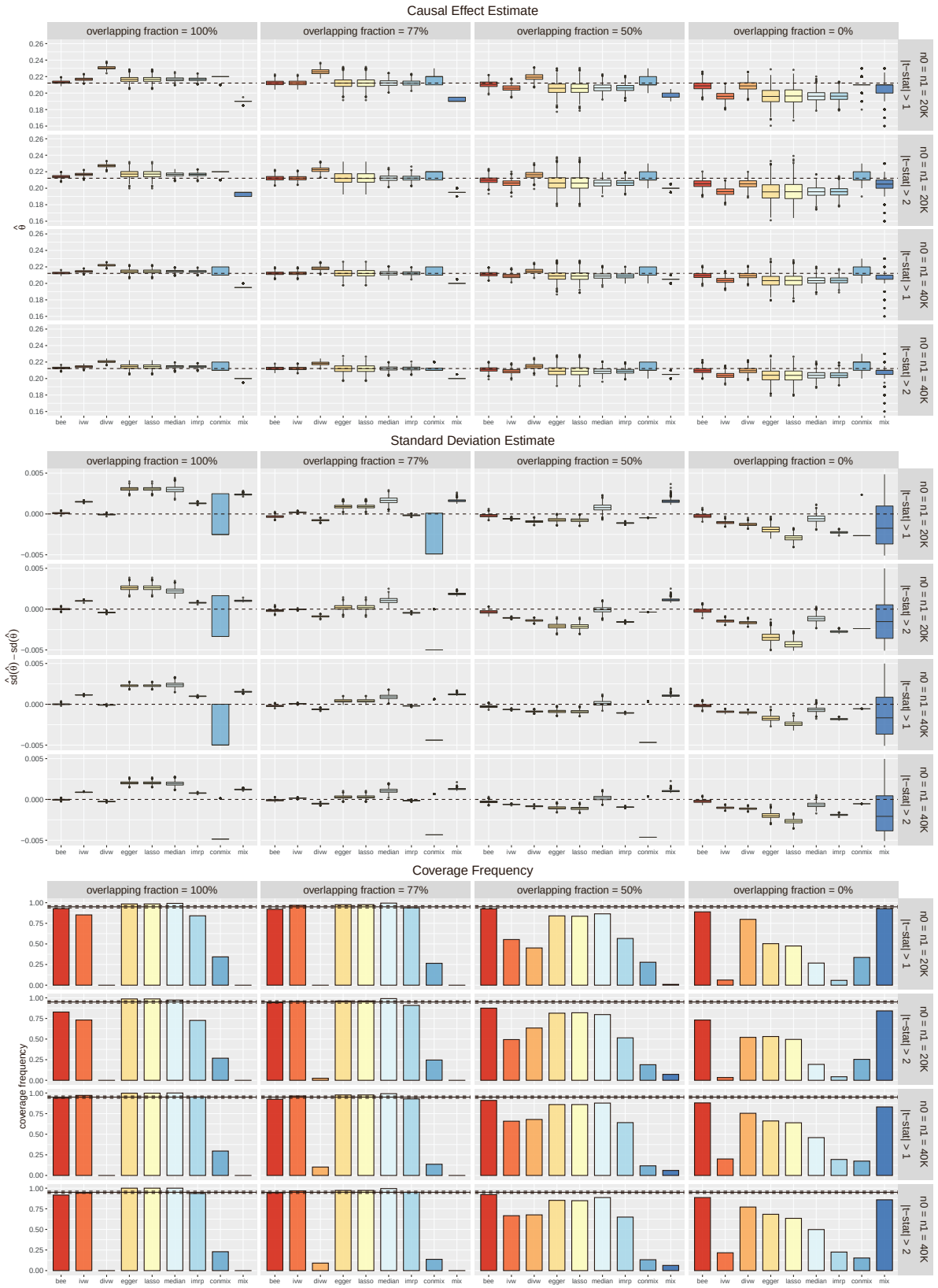

Figure S10: The investigation of univariate MR in terms of winner's curse.

2.5 Outlier test

In this section, we investigate if the MR-BEE with the IMRP pleiotropy test is able to remove the pleiotropy as resembling the outlier detection. The methods for comparsion include IMRP, MR-Lasso and MR-ConMix. Detailed setting of outliers can be found in the subsection of outlier detection setting. Here, we consider three criteria: estimation error of causal effect, true negative (TN) and true positive (TP). Here, the TN refers to the proportion of removing all outliers, while the TP refers to the proportion of not removing any valid IV. For IMRP and MR-BEE, we need to specify the threshold κ. For IMRP, we consider two thresholds: $\kappa = 0.05$ and $\kappa = 0.05/s$ where s is the number of real outliers. Regarding MR-BEE with IMRP, we not only consider this two thresholds but also consider two FDR control methods "BH" and "Sidak", where the thresholds in these two methods are 0.05. Details of the FDR control methods can be found in R package `FDRestimation`.

Figure S11 displays the results of outlier detection. As for estimation error, MR-BEE with threshold $\kappa = 0.05$ suffers from a small selection bias, because this estimator is supposed to remove many valid IVs because of false discovery. As for MR-BEE with other thresholds, they do not suffer from bias. As for other methods, they incur large bias introduced by the weak instrument bias and estimation error bias.

As for TN, the results show all methods are able to remove the true outliers. As for TP, however, only the MR-Lasso is able to keep all valid IVs. MR-BEE and IMRP with the oracle threshold (i.e., $\kappa = 0.05/s$) have large probabilities to keep every valid IV with the increasing of outlier fractions, but this probability is not 1. Other methods cannot keep valid IVs at all, although the causal effect estimates may not have biases. These results show that there exists a theoretical threshold $\kappa \asymp F_{\chi^2}(\log m)$ to distinguish the outliers and the valid IVs, but this threshold may be difficult to specify in practice. In contrast, the MR-Lasso seems to enjoy the oracle property thanks to the consistency of lasso-type regularizer (Fan, 2001).

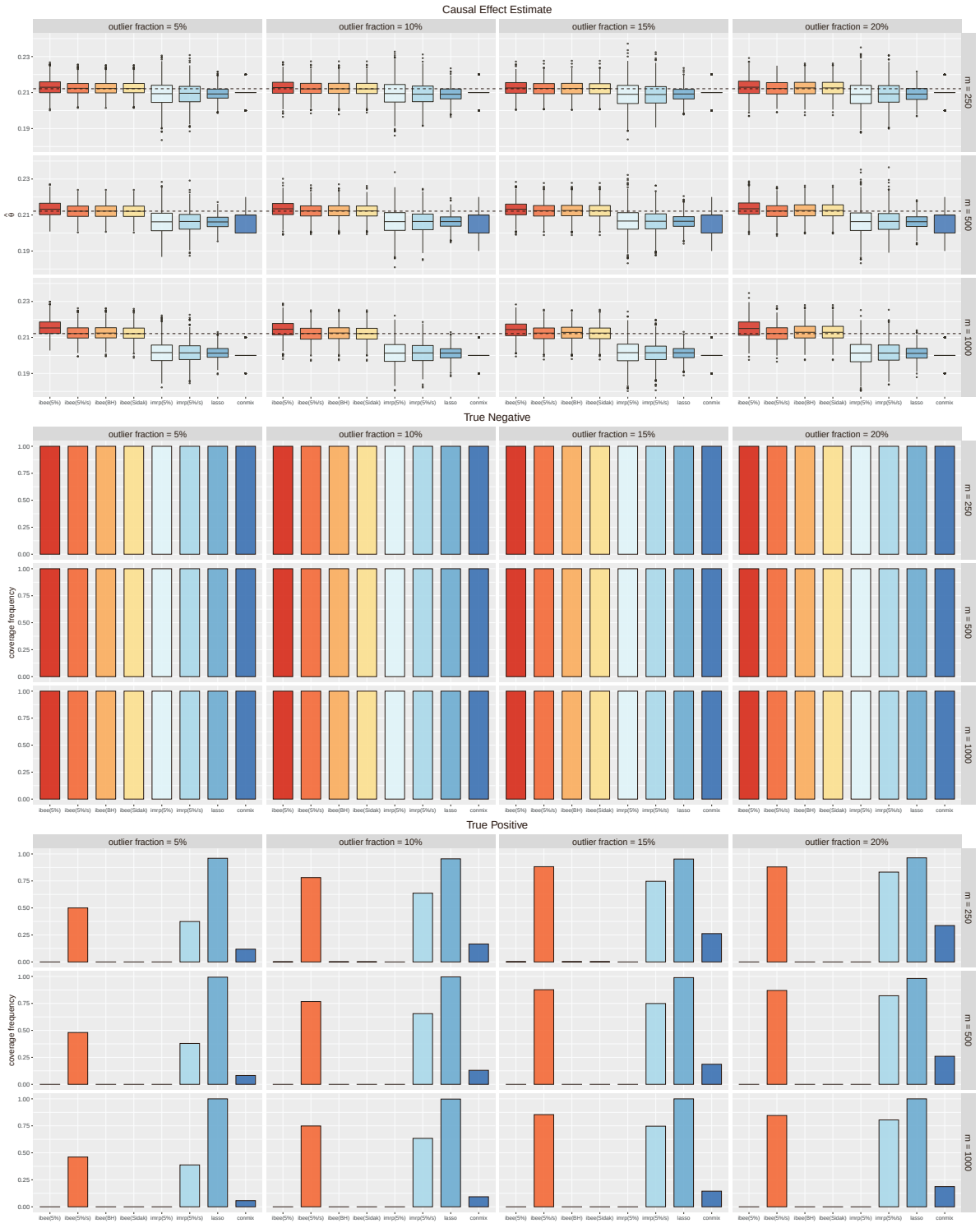

Figure S11: The investigation of univariate MR in terms of outlier detection.

2.6 Verification of Asymptotic Theroy

We next verify if the asymptotic normal distributions in Theorem 1.2 and Theorem 1.2 are correct. For a general estimate $\hat{\theta}$, the asymptotic bias and SE are $\sqrt{s}_n(\hat{\theta}-\theta)$ and $\sqrt{s}_n\text{se}(\hat{\theta})$, respectively, where $\sqrt{s}_n$ is the convergence rate of $\hat{\theta}$. If this estimate is strongly asymptotically unbiased, the asymptotic bias $s_n(\hat{\theta}-\theta)$ should also be 0. Besides, if two estimates have equal asymptotic SEs, they are equally powerful in terms of statistical efficiency. We select MR-BEE, IVW, MR-Median, and MR-Lasso to compare, only consider two overlapping fractions: 100% and 0%, set $n_0 = n_1 = n_{\min}$, and fix the causal effect $\theta = 0.5$. As for m and $n_{\min}$, we focus on the following four cases:

(1) $m = 2500, 5000, \ldots, 50000$ and $m^{0.9}/n = c_0 = 0.1$ and 0.2; we examine the direct bias: $\hat{\theta}-\theta$, asymptotic SE: $\sqrt{n_{\min}^2/m}\ \text{se}(\hat{\theta})$, and coverage frequency;

(2) $m = 250, 500, \ldots, 5000$ and $m/n = c_0 = 0.1$ and 0.2; we examine the direct bias: $\hat{\theta}-\theta$, asymptotic SE: $\sqrt{n}_{\min}\ \text{se}(\hat{\theta})$, and coverage frequency;

(3) $m = 250, 500, \ldots, 5000$ and $m^2/n = c_0 = 5$ and 10; we examine the asymptotic bias: $\sqrt{n}_{\min}(\hat{\theta}-\theta)$, asymptotic SE: $\sqrt{n}_{\min}\ \text{se}(\hat{\theta})$, and coverage frequency;

(4) $m = 250, 500, \ldots, 5000$ and $m^3/n = c_0 = 5$ and 10; we examine the asymptotic bias: $\sqrt{n}_{\min}(\hat{\theta}-\theta)$, asymptotic SE: $\sqrt{n}_{\min}\ \text{se}(\hat{\theta})$, and coverage frequency.

Note that we directly generate the estimation errors $\mathbf{W}_\beta$ and $\boldsymbol{w}_\alpha$ according to Theorem 1 because $n_{\min}$ in cases (3) and (4) can be larger than one million. %The calculations involving individual-data are extremely time-consuming in these cases.

Fig. S12 demonstrates the simulation results. In case (1), $\hat{\theta}_{\text{BEE}}$ is unbiased while the other three estimates suffer from non-removable biases. For the asymptotic SE, $\sqrt{n_{\min}^2/m}\ \text{se}(\hat{\theta}_{\text{BEE}})$ remains unchanged when $n_{\min}$ and m are sufficiently large (e.g., the bars colored in blue), verifying conclusion (iii) in Theorem 1.3. However, the coverage frequency of MR-BEE is a little larger than 0.95, meaning that the SE of $\hat{\theta}_{\text{BEE}}$ is overestimated in this extreme case. This phenomenon is reasonable because Theorem 1.4 points out that the convergence rate of the sandwich formula is $\min(\sqrt{n}_{\min}, n_{\min}/\sqrt{m}, \sqrt{m/\log m})$, which slows down as m increases. In case (2), the direct bias of $\hat{\theta}_{\text{IVW}}$ is unchanged as $n_{\min}$ tends to infinity, confirming conclusion (iii) in Theorem 1.2. As for $\hat{\theta}_{\text{BEE}}$, its asymptotic SE is a little larger than $\hat{\theta}_{\text{IVW}}$, verifying item (ii) in Theorem 1.3.

In case (3), the asymptotic bias of $\hat{\theta}_{\text{IVW}}$ is constant as $n_{\min}$ goes to infinity, illustrating that $\hat{\theta}_{\text{IVW}}$ is not strongly asymptotically unbiased. As a result, the coverage frequencies of $\hat{\theta}_{\text{IVW}}$ are significantly smaller than 0.95, confirming our claim that any inference made based on $\hat{\theta}_{\text{IVW}}$ is invalid. Besides, the asymptotic SEs of $\hat{\theta}_{\text{BEE}}$ and $\hat{\theta}_{\text{IVW}}$ are essentially the same, indicating that $\hat{\theta}_{\text{BEE}}$ and $\hat{\theta}_{\text{IVW}}$ are equally efficient as long as $m/n_{\min} \to 0$. In case (4), the asymptotic bias of IVW, MR-Median, and MR-Lasso vanish as $n_{\min}$ increases and their coverage frequencies are around 0.95, which is consistent with conclusion (i) in Theorem 1.2. The equal asymptotic SEs also indicate that $\hat{\theta}_{\text{BEE}}$ and $\hat{\theta}_{\text{IVW}}$ are equally efficient in this scenario. In addition, IVW, MR-Median, and MR-Lasso suffer from the same degree of bias when there is no pleiotropy, while MR-Median not only suffers from a large asymptotic SE but also is likely to overestimate it.

Figure S12: Investigations of MR-BEE and IVW in terms of asymptotic bias and covariance matrix.

2.7 Larger numbers of IVs

Here, we directly generate the GWAS summary data from the normal distribution using the following model:

$$\hat{\boldsymbol{\beta}}_j \sim \mathcal{N}(\mathbf{0}, \boldsymbol{\Sigma}_{\beta\beta} + \boldsymbol{\Sigma}_{W_\beta W_\beta}), \quad \hat{\alpha}_j \sim \mathcal{N}(\boldsymbol{\beta}_j^\top \boldsymbol{\theta}, \boldsymbol{\theta}^\top \boldsymbol{\Sigma}_{W_\beta W_\beta} \boldsymbol{\theta} + \sigma_{w_\alpha w_\alpha} + 2\boldsymbol{\theta}^\top \boldsymbol{\sigma}_{W_\beta w_\alpha}.)$$

This helps us to evaluate the performances of the existing methods in the cases of larger numbers of IVs.

For larger numbers of IVs, the degrees of the weak instruments are higher, MRBEE and MR.CUE are two methods consistently performing well in the no pleiotropy cases. This confirms our conjecture that the key to removing weak instrument bias is accounting for the covariance matrix of estimation errors—however, MR.CUE suffers from bias in the presence of pleiotropy. We believe this is due to the fact that MR.CUE only considers the UHP satisfying the InSide condition, which cannot address the unbalanced UHP. In addition, the univariable version of MRCML is generalized bias because it does not require the user to provide the correlation between exposure and outcome GWAS, which implies it does not account for the correlation between exposure and outcome GWAS estimation errors. In contrast, the multivariable version of MRCML requires us to provide it, and hence it is unbiased.

2.8 Additional pleiotropy simulation

We performed a univariable MR simulation to compare the performance of horizontal pleiotropy identification methods used by MRBEE and MRCML-BIC and their subsequent effects on their causal estimates. The simulation models and R code used to generate the simulated data are presented in Figure 15. In these simulations, we fixed the number of causal exposure SNPs at 100, the exposure heritability at 0.15, the true causal effect at 0.2, and the exposure and outcome GWAS sample sizes at 30k and non-overlapping and varied the mean of UHP from a value of 0 to a value of 0.1. For each UHP mean, we drew UHP effects for each SNP from a normal distribution with variance that was one fourth of the variance of the true SNP-outcome associations. We then estimated causal effects using MRBEE and MRCML-BIC. We then recorded the number of horizontally pleiotropic IVs that were identified by each method and the corresponding causal effect estimates after excluding them. These results indicate that the results of which isare presented below, which suggestreveals that MRBEE correctlyonsistently unbiasedly estimateds the causal effects and identified a stableconstant proportion of UHP IVs regardless of the UHP mean, whereas the BIC method of MVMR-cML MRCML-BIC identifieds UHP IVs at different rates as the UHP mean changeds, thus affecting the its subsequent causal effect estimate. In this simulation, the causal estimate was based on observed values of $\hat{\beta}_X$ and $\hat{\beta}_Y$, the observed SNP-exposure and SNP-outcome associations, respectively, and both methods were adjusted for GWAS estimation error.

3 Real Data Analysis

3.1 Myopia data: heritability, genetic correlation matrix, and estimation error correlation matrix

3.2 SCZ data: heritability, genetic correlation matrix, and estimation error correlation matrix

3.3 CAD data: heritability, genetic correlation matrix, and estimation error correlation matrix

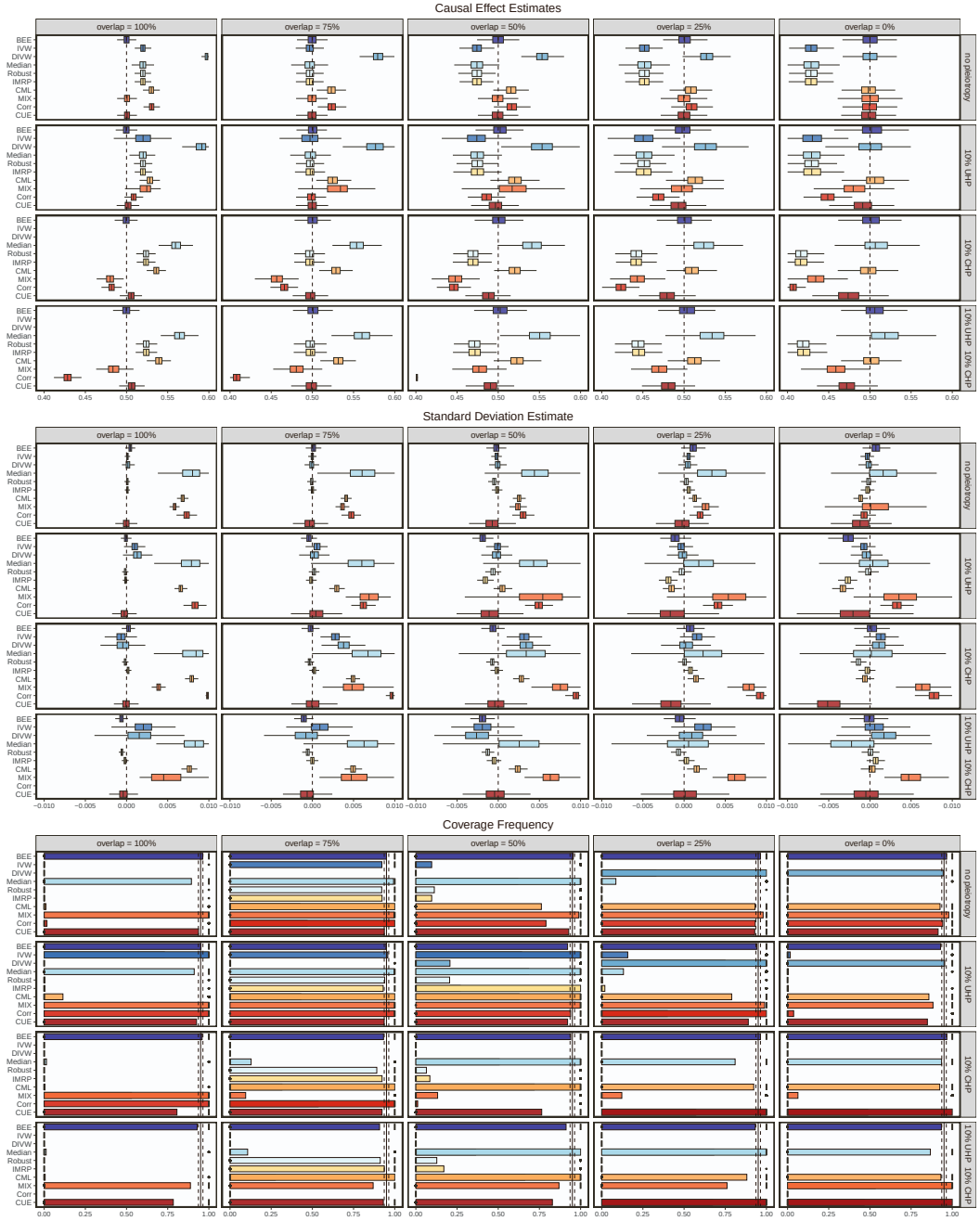

Figure S13: Investigation of UVMR approaches for UVMR model with sample sizes $n_0 = \cdots = n_6 = 20000$ and number of IVs $m = 1000$.

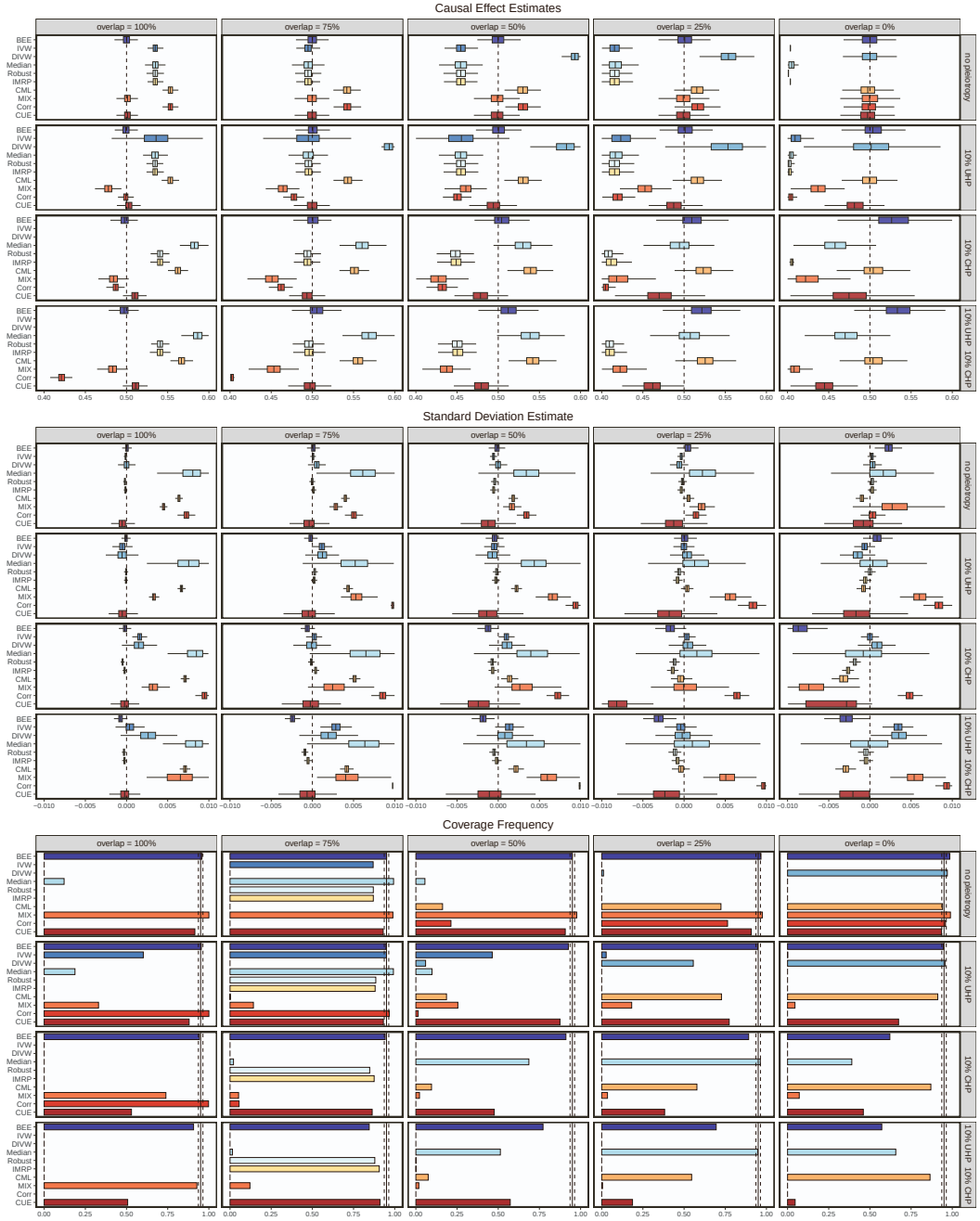

Figure S14: Investigation of UVMR approaches for UVMR model with sample sizes $n_0 = \cdots = n_6 = 20000$ and number of IVs $m = 2000$.

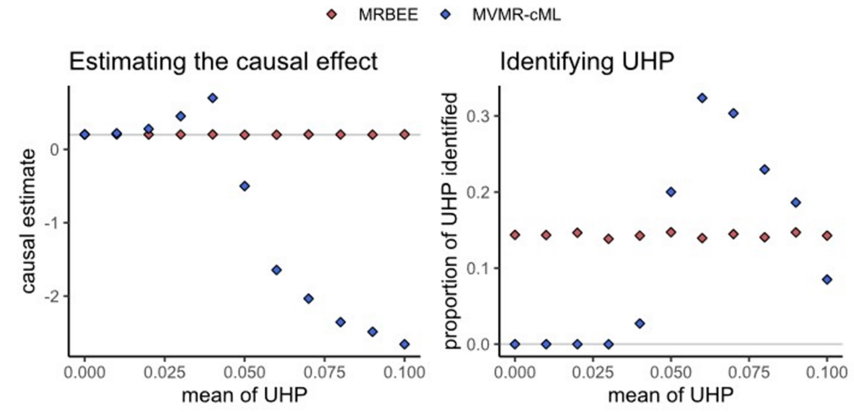

$$\beta_X \sim N\left(0, \frac{0.15}{100}\right)$$

$$\beta_Y = \beta_X \times 0.2 + \gamma$$

$$\gamma \sim N\left(\eta, \frac{0.15/100}{2} 0.2^2\right)$$

$$\eta \in \{0, 0.01, 0.02, \ldots, 0.10\}$$

$$\hat{\beta}_X = \beta_X + w_X$$

$$\hat{\beta}_Y = \beta_Y + w_Y$$

$$w_X, w_Y \overset{iid}{\sim} N\left(0, \frac{1}{30{,}000}\right)$$

```
m=100 # number of IVs
nx=ny=30000;h20.15;theta=0.2
niter=100
pleio_mean=seq(0,0.1,0.01)
byse=bxse=rep(1/sqrt(ny),m)
N=diag(sqrt(1/c(ny,nx)))
Sig_inv_l=lapply(1:m,function(h) N^2)
dims=c(niter,length(pleio_mean),2)
EST=NPLEIO=array(dim=dims)
for(p in 1:length(pleio_mean)) {
 for(iter in 1:niter) {
  bx=rnorm(m,0,sqrt(h2x/m))
  by=bx*theta
  adj=sqrt(var(by)/2)
  gamma=rnorm(m,pleio_mean[p],adj)
  by=by+gamma
  bxhat=bx+rnorm(m,0,sqrt(1/nx))
  byhat=by+rnorm(m,0,sqrt(1/ny))
  # estimate causal effect below
 }
}
```

Figure S15: These are the results of simulations described above comparing the performance of MRBEE and MRCML-BIC in identifying horizontal pleitropy and estimating the causal effect as the UHP mean changes.

References

Lin, Z., Xue, H. and Pan, W. (2023). Robust multivariable Mendelian randomization based on constrained maximum likelihood. The American Journal of Human Genetics, **110**(4), pp.592-605.

Fan. J. and Li, R. (2001). Variable selection via nonconcave penalized likelihood and its oracle properties. Journal of the American statistical Association, **96**(456), pp.1348-1360.

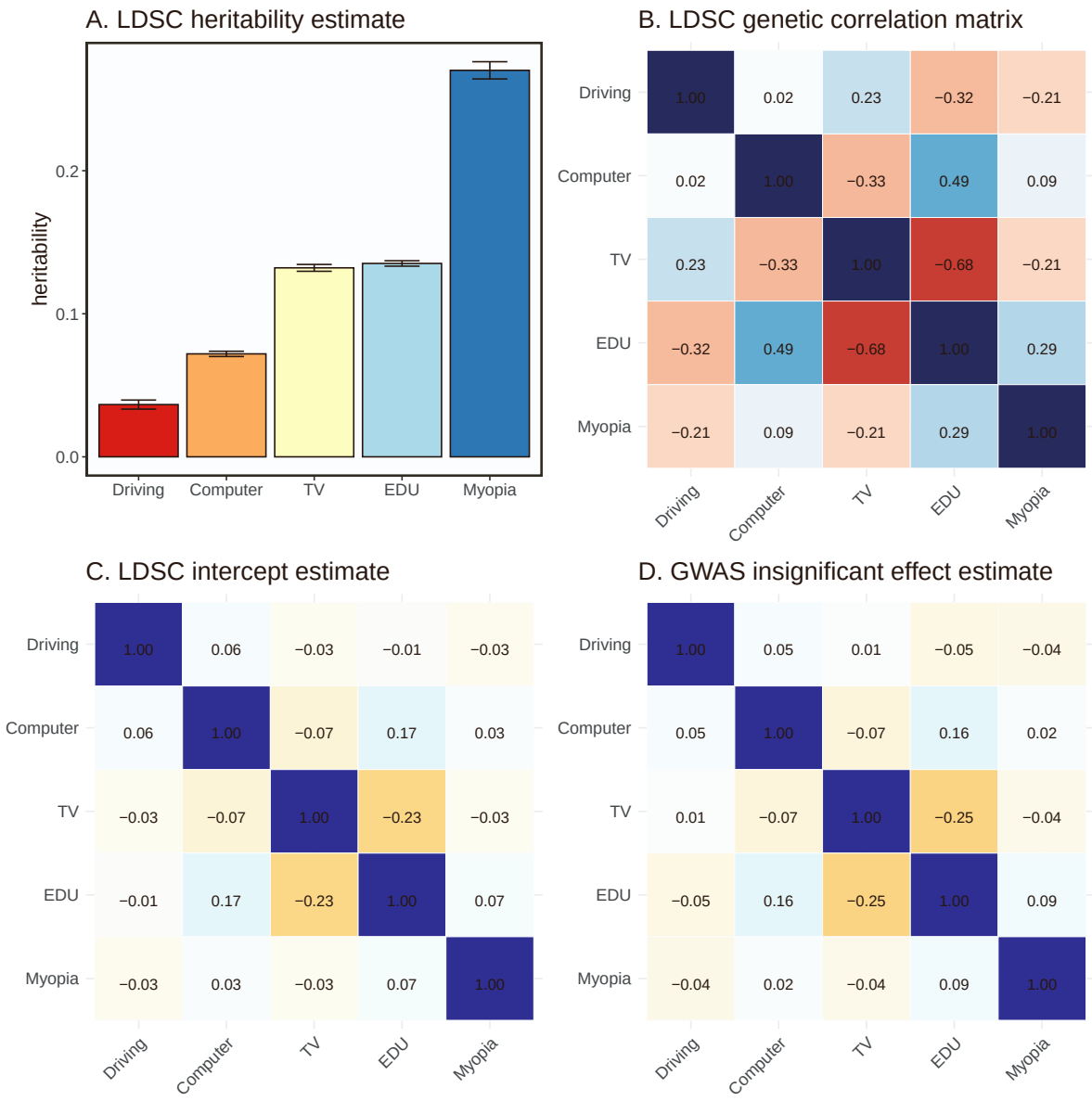

Figure S16: Myopia data. A. Heritability estimated by LDSC and the corresponding confidence intervals (radius is double SE). B. Genetic correlation matrix estimated by LDSC. C. Correlation matrix of estimation error constructed using the intercept from LDSC estimation. D. Correlation matrix of estimation error constructed using GWAS insignificant statistics.

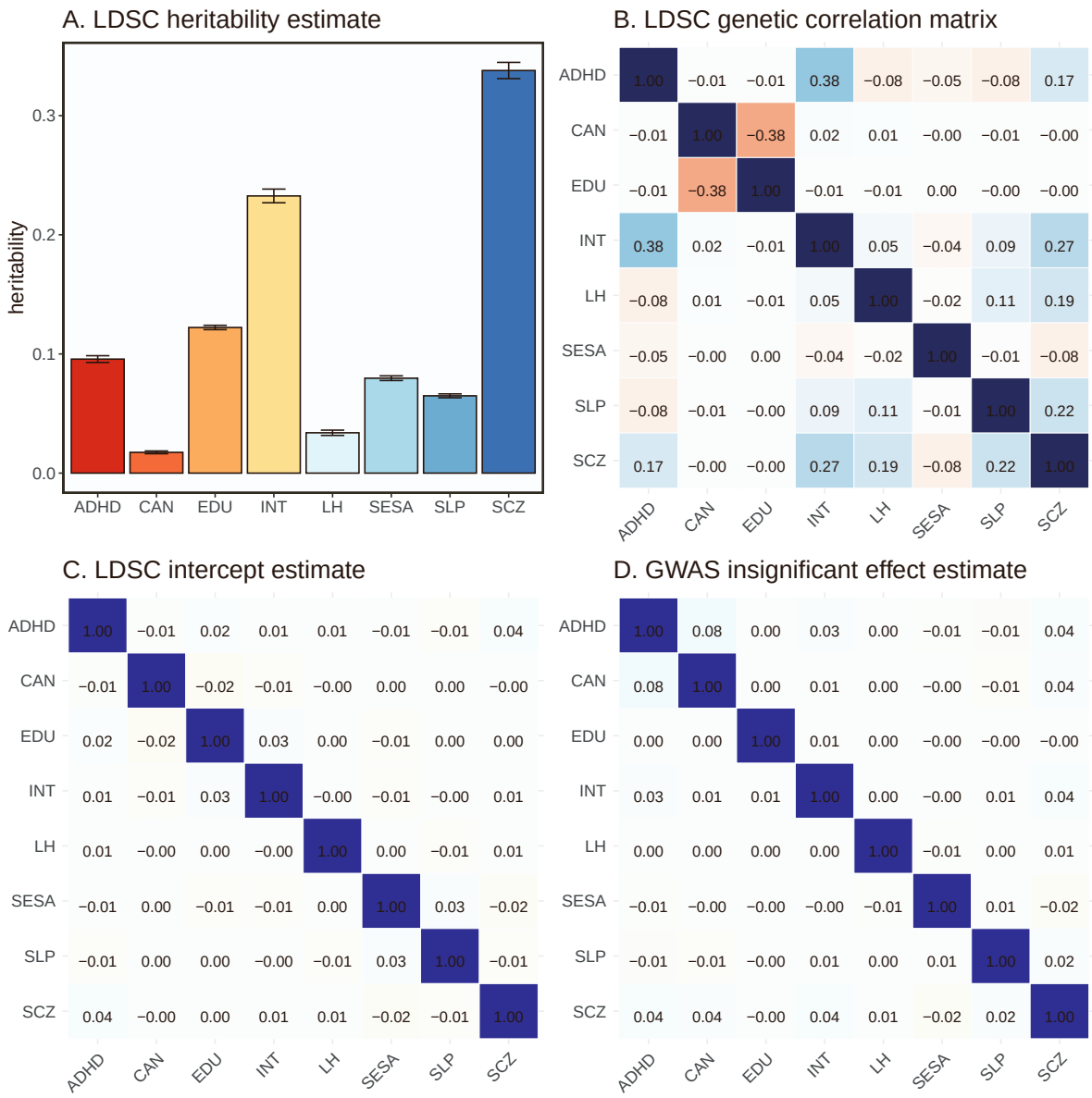

Figure S17: SCZ data. A. Heritability estimated by LDSC and the corresponding confidence intervals (radius is double SE). B. Genetic correlation matrix estimated by LDSC. C. Correlation matrix of estimation error constructed using the intercept from LDSC estimation. D. Correlation matrix of estimation error constructed using GWAS insignificant statistics.

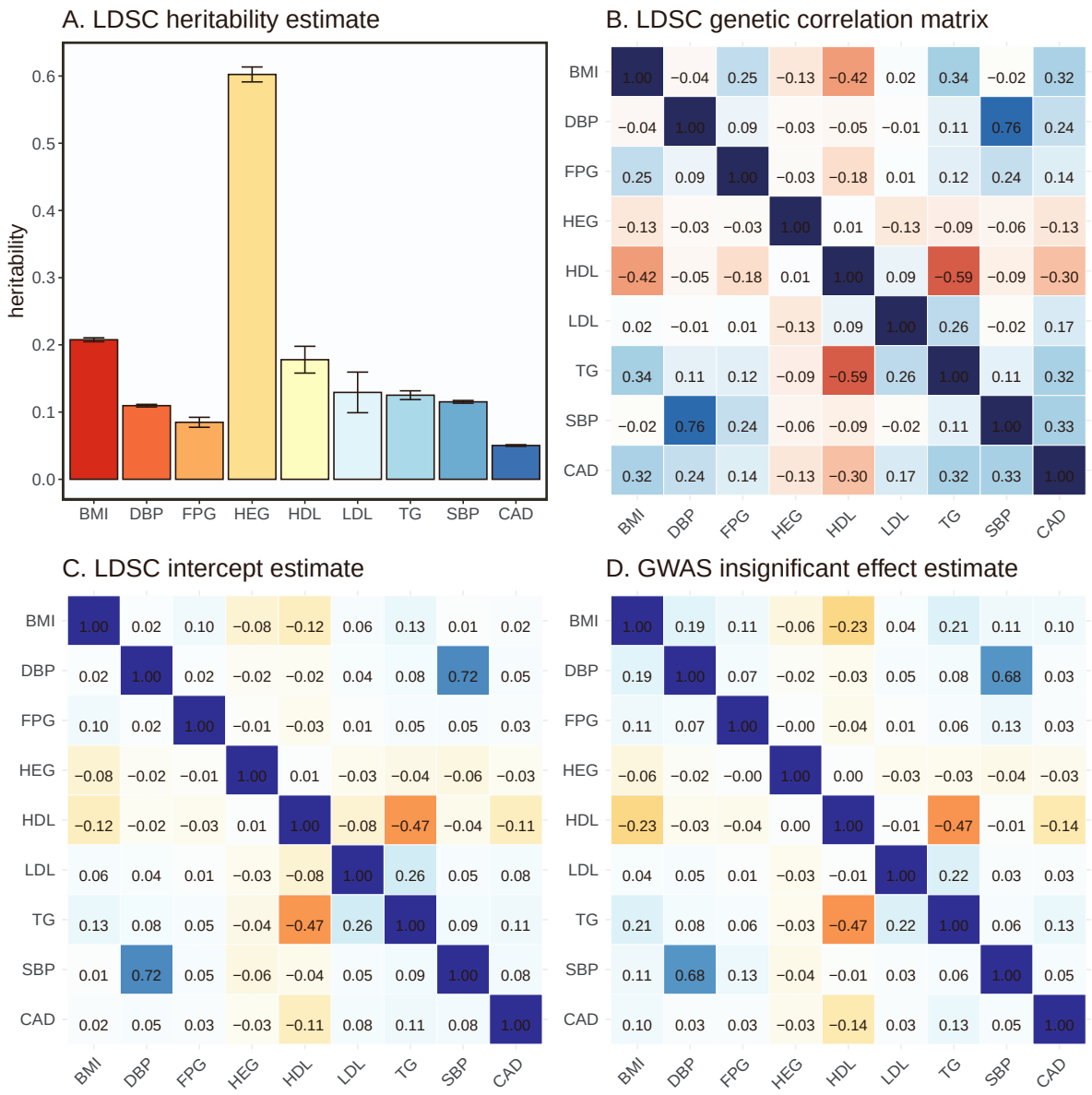

Figure S18: CAD data. A. Heritability estimated by LDSC and the corresponding confidence intervals (radius is double SE). B. Genetic correlation matrix estimated by LDSC. C. Correlation matrix of estimation error constructed using the intercept from LDSC estimation. D. Correlation matrix of estimation error constructed using GWAS insignificant statistics.

Supplementary material 2 of MRBEE: asymptotic results

Noah Lorincz-Comi, Yihe Yang, Gen Li, Xiaofeng Zhu

Contents

1 Asymptotic Results

1.1 Regular conditions

we investigate the asymptotic behavior of the multivariable IVW estimate as the number of IVs m and the minimum sample size $n_{\min}$ go to infinity. To facilitate the theoretical derivation, we specify three definitions and four regularity conditions.

Definition 1.1 (Sub-Gaussian variable)**.** *A random variable x is sub-Gaussian distributed with sub-Gaussian parameter $\tau_x > 0$ if for all $t > 0$, $\Pr(|x - E(x)| \geq t) \leq 2e^{-t^2/\tau_x^2}$.*

Definition 1.2 (Well-conditioned covariance matrix)**.** *A covariance matrix $\mathbf{\Sigma}$ is well-conditioned if there is a positive constant d_0 such that $0 < d_0^{-1} \leq \lambda_{min}(\mathbf{\Sigma}) \leq \lambda_{max}(\mathbf{\Sigma}) \leq d_0 < \infty$.*

Definition 1.3 (Strongly asymptotically unbiased estimate)**.** *Let $\hat{\boldsymbol{\theta}}$ be a consistent estimate of $\boldsymbol{\theta}$ with an asymptotic normal distribution $\sqrt{s_n}(\hat{\boldsymbol{\theta}} - \boldsymbol{\theta}) \xrightarrow{D} \mathcal{N}(\boldsymbol{\mu}_\theta, \mathbf{\Sigma}_\theta)$, where $\boldsymbol{\mu}_\theta$ is a vector with a bounded ℓ_2-norm, $\mathbf{\Sigma}_\theta$ is a well-conditioned covariance matrix, and s_n is a sequence of n. Then $\hat{\boldsymbol{\theta}}$ is called a strongly asymptotically unbiased estimate of $\boldsymbol{\theta}$ if $\boldsymbol{\mu}_\theta = \mathbf{0}$.*

Sub-Gaussianity and well-conditioned covariance matrix are two of the basic concepts in modern statistics (Vershynin, 2018). In addition, we define the strongly asymptotic unbiasedness to distinguish the consistent estimate whose squared bias vanishes with an equal and a smaller rate than its variance, respectively. If an estimate is consistent but its squared bias and variance vanish at the same rate, the classic confidence interval cannot cover the true parameter with a probability of 0.95, thus leading to invalid statistical inference (Jankova, 2018).

Condition 1.1 (Regularity conditions for multivariable MR)**.**

(C1) *For $\boldsymbol{g}_i = (g_{i1}, \ldots, g_{im})^\top$, each entry g_{ij} is a bounded sub-Gaussian with $\mathtt{E}(g_{ij})$=0, $\mathtt{var}(g_{ij})$=1, and sub-Gaussian parameter $\tau_g \in (0, \infty)$. For all $(i, j) \neq (t, s)$, g_{ij} is independent of g_{ts}.*

(C2) *For $\boldsymbol{u}_i = (u_{i1}, \ldots, u_{ip})^\top$, each entry u_{ij} is a sub-Gaussian with $\mathtt{E}(u_{ij}) = 0$, $\mathtt{var}(u_{is}) \in (0, \infty)$, and sub-Gaussian parameter $\tau_u \in (0, \infty)$; v_i is a sub-Gaussian with $\mathtt{E}(v_i) = 0$, $\mathtt{var}(v_i) \in (0, \infty)$, and sub-Gaussian parameter $\tau_v \in (0, \infty)$. Besides, $(\boldsymbol{u}_i^\top, v_i)^\top$ is independent of $(\boldsymbol{u}_t^\top, v_t)^\top$ for all $i \neq t$. Furthermore, $\boldsymbol{\Sigma}_{u \times v}$ is a well-conditioned covariance matrix of $(\boldsymbol{u}_i^\top, v_i)^\top$.*

(C3) *For $\boldsymbol{\beta}_j = (\beta_{j1}, \ldots, \beta_{jp})^\top$, $\sqrt{m}\beta_{js}$ is sub-Gaussian with $\mathtt{E}(\sqrt{m}\beta_{js}) = 0$, $\mathtt{var}(\sqrt{m}\beta_{js}) \in (0, \infty)$, and sub-Gaussian parameter $\tau_\beta \in (0, \infty)$. For all $j \neq t$, $\boldsymbol{\beta}_j$ is independent of $\boldsymbol{\beta}_t$ and $\boldsymbol{\Psi}_{\beta\beta}$ is a well-conditioned covariance matrix of $\sqrt{m}\boldsymbol{\beta}_j$.*

(C4) *The genetic variant g_{ij}, the genetic effect $\boldsymbol{\beta}_j$, the noise terms $\boldsymbol{u}_i$ and v_i, are three mutually independent groups.*

Conditions (C1)-(C4) restrict that all variables involved in this paper are sub-Gaussian distributed. In practice, g_{ij} is standardized from a binomial variable with status 0, 1, and 2. Hence, it is supposedly a bounded sub-Gaussian variable as long as its MAF is not rare. Besides, we assume $\sqrt{m}\boldsymbol{\beta}_j$ to be sub-Gaussian with a well-conditioned covariance matrix $\boldsymbol{\Psi}_{\beta\beta}$, because the cumulative covariance explained by the m IVs $\boldsymbol{\Psi}_{\beta\beta}$ should be fixed while the covariance explained by each IV $\boldsymbol{\Sigma}_{\beta\beta} \to 0$ as $m \to \infty$. This is because we adopt the infinitesimal random effect model in which $\mathrm{cov}(\boldsymbol{\beta}_j) = h_m^2/m$ (Bulik-Sullivan et al., 2015; Fisher, 1919), where h_m^2 is the additive SNP heritability explained by the m IVs. In MR analysis, the number of IVs can increase as the sample size increases because of increasing statistical power. Our theoretical work assumes that the heritability of IVs always keeps a constant. This is a reasonable assumption because the effect sizes because smaller and smaller under the infinitesimal model as the number of causal SNPs grows. In additional, the sub-Gaussian distribution is more general than the normal distribution, allowing for the possibility of partial elements in $\boldsymbol{\beta}_j$ to be a product of a continuous variable and a binary variable. This flexibility aligns with the scenario in multivariable MR analysis where the IVs from multiple exposures are combined, inevitably leading to the inclusion of numerous weak or null IVs for some exposures.

1.2 Asymptotic Results for Multivariable IVW

Theorem 1.1. *Denote* $w_{\alpha_j} = \hat{\alpha}_j - \alpha_j$ *and* $\omega_{js} = \hat{\beta}_{js} - \beta_{js}$, $s = 1, \ldots, p$. *If conditions (C1)-(C4) are satisfied, then for all* j,

$$\begin{pmatrix} \sqrt{n_0} w_{\alpha_j} \\ \sqrt{n_1} w_{\beta_{1j}} \\ \vdots \\ \sqrt{n_p} w_{\beta_{1p}} \end{pmatrix} \xrightarrow{D} \mathcal{N}\left(\begin{pmatrix} 0 \\ 0 \\ \vdots \\ 0 \end{pmatrix}, \begin{pmatrix} \sigma_{yy} & \frac{n_{01}}{\sqrt{(n_0 n_1)}}\sigma_{yx_1} & \cdots & \frac{n_{01}}{\sqrt{(n_0 n_p)}}\sigma_{yx_p} \\ \frac{n_{01}}{\sqrt{(n_0 n_1)}}\sigma_{yx_1} & \sigma_{x_1x_1} & \cdots & \frac{n_{1p}}{\sqrt{(n_1 n_p)}}\sigma_{x_1x_p} \\ \vdots & \vdots & \ddots & \vdots \\ \frac{n_{0p}}{\sqrt{(n_0 n_p)}}\sigma_{yx_p} & \frac{n_{1p}}{\sqrt{(n_1 n_p)}}\sigma_{x_1x_p} & \cdots & \sigma_{x_px_p} \end{pmatrix} \right),$$

if $n_0, \ldots, n_p$ *and* $m \to \infty$.

Theorem 1.1 demonstrates the asymptotic normal distribution of the estimation errors, from which we are able to obtain

$$\boldsymbol{\Sigma}_{W_\beta W_\beta} = \boldsymbol{\Delta}_{xx} \odot \boldsymbol{\Sigma}_{xx}, \quad \boldsymbol{\sigma}_{W_\beta w_\alpha} = \boldsymbol{\delta}_{xy} \odot \boldsymbol{\sigma}_{xy}, \quad \sigma_{w_\alpha w_\alpha} = \sigma_{yy}/n_0, \tag{1}$$

where the (j,s)th element of $\boldsymbol{\Delta}_{xx}$ is $n_{js}/(n_j n_s)$, the jth element of $\boldsymbol{\delta}_{xy}$ is $n_{j0}/(n_0 n_j)$, and the operator $\odot$ is the Hadamard product of two matrices. Our work is the first to rigorously prove this theorem under regularity conditions (C1)-(C4) and highlight the role of sample overlap.

Based on this theorem, the expectations of $\boldsymbol{S}_{\texttt{IVW}}(\boldsymbol{\theta})$ and $\mathbf{H}_{\texttt{IVW}}$ are given by

$$\mathtt{E}(\boldsymbol{S}_{\texttt{IVW}}(\boldsymbol{\theta})) = (\boldsymbol{\Delta}_{xx} \odot \boldsymbol{\Sigma}_{xx})\boldsymbol{\theta} - \boldsymbol{\delta}_{xy} \odot \boldsymbol{\sigma}_{xy}, \quad \mathtt{E}(\mathbf{H}_{\texttt{IVW}}) = \boldsymbol{\Sigma}_{\beta\beta} + \boldsymbol{\Delta}_{xx} \odot \boldsymbol{\Sigma}_{xx}. \tag{2}$$

By expressing $\boldsymbol{\sigma}_{xy} = \boldsymbol{\Sigma}_{xx}\boldsymbol{\theta} + \boldsymbol{\sigma}_{uv}$, an alternative expectation of $\boldsymbol{S}_{\texttt{IVW}}(\boldsymbol{\theta})$) is obtained:

$$\underbrace{\mathtt{E}(\boldsymbol{S}_{\texttt{IVW}}(\boldsymbol{\theta}))}_{\text{measurement error bias}} = \underbrace{\{(\boldsymbol{\Delta}_{xx} - \boldsymbol{\delta}_{xy}\mathbf{1}^\top) \odot \boldsymbol{\Sigma}_{xx}\}\boldsymbol{\theta}}_{\text{null bias}} - \underbrace{\boldsymbol{\delta}_{xy} \odot \boldsymbol{\sigma}_{uv}}_{\text{confounder bias}}. \tag{3}$$

From this expectation, it is clear that there are two sources of measurement error bias: $\{(\boldsymbol{\Delta}_{xx} - \boldsymbol{\delta}_{xy}\mathbf{1}^\top) \odot \boldsymbol{\Sigma}_{xx}\}\boldsymbol{\theta}$ comes from the measurement error, while $\{\boldsymbol{\delta}_{xy} \odot \boldsymbol{\sigma}_{uv}\}$ is caused by the confounder. Here, we call $\{(\boldsymbol{\Delta}_{xx} - \boldsymbol{\delta}_{xy}\mathbf{1}^\top) \odot \boldsymbol{\Sigma}_{xx}\}\boldsymbol{\theta}$ null bias because it always shrinks the coefficient estimate toward zero. In contrast, we term $\{\boldsymbol{\delta}_{xy} \odot \boldsymbol{\sigma}_{uv}\}$ confounder bias because $\boldsymbol{\sigma}_{uv} \neq \mathbf{0}$ implies that there are underlying confounders simultaneously affecting both $\boldsymbol{x}_i$ and y_i. Moreover, the overlapping fractions $\boldsymbol{\delta}_{xy}$ linearly trade off these two sources of biases. Generally, null bias is dominant when the elements of $\boldsymbol{\delta}_{xy}$ are small, while confounder bias dominates when the elements of $\boldsymbol{\delta}_{xy}$ are large. And there may exist a special sample overlap such that $\boldsymbol{\delta}_{xy} \odot \boldsymbol{\sigma}_{uv} = \{(\boldsymbol{\Delta}_{xx} - \boldsymbol{\delta}_{xy}\mathbf{1}^\top) \odot \boldsymbol{\Sigma}_{xx}\}\boldsymbol{\theta}$. In univariable MR, this special fraction is $n_{01}/n_0 = \sigma_{xx}\theta/\sigma_{xy}$, which guarantees that $\mathtt{E}(S_{\texttt{IVW}}(\theta)) = 0$ and $\mathtt{E}(\hat{\theta}_{\texttt{IVW}}) = \theta$. This theoretical result explains why in the empirical studies, $\hat{\theta}_{\texttt{IVW}}$ has a negative bias when n_{01}/n_0 is small, has a positive bias when n_{01}/n_0 is large, and is unbiased at this specific point.

Theorem 1.2. *Suppose conditions (C1)-(C4) hold and* m, $n_{\min} \to \infty$. *Then*

(i) if $m/\sqrt{n_{\min}} \to 0$, $\sqrt{n_{\min}}(\hat{\boldsymbol{\theta}}_{\texttt{IVW}} - \boldsymbol{\theta}) \xrightarrow{D} \mathcal{N}(\mathbf{0}, \psi_\theta \boldsymbol{\Psi}_{\beta\beta}^{-1})$;

(ii) if $m/\sqrt{n_{\min}} \to c_0$, $\sqrt{n_{\min}}(\hat{\boldsymbol{\theta}}_{\texttt{IVW}} - \boldsymbol{\theta}) \xrightarrow{D} \mathcal{N}(-c_0 \boldsymbol{\Psi}_{\beta\beta}^{-1}(\boldsymbol{\Psi}_{W_\beta W_\beta}\boldsymbol{\theta} - \boldsymbol{\psi}_{W_\beta w_\alpha}), \psi_\theta \boldsymbol{\Psi}_{\beta\beta}^{-1})$;

(iii) if $m/n_{\min} \to 0$, $||\hat{\boldsymbol{\theta}}_{\texttt{IVW}} - \boldsymbol{\theta}||_2 = O_P(m/n_{\min})$;

(iv) if $m/n_{\min} \to c_0 \in (0, \infty)$, $\hat{\boldsymbol{\theta}}_{\texttt{IVW}} - \boldsymbol{\theta} \xrightarrow{P} -c_0(\boldsymbol{\Psi}_{\beta\beta} + c_0 \boldsymbol{\Psi}_{W_\beta W_\beta})^{-1}(\boldsymbol{\Psi}_{W_\beta W_\beta}\boldsymbol{\theta} - \boldsymbol{\psi}_{W_\beta w_\alpha})$;

(v) if $m/n_{\min} \to \infty$, $\hat{\boldsymbol{\theta}}_{\texttt{IVW}} \xrightarrow{P} \boldsymbol{\Psi}^{+}_{W_\beta W_\beta}\boldsymbol{\psi}_{W_\beta w_\alpha}$;

where

$$\boldsymbol{\Psi}_{W_\beta \times w_\alpha} = \begin{pmatrix} \boldsymbol{\Psi}_{W_\beta W_\beta} & \boldsymbol{\psi}_{W_\beta w_\alpha} \\ \boldsymbol{\psi}_{W_\beta w_\alpha}^\top & \psi_{w_\alpha w_\alpha} \end{pmatrix} = \lim_{n_{\min}\to\infty} \begin{pmatrix} n_{\min}\boldsymbol{\Sigma}_{W_\beta W_\beta} & n_{\min}\boldsymbol{\sigma}_{W_\beta w_\alpha} \\ n_{\min}\boldsymbol{\sigma}_{W_\beta w_\alpha}^\top & n_{\min}\sigma_{w_\alpha w_\alpha} \end{pmatrix},$$

and $\psi_\theta = \psi_{w_\alpha w_\alpha} + \boldsymbol{\theta}^\top \boldsymbol{\Psi}_{W_\beta W_\beta}\boldsymbol{\theta} - 2\boldsymbol{\theta}^\top \boldsymbol{\psi}_{W_\beta w_\alpha}$.

Theorem 1.2 is one of two main theorems in this paper and points out five scenarios. First, if m goes to infinity with a lower rate than $\sqrt{n_{\min}}$, then $\hat{\boldsymbol{\theta}}_{\texttt{IVW}}$ is strongly asymptotically unbiased. In other words, $\hat{\boldsymbol{\theta}}_{\texttt{IVW}}$ is able to reliably infer causality only when the sample size of GWAS data is quadratically larger than the number of IVs. On the other hand, the asymptotic covariance matrix of $\hat{\boldsymbol{\theta}}_{\texttt{IVW}}$ is the inverse of the cumulative covariance matrix $\boldsymbol{\Psi}_{\beta\beta} = \sum_{j=1}^m \texttt{cov}(\boldsymbol{\beta}_j)$, therefore, it is optimal to include as many associated variants as possible in order to have $\boldsymbol{\Psi}_{\beta\beta}$ large enough. In contrast, using a few top significant variants to perform MR analysis is not recommended.

Second, if m tends to infinity with the same rate as $\sqrt{n_{\min}}$, $\sqrt{n_{\min}}(\hat{\boldsymbol{\theta}}_{\texttt{IVW}} - \boldsymbol{\theta})$ converges to an asymptotic normal distribution with a non-zero asymptotic bias $\{c_0\boldsymbol{\Psi}_{\beta\beta}^{-1}(\boldsymbol{\psi}_{W_\beta w_\alpha} - \boldsymbol{\Psi}_{W_\beta W_\beta}\boldsymbol{\theta})\}$. In this asymptotic bias, $\{c_0(\boldsymbol{\psi}_{W_\beta w_\alpha} - \boldsymbol{\Psi}_{W_\beta W_\beta}\boldsymbol{\theta})\}$ is caused by $\boldsymbol{S}_{\texttt{IVW}}(\boldsymbol{\theta})$ and $\boldsymbol{\Psi}_{\beta\beta}^{-1}$ is caused by $\mathbf{H}_{\texttt{IVW}}^{-1}$. Since the asymptotic bias and asymptotic covariance matrix are of the same order in this scenario, the inference made is invalid although the bias of $\hat{\boldsymbol{\theta}}_{\texttt{IVW}}$ is infinitesimal. When $m/n_{\min} \to 0$, $\hat{\boldsymbol{\theta}}_{\texttt{IVW}}$ still converges to $\boldsymbol{\theta}$ with a rate $O(m/n_{\min})$, but it no longer has an asymptotic normal distribution. Scenario (iv) is more serious than (iii) because the bias of $\hat{\boldsymbol{\theta}}_{\texttt{IVW}}$ will not vanish even when $\sqrt{n_{\min}}$ goes to infinity. In the fifth scenario, $\hat{\boldsymbol{\theta}}_{\texttt{IVW}}$ converges to a term irrelevant to $\boldsymbol{\theta}$.

1.3 Asymptotic Results for MRBEE

Theorem 1.3. *Suppose conditions (C1)-(C4) hold and m, $n_{\min} \to \infty$. Then*

(i) if $m/n_{\min} \to 0$, $\sqrt{n_{\min}}(\hat{\boldsymbol{\theta}}_{\mathit{BEE}} - \boldsymbol{\theta}) \xrightarrow{D} \mathcal{N}(\mathbf{0}, \psi_\theta \boldsymbol{\Psi}_{\beta\beta}^{-1})$;

(ii) if $m/n_{\min} \to c_0 \in (0, \infty)$, $\sqrt{n_{\min}}(\hat{\boldsymbol{\theta}}_{\mathit{BEE}} - \boldsymbol{\theta}) \xrightarrow{D} \mathcal{N}(\mathbf{0}, \psi_\theta \boldsymbol{\Psi}_{\beta\beta}^{-1} + c_0 \boldsymbol{\Psi}_{\beta\beta}^{-1} \boldsymbol{\Psi}_{\mathrm{BC}} \boldsymbol{\Psi}_{\beta\beta}^{-1})$;

(iii) if $m/n_{\min} \to \infty$ and $m/n_{\min}^2 \to 0$, $\sqrt{(n_{\min}^2/m)}(\hat{\boldsymbol{\theta}}_{\mathit{BEE}} - \boldsymbol{\theta}) \xrightarrow{D} \mathcal{N}(\mathbf{0}, \boldsymbol{\Psi}_{\beta\beta}^{-1} \boldsymbol{\Psi}_{\mathrm{BC}} \boldsymbol{\Psi}_{\beta\beta}^{-1})$;

where ψ_θ is defined in Theorem 1.2 and $\boldsymbol{\Psi}_{\mathrm{BC}}$ is a semi-positive symmetric matrix whose expression is shown in equation (64) in supplementary materials.

Theorem 1.3 indicates three scenarios. First, if $m/n \to 0$,$\sqrt{n_{\min}}(\hat{\boldsymbol{\theta}}_{\mathtt{BEE}} - \boldsymbol{\theta})$ converges to a normal distribution with a zero mean and the covariance matrix being exactly the same as $\hat{\boldsymbol{\theta}}_{\mathtt{IVW}}$. In other words, $\hat{\boldsymbol{\theta}}_{\mathtt{BEE}}$ is not only strongly asymptotically unbiased but also loses no efficiency in comparison to $\hat{\boldsymbol{\theta}}_{\mathtt{IVW}}$. Second, if $m/n_{\min} \to c_0 \in (0, \infty)$, there is an additional covariance matrix $c_0 \boldsymbol{\Psi}_{\beta\beta}^{-1} \boldsymbol{\Psi}_{\mathrm{BC}} \boldsymbol{\Psi}_{\beta\beta}^{-1}$ in the asymptotic normal distribution, where $\boldsymbol{\Psi}_{\mathrm{BC}}$ is introduced by the bias-correction terms:

$$\boldsymbol{\Psi}_{\mathrm{BC}} = \lim_{n_{\min} \to \infty} \mathtt{var}\left[\frac{n_{\min}}{\sqrt{m}}\left((\mathbf{W}_\beta^\top \mathbf{W}_\beta - m\boldsymbol{\Sigma}_{W_\beta W_\beta})\boldsymbol{\theta} - (\mathbf{W}_\beta^\top \boldsymbol{w}_\alpha - m\boldsymbol{\sigma}_{W_\beta w_\alpha})\right)\right]. \tag{4}$$

In this scenario, $\hat{\boldsymbol{\theta}}_{\mathtt{BEE}}$ is again strongly asymptotically unbiased with a convergence rate $\sqrt{n_{\min}}$, while $\hat{\boldsymbol{\theta}}_{\mathtt{IVW}}$ incurs a bias not vanishing asymptotically. In the third scenario, $\hat{\boldsymbol{\theta}}_{\mathtt{BEE}}$ is still strongly asymptotically unbiased with a convergence rate $\sqrt{(n_{\min}^2/m)}$, and the asymptotic distribution is dominated by the bias correction terms. Note that $\hat{\boldsymbol{\theta}}_{\mathtt{IVW}}$ is not consistent unless $m/n_{\min} \to 0$ and the inference made by $\hat{\boldsymbol{\theta}}_{\mathtt{IVW}}$ is unreliable unless $m/\sqrt{n_{\min}} \to 0$. In contrast, $\hat{\boldsymbol{\theta}}_{\mathtt{BEE}}$ is strongly asymptotically unbiased as long as $m/n_{\min}^2 \to 0$. Thus, MRBEE is superior to multivariable IVW in terms of both unbiasedness and asymptotic validity in all possible scenarios.

Theorem 1.4. *Suppose conditions (C1)-(C4) hold. Let $g_{ij}^{\{s\}}$ satisfy the condition (C1), $E(x_i^{[s]}|g_{ij}^{\{s\}}) = 0$ for all $1 \le s \le p$, and $E(y_i^{[0]}|g_{ij}^{\{0\}}) = 0$. Then*

$$\|\boldsymbol{\Sigma}_{W_\beta \times w_\alpha}^{-\frac{1}{2}} \widehat{\boldsymbol{\Sigma}}_{W_\beta \times w_\alpha} \boldsymbol{\Sigma}_{W_\beta \times w_\alpha}^{-\frac{1}{2}} - \mathbf{I}_{p+1}\|_2 = O_P\left(\frac{1}{\sqrt{M}}\right),$$

if $n_{\min}$ and $M \to \infty$.

Theorem 1.4 shows that $\widehat{\boldsymbol{\Sigma}}_{W_\beta \times w_\alpha}$ has a $O(\sqrt{M})$ convergence rate after adjusting the scale of $\boldsymbol{\Sigma}_{W_\beta \times w_\alpha}$. As there may be more than 1 million independent variants in the whole genome, $\widehat{\boldsymbol{\Sigma}}_{W_\beta \times w_\alpha}$ has high precision. Besides, $n_0, n_1, ..., n_p \to \infty$ are required such that $\sqrt{n_0}\hat{\alpha}_j^*$ and $\sqrt{n_s}\hat{\beta}_{js}^*$ are asymptotically normally distributed.

Theorem 1.5. *Under the conditions of Theorem 1.4,*

$$||\boldsymbol{\Sigma}_{\mathit{BEE}}^{-\frac{1}{2}}(\boldsymbol{\theta}) \widehat{\boldsymbol{\Sigma}}_{\mathit{BEE}}(\hat{\boldsymbol{\theta}}_{\mathit{BEE}}) \boldsymbol{\Sigma}_{\mathit{BEE}}^{-\frac{1}{2}}(\boldsymbol{\theta}) - \mathbf{I}_p||_2 = O_P\left(\max\left\{\frac{1}{\sqrt{n_{\min}}}, \frac{\sqrt{m}}{n_{\min}}, \sqrt{\frac{\log m}{m}}\right\}\right)$$

if $n_{\min}, m$ and $M \to \infty$ and $m/n_{\min}^2 \to 0$.

Theorem 1.5 shows that $\widehat{\boldsymbol{\Sigma}}_{\mathtt{BEE}}(\boldsymbol{\theta})$ has a $\min(\sqrt{n_{\min}}, \sqrt{(n_{\min}^2/m)}, \sqrt{(m/\log m)})$ convergence rate when $m/n_{\min}^2 \to 0$. The first two convergence rates are brought by $||\widehat{\mathbf{F}}_{\mathtt{BEE}} - \mathbf{F}_{\mathtt{BEE}}||_2$, while the third convergence rate is yielded by $||\widehat{\mathbf{V}}_{\mathtt{BEE}}(\hat{\boldsymbol{\theta}}_{\mathtt{BEE}}) - \mathbf{V}_{\mathtt{BEE}}(\boldsymbol{\theta})||_2$. Note that the SE estimation should be of the same importance as the causal effect estimation. Although the inference is made based on an unbiased estimate, it could still be invalid if the SE estimate is not reliable. As the dependability of the sandwich formula has been extensively investigated empirically, it is a reliable technique to obtain the SE estimate for MRBEE.

Theorem 1.6. *Assume that $|\mathcal{O}|$ is fixed and bounded and $\gamma_1^*, \ldots, \gamma_m^*$ are a series of non-random numbers. Then under the conditions of Theorem 1.5, there exists a threshold $\kappa = F_{\chi_1^2}(C_0 \log m)$ such that $\Pr(\mathcal{O} = \hat{\mathcal{O}}) \to 1$, where $\hat{\mathcal{O}} = \{j : \ F_{\chi_1^2}(t_{\gamma_j}) > \kappa\}$ and C_0 is a sufficiently large constant.*

Theorem 1.6 indicates that there is a theoretical threshold $\kappa = F_{\chi_1^2}(C_0 \log m)$ to consistently identify all horizontal pleiotropy. This threshold increases with a rate $O(\log m)$ to reduce the false discovery rate (FDR) and its concrete value can be chosen by a FDR control method (Benjamini, 1995). In practice, MRBEE iteratively applies the hypothesis test to remove the outliers and uses the remaining IVs to estimate $\boldsymbol{\theta}$. The stable estimate is regarded as $\hat{\boldsymbol{\theta}}_{\texttt{BEE}}$.

1.4 Preliminary lemmas

In this subsection, we specify some lemmas that can facilitate the proofs, most of which can be found in the existing papers. We first discuss the equivalent characterizations of sub-Gaussian and sub-exponential variables.

Lemma 1.1 (Equivalent characterizations of sub-Guassian variables)**.** *Given any random variable X, the following properties are equivalent:*

(I) there is a constant $K_1 \geq 0$ such that

$$\Pr(|X| \geq t) \leq 2\exp(-t^2/K_1^2), \quad \text{for all } t \geq 0,$$

(II) the moments of X satisfy

$$||X||_{L_p} = (E(|X|^p))^{\frac{1}{p}} \leq K_2\sqrt{p}, \quad \text{for all } p \geq 1,$$

(III) the moment generating function (MGF) of X^2 satisfies:

$$E\{\exp(\lambda^2 X^2)\} \leq \exp(K_3^2\lambda^2), \quad \text{for all } \lambda \text{ staisfying } |\lambda| \leq K_3^{-1},$$

(IV) the MGF of X^2 is bounded at some point, namely

$$E\{\exp(X^2/K_4^2)\} \leq 2,$$

(V) if $E(X) = 0$, the MGF of X satisfies

$$E\{\exp(\lambda X)\} \leq \exp(K_5^2\lambda^2), \quad \text{for all } \lambda \in \mathbb{R},$$

where $K_1, \ldots, K_5$ are certain strictly positive constants.

This lemma summarizes some well-known properties of sub-Guassian and can be found in Vershynin (2018, Proposition 2.5.2).

Lemma 1.2 (Equivalent characterizations of sub-exponential variables)**.** *Given any random variable X, the following properties are equivalent:*

(I) there is a constant $K_1 \geq 0$ such that

$$\Pr(|X| \geq t) \leq 2\exp(-t/K_1), \quad \text{for all } t \geq 0,$$

(II) the moments of X satisfy

$$||X||_{L_p} = (E(|X|^p))^{\frac{1}{p}} \leq K_2 p, \quad \text{for all } p \geq 1,$$

(III) the moment generating function (MGF) of $|X|$ satisfies:

$$E\{\exp(\lambda|X|)\} \leq \exp(K_3\lambda), \quad \text{for all } \lambda \text{ staisfying } 0 \leq \lambda \leq K_3^{-1},$$

(IV) the MGF of $|X|$ is bounded at some point, namely

$$E\{\exp(|X|/K_4)\} \leq 2,$$

(V) if $E(X) = 0$, the MGF of X satisfies

$$E\{\exp(\lambda X)\} \leq \exp(K_5^2\lambda^2), \quad \text{for all } \lambda \leq K_5^{-1},$$

where $K_1, \ldots, K_5$ are certain strictly positive constants.

This lemma summarizes some well-known properties of sub-exponential and can be found in Vershynin (2018, Proposition 2.7.1).

Lemma 1.3 (Product of sub-Gaussian variable is sub-exponential)**.** *Suppose that X, Z are two sub-Gaussian variable, then $Y = XZ$ is a sub-exponential variable. Besides, if X is a bounded sub-Gaussian variable, then then $Y = XZ$ is a sub-Gaussian variable.*

The first claim of this lemma is provided by Vershynin (2018, Proposition 2.7.7). The second claim of this lemma is a direct inference of Fan et al. (2011, Lemma A.2).

Lemma 1.4 (ℓ_2-norm of matrices with sub-Gaussian entries)**.** *Let $\boldsymbol{X}_1, \ldots, \boldsymbol{X}_n$ be n $(p \times 1)$ independent identically distributed random vector with entries $x_{i1}, \ldots, x_{ip}$ are sub-Gaussian with zero-mean. Besides, define the covariance matrix of $\boldsymbol{X}_i$ as*

$$\boldsymbol{\Sigma} = E(\boldsymbol{X}_i \boldsymbol{X}_i^\top)$$

and the related sample covariance matrix

$$\hat{\boldsymbol{\Sigma}} = \frac{1}{n} \sum_{i=1}^{n} \boldsymbol{X}_i \boldsymbol{X}_i^\top.$$

Then for every positive integer n,

$$E(||\hat{\boldsymbol{\Sigma}} - \boldsymbol{\Sigma}||_2) \leq C\left(\frac{p}{n} + \sqrt{\frac{p}{n}}\right)||\boldsymbol{\Sigma}||_2,$$

where C is certain positive constant.

This lemma is provided by Vershynin (2018, Theorem 4.7.1). It shows the convergence rate of sample covariance matrix is $\sqrt{(n/m)}$.

Lemma 1.5 (ℓ_2-norm of matrices with sub-exponential entries)**.** *Let $\boldsymbol{X}_1, \ldots, \boldsymbol{X}_n$ be n $(p \times 1)$ independent identically distributed random vector with entries $x_{i1}, \ldots, x_{ip}$ are sub-exponential with zero-mean. Besides, define the covariance matrix of $\boldsymbol{X}_i$ as*

$$\boldsymbol{\Sigma} = E(\boldsymbol{X}_i \boldsymbol{X}_i^\top)$$

and the related sample covariance matrix

$$\hat{\boldsymbol{\Sigma}} = \frac{1}{n} \sum_{i=1}^{n} \boldsymbol{X}_i \boldsymbol{X}_i^\top.$$

Then for ever $t \geq 0$, the following inequality holds with probability at least $1 - p\exp(-ct^2)$:

$$||\hat{\boldsymbol{\Sigma}} - \boldsymbol{\Sigma}||_2 \leq \max(||\boldsymbol{\Sigma}||_2 \delta, \delta^2),$$

where c is certain positive constant and $\delta = t\sqrt{p/n}$.

This lemma is the direct inference of Vershynin (2010, Theorem 5.44). Besides, by letting $t = \sqrt{p \log n}$ we further obtain

$$\mathrm{E}(|||\hat{\boldsymbol{\Sigma}} - \boldsymbol{\Sigma}|||\_2) = O\left(\sqrt{\frac{p \log n}{n}}\right)|||\boldsymbol{\Sigma}|||\_2,$$

if $\hat{\boldsymbol{\Sigma}}$ is the sample covariance matrix of sub-exponential vector. Note that in our method, the dimension p is fixed and hence we cannot chose $t = \sqrt{p \log p}$ such that the estimation bound becomes $\sqrt{(p \log p)/n}||\boldsymbol{\Sigma}||_2$.

Lemma 1.6 (Asymptotic normal distribution of Wishart matrix)**.** *Suppose $\boldsymbol{X}_1, \boldsymbol{X}_2, \ldots, \boldsymbol{X}_n$ are n IID relaxation of the p-dimensional variable $\boldsymbol{X} \sim \mathcal{N}(\mathbf{0}, \boldsymbol{\Sigma})$ with a well-conditioned covariance matrix $\boldsymbol{\Sigma}$. Besides, define the sample covariance matrix of $\boldsymbol{\Sigma}$ as*

$$\hat{\boldsymbol{\Sigma}} = \frac{1}{n} \sum_{i=1}^{n} \boldsymbol{X}_i \boldsymbol{X}_i^{\top}.$$

If p is a fixed number, then as $n \to \infty$,

$$\sqrt{n}(vec(\hat{\boldsymbol{\Sigma}}) - vec(\boldsymbol{\Sigma})) \xrightarrow{D} \mathcal{N}\bigg(\mathbf{0}, (\mathbf{I}_{p^2} + \mathbf{K}_{p^2})(\boldsymbol{\Sigma} \otimes \boldsymbol{\Sigma})\bigg),$$

where $\mathbf{K}_{p^2}$ is the so-called commutation matrix, which is able to ensure $\mathbf{K}_{p^2} vec(\mathbf{A}) = vec(\mathbf{A}')$ for all $(p \times p)$ matrix.

This lemma can be found in Muirhead (2009, equation (5), p90).

1.5 Specific Lemmas

In this subsection, we specify the following lemmas that are made based on the preliminary lemmas.

Lemma 1.7 (Asymptotic normal distribution of sub-Gaussian and sub-exponential variables)**.** *Suppose $X_1, \ldots, X_n$ are n independent sub-Gaussian or sub-exponential variables with mean-zero and variance $\sigma_1^2, \ldots, \sigma_n^2$. Then*

$$\lim_{n\to\infty} \frac{1}{\sqrt{n}} \sum_{i=1}^{n} X_i \xrightarrow{D} \mathcal{N}(0, \sigma_x^2),$$

where

$$\sigma_x^2 = \lim_{n\to\infty} \frac{1}{n} \sum_{i=1}^{n} \sigma_i^2.$$

Proof of Lemma 1.7. It is easy to verify the Lyapunov's condition: for all fixed $\delta > 0$,

$$\lim_{n\to\infty} \frac{1}{n^{1+\delta}} \sum_{i=1}^{n} \mathrm{E}(|X_i|^{2+2\delta}) \leq \frac{\sqrt{2K_2 + 2K_2\delta}^{2+2\delta}}{n^{\delta}} \to 0$$

by the (II) of Lemma 1.1, if $X_1, \ldots, X_n$ are sub-Gaussian variables;

$$\lim_{n\to\infty} \frac{1}{n^{1+\delta}} \sum_{i=1}^{n} \mathrm{E}(|X_i|^{2+2\delta}) \leq \frac{(2K_2 + 2K_2\delta)^{2+2\delta}}{n^{\delta}} \to 0$$

by the (II) of Lemma 1.2, if $X_1, \ldots, X_n$ are sub-exponential variables. And hence the asymptotic normal distribution holds. □

Lemma 1.8 (Asymptotic normal distribution of estimation error)**.** *Let*

$$\xi_j^{[s]} = \frac{1}{\sqrt{n_s}} \sum_{i=1}^{n_s} g_{ij}^{[s]} x_{i,-j}^{[s]},$$

where

$$x_{i,-j}^{[s]} = x_i^{[s]} - \beta_{js} g_{i,j}^{[s]},$$

$s = 0, 1, \ldots, p$, $x_{i,-j}^{[0]}$ represents $y_{i,-j}^{[0]}$ and $\beta j0$ represent α_j. Then

$$\xi_j^{[s]} \xrightarrow{D} \mathcal{N}(0, \sigma_{x_s x_s} - \sigma_{\beta_s \beta_s}),$$

where $\sigma_{x_0 x_0}$ represents σ_{yy} and $\sigma_{\beta_0 \beta_0}$ represents $\boldsymbol{\theta}^\top \boldsymbol{\Sigma}_{\beta\beta} \theta$.

Proof of Lemma 1.8. Note that both $g_{ij}^{[s]}$ and $x_{i,-j}^{[s]}$ are sub-Gaussian ($x_{i,-j}^{[s]}$ is the product of a sub-Gaussian variable and a bounded sub-Gaussian variable), and it holds $\mathrm{E}(g_{ij}^{[s]} x_{i,-j}^{[s]}) = 0$ and

$$\mathrm{var}(g_{ij}^{[s]} x_{i,-j}^{[s]}) = \mathrm{var}(g_{ij}^{[s]}) \times \mathrm{var}(x_{i,-j}^{[s]}) = \sigma_{x_s x_s} - \sigma_{\beta_s \beta_s}. \tag{5}$$

As a result,

$$\xi_j^{[s]} = \frac{1}{\sqrt{n_s}} \sum_{i=1}^{n_s} g_{ij}^{[s]} x_{i,-j}^{[s]} \xrightarrow{D} \mathcal{N}(0, \sigma_{x_s x_s} - \sigma_{\beta_s \beta_s}), \tag{6}$$

according Lemma 1.7. □

Lemma 1.9 (Asymptotic normality of bias-correction terms)**.** *Let*

$$\boldsymbol{\zeta}_j = \left(\frac{n_{\min}}{n_1}\xi_j^{[1]}, \frac{n_{\min}}{n_2}\xi_j^{[2]}, \ldots, \frac{n_{\min}}{n_p}\xi_j^{[p]}, \frac{n_{\min}}{n_0}\xi_j^{[0]} \right)^\top.$$

Under the conditions (C1)-(C4),

$$\lim_{m\to\infty} \frac{1}{\sqrt{m}} \sum_{j=1}^{m} (vec(\boldsymbol{\zeta}_j\boldsymbol{\zeta}_j^\top) - vec(\boldsymbol{\Psi}_{W_\beta \times w_\alpha})) \xrightarrow{D} \mathcal{N}\Big(\mathbf{0}, (\mathbf{I}_{(p+1)^2} + \mathbf{K}_{(p+1)^2})(\boldsymbol{\Psi}_{W_\beta \times w_\alpha} \otimes \boldsymbol{\Psi}_{W_\beta \times w_\alpha}) \Big).$$

as $n_{\min}, m \to \infty$.

Proof of Lemma 1.9. By using Lemma 1.7, $\boldsymbol{\zeta}_j$ follows $\mathcal{N}(0, \boldsymbol{\Psi}_{W_\beta \times w_\alpha})$ as $n_{\min} \to \infty$. Then by using Lemma 1.6, this lemma holds. □

Lemma 1.10 (Asymptotic normality of residual term)**.** *Under the conditions (C1)-(C4),*

$$\lim_{m\to\infty} \frac{1}{\sqrt{m}} \sum_{j=1}^{m} \sqrt{m}\boldsymbol{\beta}_j \xi_j^{[s]} \xrightarrow{D} \mathcal{N}(0, \sigma_{x_s x_s} \boldsymbol{\Sigma}_{\beta\beta}),$$

and

$$\lim_{m\to\infty} \frac{1}{m} \sum_{j=1}^{m} \sqrt{m}\boldsymbol{\beta}_j \sqrt{m}\boldsymbol{\beta}_j^\top \xi_j^{[s]} \xi_j^{[k]} \xrightarrow{P} \frac{n_{sk}}{\sqrt{n_s n_k}} \sigma_{x_s x_k} \boldsymbol{\Sigma}_{\beta\beta},$$

for $s = 0, \ldots, p$*, where* $\sigma_{x_0 x_k}$ *represents* $\sigma_{y x_k} = \sum_{l=1}^{p} \theta_l \sigma_{x_l x_k}$.

Proof of Lemma 1.10. By condition (C4), $\sqrt{m}\boldsymbol{\beta}_j$ is independent of $\xi_j^{[s]}$. By Lemma 1.3, $\sqrt{m}\boldsymbol{\beta}_j \xi_j^{[s]}$ is sub-exponential with mean $\mathbf{0}$ and covariance matrix

$$\begin{aligned} \mathrm{cov}(\sqrt{m}\boldsymbol{\beta}_j \xi_j^{[s]}) &= \mathrm{cov}(\sqrt{m}\boldsymbol{\beta}_j) \times \mathrm{var}(\xi_j^{[s]}) \\ &= (\sigma_{x_s x_s} - \sigma_{\beta_s \beta_s}) \boldsymbol{\Sigma}_{\beta\beta}. \end{aligned} \tag{7}$$

Hence, by Lemma 1.6,

$$\lim_{m\to\infty} \frac{1}{\sqrt{m}} \sum_{j=1}^{m} \sqrt{m}\boldsymbol{\beta}_j \xi_j^{[s]} \xrightarrow{D} \mathcal{N}(0, \sigma_{x_s x_s} \boldsymbol{\Sigma}_{\beta\beta}).$$

On the other hand, $\boldsymbol{\beta}_j \xi_j^{[s]}$ is sub-exponential variable according to Lemma 1.3, and

$$\begin{aligned} \mathrm{cov}(\sqrt{m}\boldsymbol{\beta}_j \xi_j^{[s]}, \sqrt{m}\boldsymbol{\beta}_j \xi_j^{[k]}) &= \mathrm{cov}(\xi_j^{[s]}, \xi_j^{[k]}) \times \boldsymbol{\Sigma}_{\beta\beta} \\ &= \frac{n_{sk}}{\sqrt{n_s n_k}} (\sigma_{x_s x_k} - \sigma_{\beta_s \beta_k}) \boldsymbol{\Sigma}_{\beta\beta}. \end{aligned} \tag{8}$$

Hence, by using Lemma 1.5

$$\lim_{m\to\infty} \frac{1}{m} \sum_{j=1}^{m} \sqrt{m}\boldsymbol{\beta}_j \sqrt{m}\boldsymbol{\beta}_j^\top \xi_j^{[s]} \xi_j^{[k]} \xrightarrow{P} \frac{n_{sk}}{\sqrt{n_s n_k}} \sigma_{x_s x_k} \boldsymbol{\Sigma}_{\beta\beta}.$$

□

1.6 Proofs of Theorems for IVW

Proof of Theorem 1.1. As for the estimation error $\boldsymbol{\omega}_\alpha$, we have

$$w_{\alpha_j} = \frac{\boldsymbol{g}_j^{[0]\top}\boldsymbol{y}^{[0]}}{n_0} - \alpha_j = \frac{\boldsymbol{g}_j^{[0]\top}\boldsymbol{y}_{-j}^{[0]}}{n_0}, \tag{9}$$

where

$$\boldsymbol{y}_{-j}^{[0]} = \boldsymbol{y}^{[0]} - \alpha_j \boldsymbol{g}_j^{[0]} = \sum_{s\neq j}^{m} \alpha_t \boldsymbol{g}_t^{[0]} + \mathbf{U}^{[0]}\boldsymbol{\theta} + \boldsymbol{v}^{[0]}, \tag{10}$$

and $\mathbf{U}^{[0]}$ and $\boldsymbol{v}^{[0]}$ are the corresponding noise terms in the outcome GWAS cohort. According to Lemma 1.8,

$$\xi_j^{[0]} = \frac{1}{\sqrt{n_0}} \sum_{i=1}^{n_0} g_{ij}^{[0]} y_{i,-j}^{[0]} \xrightarrow{D} \mathcal{N}(0, \sigma_{yy} - \boldsymbol{\theta}^\top \boldsymbol{\Sigma}_{\beta\beta}\boldsymbol{\theta}). \tag{11}$$

As for the estimation error $w_{\beta_{js}}$, we have

$$w_{\beta_{js}} = \frac{\boldsymbol{g}_j^{[s]\top}\boldsymbol{x}^{[s]}}{n_s} - \beta_{js} = \frac{\boldsymbol{g}_j^{[s]\top}\boldsymbol{x}_{-j}^{[s]}}{n_s}, \tag{12}$$

where

$$\boldsymbol{x}_{-j}^{[s]} = \boldsymbol{x}^{[s]} - \boldsymbol{g}_j^{[s]}\beta_{js} = \sum_{t\neq j} \beta_{ts}\boldsymbol{g}_t^{[s]} + \boldsymbol{u}^{[s]}. \tag{13}$$

Let

$$\xi_j^{[s]} = \frac{\boldsymbol{g}_j^{[s]\top}\boldsymbol{x}_{-j}^{[s]}}{\sqrt{n_s}} = \frac{1}{\sqrt{n}_s} \sum_{i=1}^{n_s} g_{ij}^{[s]} x_{i,-j}^{[s]}, \tag{14}$$

where $x_{i,-j}^{[s]}$ is the ith element in vector $\boldsymbol{x}_{-j}^{[s]}$. According to Lemma 1.8,

$$\xi_j^{[s]} = \frac{1}{\sqrt{n}_s} \sum_{i=1}^{n_s} g_{ij}^{[s]} x_{i,-j}^{[s]} \xrightarrow{D} \mathcal{N}(0, \sigma_{x_s x_s} - \sigma_{\beta_s\beta_s}). \tag{15}$$

Now we show the covariance between $\xi_j^{[s]}$ and $\xi_j^{[k]}$:

$$\mathrm{cov}(\xi_j^{[s]}, \xi_j^{[k]}) = \mathrm{E}\left(\frac{\boldsymbol{x}_{-j}^{[s]\top}\boldsymbol{g}_j^{[s]}\boldsymbol{g}_j^{[k]\top}\boldsymbol{x}_{-j}^{[k]}}{\sqrt{n_s n_k}}\right), \tag{16}$$

where $\boldsymbol{x}_{-j}^{[0]}$ represents $\boldsymbol{y}_{-j}^{[0]}$ for simplicity. Denote $\mathbf{Q}^{[sk]} = (Q_{it}^{[sk]})$ being a $(n_s \times n_k)$ matrix whose (i,t)th element is

$$Q_{it}^{[sk]} = \mathrm{E}(g_{ij}^{[s]} g_{tj}^{[k]}) = \begin{cases} 1, & (i,t) \in \mathcal{Q}^{[sk]}, \\ 0, & (i,t) \notin \mathcal{Q}^{[sk]}, \end{cases} \tag{17}$$

where

$$\mathcal{Q}^{[sk]} = \{(i,t):\ g_{ij}^{[s]} \text{ and } g_{tj}^{[k]} \text{ come from the same individual}\}. \tag{18}$$

As a result,

$$\begin{aligned}\operatorname{cov}(\xi_j^{[s]}, \xi_j^{[k]}) &= \mathrm{E}\left(\frac{\boldsymbol{x}_{-j}^{[s]\top}\mathbf{Q}^{[sk]}\boldsymbol{x}_{-j}^{[k]}}{\sqrt{n_s n_k}}\right) = \frac{1}{\sqrt{n_s n_k}} \sum_{(i,t)\in\mathcal{Q}^{[sk]}} \mathrm{E}(x_{i,-j}^{[s]} x_{t,-j}^{[k]}) \\ &= \frac{n_{sk}}{\sqrt{n_s n_k}}\left(\sigma_{x_s x_k} - \sigma_{\beta_s\beta_k}\right), \end{aligned} \tag{19}$$

where $\sigma_{x_0 x_k}$ represents $\sigma_{y x_k}$ for simplicity, and $\sigma_{\beta_0\beta_k}$ represents

$$\sigma_{\beta_0\beta_k} = \operatorname{cov}(\sqrt{m}\boldsymbol{\beta}_j^\top\boldsymbol{\theta}, \sqrt{m}\beta_{jk}) = \sum_{l=1}^{p} \theta_l \sigma_{\beta_l\beta_k}. \tag{20}$$

Finally, we show $\xi_j^{[s]}$ is uncorrelated with $\xi_t^{[s]}$ for all $t \neq j$ and $s = 0, \ldots, p$. Specifically,

$$\operatorname{cov}(\xi_j^{[s]}, \xi_t^{[s]}) = \mathrm{E}\left(\frac{\boldsymbol{x}_{-j}^{[s]\top}\boldsymbol{g}_j^{[s]}\boldsymbol{g}_t^{[s]\top}\boldsymbol{x}_{-j}^{[s]}}{n_s}\right). \tag{21}$$

According the model setting, $\boldsymbol{g}_j^{[s]}$ is independent of $\boldsymbol{g}_t^{[s]}$ for all $t \neq s$. Therefore, $\operatorname{cov}(\xi_j^{[s]}, \xi_t^{[s]}) = 0$.

Note that if $m \to \infty$, $\boldsymbol{\Sigma}_{\beta\beta} = \frac{1}{m}\boldsymbol{\Psi}_{\beta\beta}$ vanishes. And so Theorem 1.1 is proved. □

Proof of Theorem 1.2. Before showing the proof, we first recall the following definitions: m is the number of IVs, $n_{\min}$ is the minimum sample size,

$$\boldsymbol{\Sigma}_{\beta\beta} = \lim_{m\to\infty} \frac{1}{m}\sum_{j=1}^{m} \boldsymbol{\beta}_j\boldsymbol{\beta}_j^\top, \quad \boldsymbol{\Psi}_{\beta\beta} = m\boldsymbol{\Sigma}_{\beta\beta},$$

$$\boldsymbol{\Sigma}_{W_\beta W_\beta} = \lim_{m\to\infty} \frac{1}{m}\sum_{j=1}^{m} \boldsymbol{w}_{\beta_j}\boldsymbol{w}_{\beta_j}^\top, \quad \boldsymbol{\Psi}_{W_\beta W_\beta} = n_{\min}\boldsymbol{\Sigma}_{W_\beta W_\beta},$$

$$\boldsymbol{\sigma}_{W_\beta w_\alpha} = \lim_{m\to\infty} \frac{1}{m}\sum_{j=1}^{m} w_{\alpha_j}\boldsymbol{w}_{\beta_j}, \quad \boldsymbol{\psi}_{W_\beta w_\alpha} = n_{\min}\boldsymbol{\sigma}_{W_\beta w_\alpha},$$

$$\sigma_{w_\alpha w_\alpha} = \lim_{m\to\infty} \frac{1}{m}\sum_{j=1}^{m} w_{\alpha_j}^2, \quad \psi_{w_\alpha w_\alpha} = n_{\min}\sigma_{w_\alpha w_\alpha}.$$

The score function of IVW is

$$-\frac{1}{m}\hat{\mathbf{B}}^\top(\hat{\boldsymbol{a}} - \hat{\mathbf{B}}\hat{\boldsymbol{\theta}}_{\mathrm{IVW}}) = -\frac{1}{m}\hat{\mathbf{B}}^\top(\hat{\boldsymbol{a}} - \hat{\mathbf{B}}\boldsymbol{\theta}) + \frac{1}{m}\hat{\mathbf{B}}^\top\hat{\mathbf{B}}(\hat{\boldsymbol{\theta}}_{\mathrm{IVW}} - \boldsymbol{\theta}) \tag{22}$$

which leads to

$$\mathbf{H}_{\mathrm{IVW}}(\hat{\boldsymbol{\theta}}_{\mathrm{IVW}} - \boldsymbol{\theta}) = -\boldsymbol{S}_{\mathrm{IVW}}(\boldsymbol{\theta}), \tag{23}$$

where

$$\mathbf{H}_{\mathrm{IVW}} = \frac{1}{m}\hat{\mathbf{B}}^\top\hat{\mathbf{B}}, \quad \boldsymbol{S}_{\mathrm{IVW}}(\boldsymbol{\theta}) = -\frac{1}{m}\hat{\mathbf{B}}^\top(\hat{\boldsymbol{a}} - \hat{\mathbf{B}}\boldsymbol{\theta}). \tag{24}$$

We first work with the Hessian matrix $\mathbf{H}_{\mathrm{IVW}}$:

$$\begin{aligned} m\mathbf{H}_{\mathrm{IVW}} &= \hat{\mathbf{B}}^\top\hat{\mathbf{B}} = \mathbf{B}^\top\mathbf{B} + \mathbf{B}^\top\mathbf{W}_\beta + \mathbf{W}_\beta^\top\mathbf{B} + \mathbf{W}_\beta^\top\mathbf{W}_\beta \\ &= \mathbf{J}_1 + \mathbf{J}_2 + \mathbf{J}_3 + \mathbf{J}_4. \end{aligned} \tag{25}$$

As for $\mathbf{J}_1$,

$$\mathbf{J}_1 = \sum_{j=1}^{m} \boldsymbol{\beta}_j\boldsymbol{\beta}_j^\top \xrightarrow{P} \boldsymbol{\Psi}_{\beta\beta}. \tag{26}$$

As for $\mathbf{J}_2$,

$$\begin{aligned} \|\sqrt{n}_{\min}\mathbf{J}_2\|_2 &= \left\| \frac{1}{\sqrt{m}}\sum_{j=1}^{m} (\sqrt{n}_{\min}\boldsymbol{w}_{\beta_j})(\sqrt{m}\boldsymbol{\beta}_j)^\top \right\|_2 \\ &\le \sqrt{\left\| \frac{1}{m}\sum_{j=1}^{m} (\sqrt{n}_{\min}\boldsymbol{w}_{\beta_j})(\sqrt{n}_{\min}\boldsymbol{w}_{\beta_j})^\top \right\|_2} \times \sqrt{\left\| \frac{1}{m}\sum_{j=1}^{m} (\sqrt{m}\boldsymbol{\beta}_j)(\sqrt{m}\boldsymbol{\beta}_j)^\top \right\|_2} \\ &\le \lambda_{\max}^{\frac{1}{2}}(\boldsymbol{\Psi}_{W_\beta W_\beta}) \times \lambda_{\max}^{\frac{1}{2}}(\boldsymbol{\Psi}_{\beta\beta}), \end{aligned} \tag{27}$$

which means

$$\|\mathbf{J}_2\|_2 = O_P(1/\sqrt{n}_{\min}). \tag{28}$$

As for $\mathbf{J}_3$, it has the same order as $\mathbf{J}_2$. As for $\mathbf{J}_4$,

$$\frac{n_{\min}}{m}\mathbf{J}_4 = \frac{1}{m}\sum_{j=1}^{m} (\sqrt{n}_{\min}\boldsymbol{w}_{\beta_j})(\sqrt{n}_{\min}\boldsymbol{w}_{\beta_j})^\top \xrightarrow{P} \boldsymbol{\Psi}_{W_\beta W_\beta} \tag{29}$$

Hence:

(1) If $m/n_{\min} \to 0$,

$$\|\mathbf{J}_4\|_2 \leq \lambda_{\max}(\mathbf{\Psi}_{W_\beta W_\beta}) \times \frac{m}{n_{\min}} \to 0. \tag{30}$$

Therefore,

$$m\mathbf{H}_{\text{IVW}} \xrightarrow{P} \mathbf{\Psi}_{\beta\beta}. \tag{31}$$

(2) If $m/n_{\min} \to c_0 \in (0, \infty)$, then

$$\mathbf{J}_4 = \frac{m}{n_{\min}} \times \frac{1}{m} \sum_{j=1}^{m} (\sqrt{n}_{\min} \boldsymbol{w}_{\beta_j})(\sqrt{n}_{\min} \boldsymbol{w}_{\beta_j})^\top \xrightarrow{P} c_0 \mathbf{\Psi}_{W_\beta W_\beta}. \tag{32}$$

Therefore,

$$m\mathbf{H}_{\text{IVW}} \xrightarrow{P} \mathbf{\Psi}_{\beta\beta} + c_0 \mathbf{\Psi}_{W_\beta W_\beta}. \tag{33}$$

(3) If $m/n_{\min} \to \infty$ and $m/n_{\min}^{1+\tau} \to c_0 \in (0, +\infty)$ with certain constant $\tau > 0$, then

$$\frac{1}{n_{\min}^{\tau}} \mathbf{J}_4 = \frac{m}{n_{\min}^{1+\tau}} \times \frac{1}{m} \sum_{j=1}^{m} (\sqrt{n}_{\min} \boldsymbol{w}_{\beta_j})(\sqrt{n}_{\min} \boldsymbol{w}_{\beta_j})^\top \xrightarrow{P} c_0 \mathbf{\Psi}_{W_\beta W_\beta}. \tag{34}$$

Therefore,

$$\frac{m}{n_{\min}^{\tau}} \mathbf{H}_{\text{IVW}} = c_0 n_{\min} \mathbf{H}_{\text{IVW}} \xrightarrow{P} c_0 \mathbf{\Psi}_{W_\beta W_\beta}. \tag{35}$$

We then work with $\boldsymbol{S}_{\text{IVW}}(\theta)$:

$$\begin{aligned} m\boldsymbol{S}_{\text{IVW}}(\theta) &= -\mathbf{B}^\top \boldsymbol{w}_\alpha - \mathbf{W}_\beta^\top \boldsymbol{w}_\alpha + \mathbf{B}^\top \mathbf{W}_\beta \boldsymbol{\theta} + \mathbf{W}_\beta^\top \mathbf{W}_\beta \boldsymbol{\theta} \\ &= \boldsymbol{K}_1 + \boldsymbol{K}_2 + \boldsymbol{K}_3 + \boldsymbol{K}_4. \end{aligned} \tag{36}$$

As for $\boldsymbol{K}_1 + \boldsymbol{K}_3$,

$$\sqrt{n}_{\min}(\boldsymbol{K}_1 + \boldsymbol{K}_3) = \frac{1}{\sqrt{m}} \sum_{j=1}^{m} (-\sqrt{n}_{\min} w_{\alpha_j} + \sqrt{n}_{\min} \boldsymbol{w}_{\beta_j}^\top \boldsymbol{\theta})(\sqrt{m}\boldsymbol{\beta}_j) \xrightarrow{D} \mathcal{N}(\mathbf{0}, \psi_\theta \mathbf{\Psi}_{\beta\beta}), \tag{37}$$

where

$$\psi_\theta = \psi_{w_\alpha w_\alpha} + \boldsymbol{\theta}^\top \mathbf{\Psi}_{W_\beta W_\beta} \boldsymbol{\theta} - 2\boldsymbol{\theta}^\top \boldsymbol{\psi}_{W_\beta w_\alpha}. \tag{38}$$

As for $\boldsymbol{K}_2$,

$$\frac{n_{\min}}{m} \boldsymbol{K}_2 = -\frac{1}{m} \sum_{j=1}^{m} (\sqrt{n}_{\min} w_{\alpha_j})(\sqrt{n}_{\min} \boldsymbol{w}_{\beta_j}) \xrightarrow{P} -\boldsymbol{\psi}_{W_\beta w_\alpha}. \tag{39}$$

As for $\boldsymbol{K}_4$,

$$\frac{n_{\min}}{m} \boldsymbol{K}_4 = \left(\frac{1}{m} \sum_{j=1}^{m} (\sqrt{n}_{\min} \boldsymbol{w}_{\beta_j} \sqrt{n}_{\min} \boldsymbol{w}_{\beta_j} \right) \boldsymbol{\theta} \xrightarrow{P} \mathbf{\Psi}_{W_\beta W_\beta} \boldsymbol{\theta}, \tag{40}$$

Jointing these results, we summary the asymptotic behavior of $\hat{\boldsymbol{\theta}}_{\text{IVW}}$:

(1) If $m/\sqrt{n}_{\min} \to 0$, then

$$\sqrt{n}_{\min}||\boldsymbol{K}_2 + \boldsymbol{K}_4|| = O_P\left(\frac{m}{\sqrt{n}_{\min}}\right) = o_P(1). \tag{41}$$

Therefore,

$$\sqrt{n}_{\min} \times m\boldsymbol{S}_{\text{IVW}}(\boldsymbol{\theta}) = \sqrt{n}_{\min}(\boldsymbol{K}_1 + \boldsymbol{K}_3) + o_P(1) \xrightarrow{D} \mathcal{N}(\mathbf{0}, \psi_\theta \boldsymbol{\Psi}_{\beta\beta}). \tag{42}$$

Note that when $m/n_{\min} \to 0$, $m\mathbf{H}_{\text{IVW}} \xrightarrow{P} \boldsymbol{\Psi}_{\beta\beta}$. Therefore,

$$\sqrt{n}_{\min}(\hat{\boldsymbol{\theta}}_{\text{IVW}} - \boldsymbol{\theta}) = -\sqrt{n}_{\min}(m\mathbf{H}_{\text{IVW}})^{-1}(m\boldsymbol{S}_{\text{IVW}}(\theta)) \xrightarrow{D} \mathcal{N}(\mathbf{0}, \psi_\theta \boldsymbol{\Psi}_{\beta\beta}^{-1}), \tag{43}$$

(2) If $m/\sqrt{n}_{\min} \to c_0$, then

$$\sqrt{n}_{\min}(\boldsymbol{K}_2 + \boldsymbol{K}_4) \to -c_0\boldsymbol{\psi}_{W_\beta w_\alpha} + c_0\boldsymbol{\Psi}_{W_\beta W_\beta}\boldsymbol{\theta}, \tag{44}$$

and hence

$$\sqrt{n}_{\min} \times m\boldsymbol{S}_{\text{IVW}}(\boldsymbol{\theta}) \xrightarrow{D} \mathcal{N}(-c_0(\boldsymbol{\psi}_{W_\beta w_\alpha} + \boldsymbol{\Psi}_{W_\beta W_\beta}\boldsymbol{\theta}), \psi_\theta \boldsymbol{\Psi}_{\beta\beta}). \tag{45}$$

Note that when $m/n_{\min} \to 0$, $m\mathbf{H}_{\text{IVW}} \xrightarrow{P} \boldsymbol{\Psi}_{\beta\beta}$. Therefore,

$$\begin{aligned}\sqrt{n}_{\min}(\hat{\boldsymbol{\theta}}_{\text{IVW}} - \boldsymbol{\theta}) &= -\sqrt{n}_{\min}(m\mathbf{H}_{\text{IVW}})^{-1}(m\boldsymbol{S}_{\text{IVW}}(\theta)) \\ &\xrightarrow{D} \mathcal{N}(c_0\boldsymbol{\Psi}_{\beta\beta}^{-1}(\boldsymbol{\psi}_{W_\beta w_\alpha} - \boldsymbol{\Psi}_{W_\beta W_\beta}\boldsymbol{\theta}), \psi_\theta \boldsymbol{\Psi}_{\beta\beta}^{-1}).\end{aligned} \tag{46}$$

(3) If $m/\sqrt{n}_{\min} \to \infty$ and $m/n_{\min} \to c_0$, then $||\boldsymbol{K}_1 + \boldsymbol{K}_3||_2 = O_P(1/\sqrt{n}_{\min})$,

$$\boldsymbol{K}_2 + \boldsymbol{K}_4 \xrightarrow{P} -c_0\boldsymbol{\psi}_{W_\beta w_\alpha} + c_0\boldsymbol{\Psi}_{W_\beta W_\beta}\boldsymbol{\theta}, \tag{47}$$

and

$$m\mathbf{H}_{\text{IVW}} \xrightarrow{P} \boldsymbol{\Psi}_{\beta\beta} + c_0\boldsymbol{\Psi}_{W_\beta W_\beta}. \tag{48}$$

Hence,

$$\hat{\boldsymbol{\theta}}_{\text{IVW}} - \boldsymbol{\theta} \xrightarrow{P} c_0(\boldsymbol{\Psi}_{\beta\beta} + c_0\boldsymbol{\Psi}_{W_\beta W_\beta})^{-1}(\boldsymbol{\psi}_{W_\beta w_\alpha} - \boldsymbol{\Psi}_{W_\beta W_\beta}\boldsymbol{\theta}). \tag{49}$$

Note that if $c_0 = 0$, then (iii) in Theorem 1.2 holds.

(4) If $m/n_{\min} \to \infty$ and $m/n_{\min}^{1+\tau} \to c_0$, then

$$\frac{1}{n_{\min}^{\tau}}(\boldsymbol{K}_2 + \boldsymbol{K}_4) \xrightarrow{P} -c_0\boldsymbol{\psi}_{W_\beta w_\alpha} + c_0\boldsymbol{\Psi}_{W_\beta W_\beta}\boldsymbol{\theta} \tag{50}$$

and

$$\frac{m}{n_{\min}^{\tau}}\mathbf{H}_{\text{IVW}} \xrightarrow{P} c_0\boldsymbol{\Psi}_{W_\beta W_\beta}. \tag{51}$$

Therefore,

$$\hat{\boldsymbol{\theta}}_{\text{IVW}} \xrightarrow{P} \boldsymbol{\Psi}_{W_\beta W_\beta}^{-1}\boldsymbol{\psi}_{W_\beta w_\alpha}. \tag{52}$$

Now Theorem 1.2 is proved. □

1.7 Proofs of Theorems for MRBEE

Proofs of Theorem 1.3. Note that

$$\mathbf{0} = \boldsymbol{S}_{\mathrm{BEE}}(\hat{\boldsymbol{\theta}}_{\mathrm{BEE}}) = \boldsymbol{S}_{\mathrm{BEE}}(\boldsymbol{\theta}) + \mathbf{H}_{\mathrm{BEE}}(\hat{\boldsymbol{\theta}}_{\mathrm{BEE}} - \boldsymbol{\theta}), \tag{53}$$

where

$$\boldsymbol{S}_{\mathrm{BEE}}(\boldsymbol{\theta}) = -\frac{1}{m}\hat{\mathbf{B}}^\top(\hat{\boldsymbol{\alpha}} - \hat{\mathbf{B}}\boldsymbol{\theta}) - \boldsymbol{\Sigma}_{W_\beta W_\beta}\boldsymbol{\theta} + \boldsymbol{\sigma}_{W_\beta w_\alpha}, \tag{54}$$

and

$$\mathbf{H}_{\mathrm{BEE}} = \frac{1}{m}\hat{\mathbf{B}}^\top\hat{\mathbf{B}} - \boldsymbol{\Sigma}_{W_\beta W_\beta}. \tag{55}$$

As for $\boldsymbol{S}_{\mathrm{BEE}}(\boldsymbol{\theta})$,

$$\begin{aligned} m\boldsymbol{S}_{\mathrm{BEE}}(\boldsymbol{\theta}) &= -(\mathbf{B} + \mathbf{W}_\beta)^\top(\boldsymbol{\alpha} + \boldsymbol{w}_\alpha - \mathbf{B}\boldsymbol{\theta} - \mathbf{W}_\beta\boldsymbol{\theta}) - m\boldsymbol{\Sigma}_{W_\beta W_\beta} + m\boldsymbol{\sigma}_{W_\beta w_\alpha} \\ &= -\left\{\mathbf{B}^\top(\boldsymbol{w}_\alpha - \mathbf{W}_\beta\boldsymbol{\theta})\right\} + \left\{\left(\mathbf{W}_\beta^\top\mathbf{W}_\beta - m\boldsymbol{\Sigma}_{W_\beta W_\beta}\right)\boldsymbol{\theta}\right\} - \left\{\mathbf{W}_\beta^\top\boldsymbol{w}_\alpha - m\boldsymbol{\sigma}_{W_\beta w_\alpha}\right\} \\ &= \boldsymbol{K}_1 + \boldsymbol{K}_2 + \boldsymbol{K}_3. \end{aligned} \tag{56}$$

Here, we define a new vector $\boldsymbol{\vartheta} = (\boldsymbol{\theta}^\top, 1)^\top$, an alternative vector

$$\boldsymbol{\zeta}_j = \left(\frac{n_{\min}}{n_1}\xi_j^{[1]}, \frac{n_{\min}}{n_2}\xi_j^{[2]}, \ldots, \frac{n_{\min}}{n_p}\xi_j^{[p]}, \frac{n_{\min}}{n_0}\xi_j^{[0]}\right)^\top,$$

where

$$\xi_j^{[s]} = \frac{1}{\sqrt{n}_s}\sum_{i=1}^{n_s} g_{ij}^{[s]}x_{is}^{[s]}, \quad s = 0, 1, \ldots, p,$$

and a new covariance matrix

$$\mathrm{cov}(\boldsymbol{\zeta}_j) = \boldsymbol{\Psi}_{W_\beta \times w_\alpha} = \begin{pmatrix} \boldsymbol{\Psi}_{W_\beta W_\beta} & \boldsymbol{\psi}_{W_\beta w_\alpha} \\ \boldsymbol{\psi}_{W_\beta w_\alpha}^\top & \psi_{w_\alpha w_\alpha} \end{pmatrix}. \tag{57}$$

As for $\boldsymbol{K}_1$, it can be rewritten as

$$\begin{aligned} \sqrt{n}_{\min}\boldsymbol{K}_1 &= -\sum_{j=1}^{m}\sqrt{n}_{\min}(w_{\alpha_j} - \boldsymbol{w}_{\beta_j}^\top\boldsymbol{\theta})\boldsymbol{\beta}_j = \frac{1}{\sqrt{m}}\sum_{j=1}^{m}(\sqrt{n}_{\min}\boldsymbol{\zeta}_j^\top\boldsymbol{\vartheta})(\sqrt{m}\boldsymbol{\beta}_j) \\ &\xrightarrow{D} \mathcal{N}(\mathbf{0}, \psi_\theta\boldsymbol{\Psi}_{\beta\beta}), \end{aligned} \tag{58}$$

where ψ_θ defined in (38) can be rewritten as

$$\psi_\theta = \boldsymbol{\vartheta}^\top\boldsymbol{\Psi}_{W_\beta \times w_\alpha}\boldsymbol{\vartheta}. \tag{59}$$

As for $\boldsymbol{K}_2 + \boldsymbol{K}_3$, it can be rewritten as

$$\begin{aligned} \boldsymbol{K}_2 + \boldsymbol{K}_3 &= \mathbf{I}_{p+1}^{1:p}\begin{pmatrix} \mathbf{W}_\beta^\top\mathbf{W}_\beta - m\boldsymbol{\Sigma}_{W_\beta W_\beta} & \mathbf{W}_\beta^\top\boldsymbol{w}_\alpha - m\boldsymbol{\sigma}_{W_\beta w_\alpha} \\ \boldsymbol{w}_\alpha^\top\mathbf{W}_\beta - m\boldsymbol{\sigma}_{W_\beta w_\alpha}^\top & \boldsymbol{w}_\alpha^\top\boldsymbol{w}_\alpha - m\sigma_{w_\alpha w_\alpha} \end{pmatrix}\begin{pmatrix} \boldsymbol{\theta} \\ -1 \end{pmatrix} \\ &= \frac{\sqrt{m}}{n_{\min}}\mathbf{I}_{p+1}^{1:p}\left(\frac{1}{\sqrt{m}}\sum_{j=1}^{m}\boldsymbol{\zeta}_j\boldsymbol{\zeta}_j^\top - \boldsymbol{\Psi}_{W_\beta \times w_\alpha}\right)\boldsymbol{\vartheta} \\ &= \frac{\sqrt{m}}{n_{\min}}\mathbf{I}_{p+1}^{1:p}\mathbf{K}_4\boldsymbol{\vartheta}, \end{aligned} \tag{60}$$

where $\mathbf{I}_{p+1}^{1:p}$ is a $(p \times (p+1))$ matrix consisting of the first p row of $\mathbf{I}_{p+1}$ and

$$\mathbf{K}_4 = \frac{1}{\sqrt{m}} \sum_{j=1}^{m} \boldsymbol{\zeta}_j \boldsymbol{\zeta}_j^\top - \boldsymbol{\Psi}_{W_\beta \times w_\alpha}. \tag{61}$$

According to Lemma 1.6,

$$\mathrm{vec}(\mathbf{K}_4) \xrightarrow{D} \mathcal{N}\bigg(\mathbf{0}, (\mathbf{I}_{(p+1)^2} + \mathbf{K}_{(p+1)^2})(\boldsymbol{\Psi}_{W_\beta \times w_\alpha} \otimes \boldsymbol{\Psi}_{W_\beta \times w_\alpha})\bigg). \tag{62}$$

As a result,

$$\frac{n_{\min}}{\sqrt{m}}(\boldsymbol{K}_2 + \boldsymbol{K}_3) \xrightarrow{D} \mathcal{N}(\mathbf{0}, \boldsymbol{\Sigma}_{\mathrm{BC}}) \tag{63}$$

where

$$\boldsymbol{\Sigma}_{\mathrm{BC}} = \underbrace{\bigg[\boldsymbol{\vartheta}^\top \otimes \mathbf{I}_{p+1}^{1:p}\bigg]}_{p\times(p+1)^2} \underbrace{\bigg[(\mathbf{I}_{(p+1)^2} + \mathbf{K}_{(p+1)^2})(\boldsymbol{\Psi}_{W_\beta \times w_\alpha} \otimes \boldsymbol{\Psi}_{W_\beta \times w_\alpha})\bigg]}_{(p+1)^2\times(p+1)^2} \underbrace{\bigg[\boldsymbol{\vartheta}^\top \otimes \mathbf{I}_{p+1}^{1:p}\bigg]^\top}_{(p+1)^2\times p}. \tag{64}$$

Now we show $\boldsymbol{K}_1$ and $\boldsymbol{K}_2 + \boldsymbol{K}_3$ are uncorrelated. Note that $\boldsymbol{\beta}_j$ is independent of $\boldsymbol{w}_{\beta_j}$ and w_{α_j}, and hence $\boldsymbol{K}_1$ and $\boldsymbol{K}_2 + \boldsymbol{K}_3$ are uncorrelated. So far, we can obtain:

(1) If $m/n_{\min} \to 0$,

$$\sqrt{n}_{\min} \times m\boldsymbol{S}_{\mathrm{BEE}}(\boldsymbol{\theta}) = \sqrt{n}_{\min}\boldsymbol{K}_1 + o_P(1) \xrightarrow{D} \mathcal{N}(\mathbf{0}, \psi_\theta \boldsymbol{\Psi}_{\beta\beta}). \tag{65}$$

(2) If $m/n_{\min} \to c_0$,

$$\sqrt{n}_{\min} \times m\boldsymbol{S}_{\mathrm{BEE}}(\boldsymbol{\theta}) = \sqrt{n}_{\min}\boldsymbol{K}_1 + \sqrt{n}_{\min}(\boldsymbol{K}_2 + \boldsymbol{K}_3) \xrightarrow{D} \mathcal{N}(\mathbf{0}, \psi_\theta \boldsymbol{\Psi}_{\beta\beta} + c_0\boldsymbol{\Sigma}_{\mathrm{BC}}). \tag{66}$$

(3) If $m/n_{\min} \to \infty$ and $\sqrt{m}/n_{\min} \to 0$,

$$\frac{n_{\min}}{\sqrt{m}} \times m\boldsymbol{S}_{\mathrm{BEE}}(\boldsymbol{\theta}) = \frac{n_{\min}}{\sqrt{m}}(\boldsymbol{K}_2 + \boldsymbol{K}_3) + \frac{n_{\min}}{\sqrt{m}}\boldsymbol{K}_1 \xrightarrow{D} \mathcal{N}(\mathbf{0}, \boldsymbol{\Sigma}_{\mathrm{BC}}), \tag{67}$$

where

$$\frac{n_{\min}}{\sqrt{m}}\boldsymbol{K}_1 = \sqrt{\frac{n_{\min}}{m}} \times \sqrt{n}_{\min}\boldsymbol{K}_1 = O_P\bigg(\sqrt{\frac{n_{\min}}{m}}\bigg) = o_P(1). \tag{68}$$

Now we move to $\mathbf{H}_{\mathrm{BEE}}$:

$$\begin{aligned} m\mathbf{H}_{\mathrm{BEE}} &= \mathbf{B}^\top\mathbf{B} + \bigg(\mathbf{W}_\beta^\top\mathbf{W}_\beta - m\boldsymbol{\Sigma}_{W_\beta W_\beta}\bigg) + \mathbf{B}^\top\mathbf{W}_\beta + \mathbf{W}_\beta^\top\mathbf{B} \\ &= \mathbf{J}_1 + \mathbf{J}_2 + \mathbf{J}_3 + \mathbf{J}_4. \end{aligned} \tag{69}$$

As for $\mathbf{J}_1 = \mathbf{B}^\top\mathbf{B}$, we have

$$\begin{aligned} ||\mathbf{J}_1 - \boldsymbol{\Psi}_{\beta\beta}||_2 &= \bigg\|\frac{1}{m}\sum_{j=1}^{m}\sqrt{m}\boldsymbol{\beta}_j\sqrt{m}\boldsymbol{\beta}_j^\top - \boldsymbol{\Psi}_{\beta\beta}\bigg\|_2 \\ &= O_P\bigg(\frac{1}{\sqrt{m}}\bigg). \end{aligned} \tag{70}$$

As for $\mathbf{J}_2 = \mathbf{W}_\beta^\top \mathbf{W}_\beta - m\mathbf{\Sigma}_{W_\beta W_\beta}$, we have

$$\mathbf{J}_2 = \sum_{j=1}^{m} \left(\boldsymbol{w}_{\beta_j} \boldsymbol{w}_{\beta_j}^\top - \mathbf{\Sigma}_{W_\beta W_\beta} \right) = \frac{\sqrt{m}}{n_{\min}} \frac{1}{\sqrt{m}} \sum_{j=1}^{m} \left(\boldsymbol{\xi}_j \boldsymbol{\xi}_j^\top - \mathbf{\Psi}_{W_\beta W_\beta} \right). \tag{71}$$

As a result,

$$\frac{n_{\min}}{\sqrt{m}} \mathrm{vec}(\mathbf{J}_2) \xrightarrow{D} \mathcal{N}(\mathbf{0}, (\mathbf{I}_{p^2} + \mathbf{K}_{p^2})(\mathbf{\Psi}_{W_\beta W_\beta} \otimes \mathbf{\Psi}_{W_\beta W_\beta})), \tag{72}$$

which means $||\mathbf{J}_2|| = O_P(\sqrt{m}/n_{\min})$. As for $\mathbf{J}_3 = \mathbf{B}^\top \mathbf{W}_\beta$,

$$\begin{aligned}
\sqrt{n}_{\min} ||\mathbf{J}_3||_2 &= \left\| \frac{1}{\sqrt{m}} \sum_{j=1}^{m} \sqrt{m} \boldsymbol{\beta}_j \sqrt{n}_{\min} \boldsymbol{\omega}_{\beta_j}^\top \right\|_2 \\
&\leq \sqrt{\left\| \frac{1}{m} \sum_{j=1}^{m} \sqrt{m} \boldsymbol{\beta}_j \sqrt{m} \boldsymbol{\beta}_j^\top \right\|_2} \sqrt{\left\| \frac{1}{m} \sum_{j=1}^{m} \sqrt{n}_{\min} \boldsymbol{\omega}_{\beta_j} \sqrt{n}_{\min} \boldsymbol{\omega}_{\beta_j}^\top \right\|_2} \\
&\leq \lambda_{\max}^{\frac{1}{2}}(\mathbf{\Psi}_{\beta\beta}) \times \lambda_{\max}^{\frac{1}{2}}(\mathbf{\Psi}_{W_\beta W_\beta}),
\end{aligned} \tag{73}$$

which means

$$||\mathbf{J}_3||_2 = O_P\left(\frac{1}{\sqrt{n}_{\min}} \right) \tag{74}$$

As for $\mathbf{J}_4$, it is easy to see $||\mathbf{J}_4||_2^2 = ||\mathbf{J}_3||_2^2$. Hence, for all three scenarios in Theorem 1.3,

$$||m\mathbf{H}_{\mathrm{BEE}} - \mathbf{\Psi}_{\beta\beta}||_2 = O_P\left\{ \max\left(\frac{1}{\sqrt{m}}, \frac{1}{\sqrt{n}_{\min}}, \frac{\sqrt{m}}{n_{\min}} \right) \right\}. \tag{75}$$

And hence, according to the Slutsky's theorem,

(1) If $m/n_{\min} \to 0$,

$$\sqrt{n}_{\min}(\hat{\boldsymbol{\theta}}_{\mathrm{BEE}} - \boldsymbol{\theta}) = -\sqrt{n}_{\min} \mathbf{\Psi}_{\beta\beta}^{-1} \boldsymbol{K}_1 \xrightarrow{D} \mathcal{N}(\mathbf{0}, \psi_\theta \mathbf{\Psi}_{\beta\beta}^{-1}). \tag{76}$$

(2) If $m/n_{\min} \to c_0$,

$$\sqrt{n}_{\min}(\hat{\boldsymbol{\theta}}_{\mathrm{BEE}} - \boldsymbol{\theta}) = -\sqrt{n}_{\min} \mathbf{\Psi}_{\beta\beta}^{-1} (\boldsymbol{K}_1 + \boldsymbol{K}_2 + \boldsymbol{K}_3) \xrightarrow{D} \mathcal{N}(\mathbf{0}, \psi_\theta \mathbf{\Psi}_{\beta\beta}^{-1} + c_0 \mathbf{\Psi}_{\beta\beta}^{-1} \mathbf{\Psi}_{\mathrm{BC}} \mathbf{\Psi}_{\beta\beta}^{-1}). \tag{77}$$

(2) If $m/n_{\min} \to \infty$ and $m/n_{\min}^2 \to 0$,

$$\sqrt{n_{\min}^2/m}(\hat{\boldsymbol{\theta}}_{\mathrm{BEE}} - \boldsymbol{\theta}) = -\frac{n_{\min}}{\sqrt{m}} \mathbf{\Psi}_{\beta\beta}^{-1} (\boldsymbol{K}_2 + \boldsymbol{K}_3) \xrightarrow{D} \mathcal{N}(\mathbf{0}, \mathbf{\Psi}_{\beta\beta}^{-1} \mathbf{\Psi}_{\mathrm{BC}} \mathbf{\Psi}_{\beta\beta}^{-1}). \tag{78}$$

Thus, Theorem 1.3 is proved. □

Proof of Theorem 1.4. Similar to $\xi_j^{[s]}$, we define $\eta_j^{\{s\}}$ as

$$\eta_j^{\{s\}} = \frac{\boldsymbol{g}_j^{\{s\}\top}\boldsymbol{x}^{[s]}}{\sqrt{n_s}} = \frac{1}{\sqrt{n_s}}\sum_{i=1}^{n_s} g_{ij}^{\{s\}} x_i^{[s]}. \tag{79}$$

By using similar deduction as which in the proof of Theorem 1,

$$\eta_j^{\{s\}} \xrightarrow{D} \mathcal{N}(0, \sigma_{x_s x_s}) \tag{80}$$

and

$$\operatorname{cov}(\eta_j^{\{s\}}, \eta_j^{\{k\}}) = \frac{n_{sk}}{\sqrt{n_s n_k}}\sigma_{x_s x_k}. \tag{81}$$

Denote $\boldsymbol{\eta}_j = (\eta_j^{\{1\}}, \ldots, \eta_j^{\{p\}}, \eta_j^{\{0\}})$ where $\eta_j^{\{0\}}$ represents $\frac{1}{\sqrt{n_0}}\boldsymbol{g}_j^{\{s\}\top}\boldsymbol{y}^{[0]}$. Then we have

$$\operatorname{cov}(\boldsymbol{\eta}_j) = \mathbf{D}_\eta^{-1}\boldsymbol{\Sigma}_{W_\beta \times w_\alpha}\mathbf{D}_\eta^{-1}, \tag{82}$$

where

$$\mathbf{D}_\eta = \operatorname{diag}\left(\frac{1}{\sqrt{n_1}}, \ldots, \frac{1}{\sqrt{n_p}}, \frac{1}{\sqrt{n_0}}\right). \tag{83}$$

By using Lemma 1.4,

$$\left\| \frac{1}{M}\sum_{j=1}^{M} \boldsymbol{\eta}_j\boldsymbol{\eta}_j^\top - \operatorname{cov}(\boldsymbol{\eta}_j) \right\|_2 = O_P\left(\frac{1}{\sqrt{M}}\right), \tag{84}$$

and hence

$$\begin{aligned} \|\boldsymbol{\Sigma}_{W_\beta \times w_\alpha}^{-\frac{1}{2}}\hat{\boldsymbol{\Sigma}}_{W_\beta \times w_\alpha}\boldsymbol{\Sigma}_{W_\beta \times w_\alpha}^{\frac{1}{2}} - \mathbf{I}_{p+1}\|_2 &\le \lambda_{\min}^{-1}(\operatorname{cov}(\boldsymbol{\eta}_j)) \left\| \frac{1}{M}\sum_{j=1}^{M} \boldsymbol{\eta}_j\boldsymbol{\eta}_j^\top - \operatorname{cov}(\boldsymbol{\eta}_j) \right\|_2 \\ &= O_P\left(\frac{1}{\sqrt{M}}\right). \end{aligned} \tag{85}$$

Thus, Theorem 1.4 is proved. □

Proof of Theorem 1.5. Note that

$$\begin{aligned}\boldsymbol{S}_j(\boldsymbol{\theta}) &= -(\hat{\alpha}_j - \boldsymbol{\theta}^\top \hat{\boldsymbol{\beta}}_j)\hat{\boldsymbol{\beta}}_j - \boldsymbol{\Sigma}_{W_\beta W_\beta}\boldsymbol{\theta} + \boldsymbol{\sigma}_{W_\beta w_\alpha} \\ &= (w_{\alpha_j} - \boldsymbol{\theta}^\top \boldsymbol{w}_{\beta_j})\boldsymbol{\beta}_j + \Big\{(w_{\alpha_j} - \boldsymbol{\theta}^\top \boldsymbol{w}_{\beta_j})\boldsymbol{w}_{\beta_j} - \boldsymbol{\Sigma}_{W_\beta W_\beta}\boldsymbol{\theta} + \boldsymbol{\sigma}_{W_\beta w_\alpha}\Big\} \\ &= \boldsymbol{J}_{1j} + \boldsymbol{J}_{2j}. \end{aligned} \tag{86}$$

Note that both $\boldsymbol{J}_{1j}$ and $\boldsymbol{J}_{2j}$ are sub-exponential variables with zero mean and covariance matrix

$$\mathrm{cov}(\boldsymbol{J}_{1j}) = \frac{1}{mn_{\min}}\psi_\theta \boldsymbol{\Psi}_{\beta\beta}, \quad \mathrm{cov}(\boldsymbol{J}_{2j}) = \frac{1}{n_{\min}^2}\boldsymbol{\Sigma}_{\mathrm{BC}}. \tag{87}$$

Therefore, we obtain

$$\mathrm{cov}(\boldsymbol{S}_j(\boldsymbol{\theta})) = \boldsymbol{\Sigma}_S = \begin{cases} \frac{1}{mn_{\min}}\psi_\theta \boldsymbol{\Psi}_{\beta\beta}, & \text{if } m/n_{\min} \to 0, \\ \frac{1}{mn_{\min}}\psi_\theta \boldsymbol{\Psi}_{\beta\beta} + \frac{c_0}{mn_{\min}}\boldsymbol{\Sigma}_{\mathrm{BC}}, & \text{if } m/n_{\min} \to c_0, \\ \frac{1}{n_{\min}^2}\boldsymbol{\Sigma}_{\mathrm{BC}},, & \text{if } m/n_{\min} \to \infty \text{ and } \sqrt{m}/n_{\min} \to 0. \end{cases} \tag{88}$$

Then by using Lemma 1.5,

$$\left\| \frac{1}{m}\sum_{j=1}^m \boldsymbol{S}_j(\boldsymbol{\theta})\boldsymbol{S}_j(\boldsymbol{\theta})^\top - \boldsymbol{\Sigma}_S \right\|_2 = O_P\left(\sqrt{\frac{\log m}{m}}\right)||\boldsymbol{\Sigma}_S||_2. \tag{89}$$

By using the Slutsky's theorem,

$$\left\| \frac{1}{m}\sum_{j=1}^m \hat{\boldsymbol{S}}_j(\hat{\boldsymbol{\theta}}_{\mathrm{BEE}})\hat{\boldsymbol{S}}_j(\hat{\boldsymbol{\theta}}_{\mathrm{BEE}})^\top - \boldsymbol{\Sigma}_S \right\|_2 = O_P\left(\sqrt{\frac{\log m}{m}}\right)||\boldsymbol{\Sigma}_S||_2. \tag{90}$$

where

$$\hat{\boldsymbol{S}}_j(\hat{\boldsymbol{\theta}}_{\mathrm{BEE}}) = -(\hat{\boldsymbol{\theta}}_{\mathrm{BEE}}^\top \hat{\boldsymbol{\beta}}_j - \hat{\alpha}_j)\hat{\boldsymbol{\beta}}_j + \hat{\boldsymbol{\Sigma}}_{W_\beta W_\beta}\hat{\boldsymbol{\theta}}_{\mathrm{BEE}} - \hat{\boldsymbol{\sigma}}_{W_\beta w_\alpha} \tag{91}$$

On the other hand, according to the proof of Theorem 1.3,

$$\|m\hat{\mathbf{F}}_{\mathrm{BEE}} - \boldsymbol{\Psi}_{\beta\beta}||_2 = O_P\Big\{ \max\left(\frac{1}{\sqrt{m}}, \frac{1}{\sqrt{n}_{\min}}, \frac{\sqrt{m}}{n_{\min}}\right)\Big\}. \tag{92}$$

Note that Bickel and Levina (2008, A22(p223)) illustrates

$$\|\mathbf{A}_1\mathbf{A}_2\mathbf{A}_3 - \mathbf{B}_1\mathbf{B}_2\mathbf{B}_3||_2 = O_P\Big\{ \max\Big(||\mathbf{A}_1 - \mathbf{B}_1||_2, ||\mathbf{A}_2 - \mathbf{B}_2||_2, ||\mathbf{A}_3 - \mathbf{B}_3||_2\Big)\Big\}, \tag{93}$$

where $\mathbf{A}_1, \mathbf{A}_2, \mathbf{A}_3, \mathbf{B}_1, \mathbf{B}_2, \mathbf{B}_3$ are six matrices with non-diverging maximum singular values. Hence,

$$\begin{aligned}||\hat{\boldsymbol{\Sigma}}_{\mathrm{BEE}}(\hat{\boldsymbol{\theta}}_{\mathrm{BEE}}) - \boldsymbol{\Sigma}_{\mathrm{BEE}}(\boldsymbol{\theta})||_2 &= \left\|(m\hat{\mathbf{F}}_{\mathrm{BEE}})^{-1}\Big(\sum_{j=1}^m \hat{\boldsymbol{S}}_j(\hat{\boldsymbol{\theta}}_{\mathrm{BEE}})\hat{\boldsymbol{S}}_j(\hat{\boldsymbol{\theta}}_{\mathrm{BEE}})^\top\Big)(m\hat{\mathbf{F}}_{\mathrm{BEE}})^{-1} - m\boldsymbol{\Psi}_{\beta\beta}^{-1}\boldsymbol{\Sigma}_S\boldsymbol{\Psi}_{\beta\beta}^{-1}\right\|_2 \\ &= O_P\Big\{ \max\left(\sqrt{\frac{\log m}{m}}, \frac{1}{\sqrt{n}_{\min}}, \frac{\sqrt{m}}{n_{\min}}\right)\Big\}||m\boldsymbol{\Sigma}_S||_2, \end{aligned} \tag{94}$$

and consequently

$$||\boldsymbol{\Sigma}_{\mathrm{BEE}}^{-\frac{1}{2}}(\boldsymbol{\theta})\hat{\boldsymbol{\Sigma}}_{\mathrm{BEE}}(\boldsymbol{\theta})\boldsymbol{\Sigma}_{\mathrm{BEE}}^{-\frac{1}{2}}(\boldsymbol{\theta}) - \mathbf{I}_p||_2 = O_P\Big\{ \max\left(\sqrt{\frac{\log m}{m}}, \frac{1}{\sqrt{n}_{\min}}, \frac{\sqrt{m}}{n_{\min}}\right)\Big\}. \tag{95}$$

Thus, Theorem 1.5 is proved. □

Proof of Theorem 1.6. Note that $||\hat{\boldsymbol{\theta}}_{\text{BEE}} - \boldsymbol{\theta}||_2 = O_P(n_{\min}^{-\frac{1}{2}})$ and hence $\hat{\alpha}_j - \hat{\boldsymbol{\beta}}_j^\top \hat{\boldsymbol{\theta}}_{\text{BEE}}$ and $\hat{\alpha}_j - \hat{\boldsymbol{\beta}}_j^\top \boldsymbol{\theta}$ have the same distribution. For $j \in \mathcal{O}^c$,

$$\begin{aligned}\hat{\gamma}_j = \varepsilon_j = \hat{\alpha}_j - \hat{\boldsymbol{\beta}}_j^\top \hat{\boldsymbol{\theta}}_{\text{BEE}} &= w_{\alpha_j} - \boldsymbol{w}_{\beta_j}^\top \boldsymbol{\theta} + \boldsymbol{w}_{\beta_j}^\top (\hat{\boldsymbol{\theta}}_{\text{BEE}} - \boldsymbol{\theta}) \\ &\sim \mathcal{N}(0, \sigma_{\varepsilon\varepsilon}),\end{aligned} \tag{96}$$

where

$$\sigma_{\varepsilon\varepsilon} = \boldsymbol{\theta}^\top \boldsymbol{\Sigma}_{W_\beta w_\alpha} \boldsymbol{\theta} + \sigma_{\omega_\gamma \omega_\gamma} - 2\boldsymbol{\theta}^\top \boldsymbol{\sigma}_{W_\beta w_\alpha}. \tag{97}$$

As a result,

$$\frac{\hat{\gamma}_j^2}{\sigma_{\varepsilon\varepsilon}} \sim \chi_1^2. \tag{98}$$

Denote $\kappa^* = F_{\chi_1^2}^{-1}(\kappa)$. Then by using Lemma A.1 of Huang et al. (2012),

$$\begin{aligned}\Pr\left(\max_{j\in\mathcal{O}^c} \frac{\hat{\gamma}_j^2}{\sigma_{\varepsilon\varepsilon}} \le \kappa^*\right) &= 1 - \Pr\left(\max_{j\in\mathcal{O}^c} \frac{\hat{\gamma}_j^2}{\sigma_{\varepsilon\varepsilon}} > \kappa^*\right) \\ &\ge 1 - (m - |\mathcal{O}|) \Pr\left(\frac{\hat{\gamma}_j^2}{\sigma_{\varepsilon\varepsilon}} > \kappa^*\right) \\ &\ge 1 - m \Pr\left(\frac{\hat{\gamma}_j^2}{\sigma_{\varepsilon\varepsilon}} > \kappa^*\right) \\ &\ge 1 - m \exp\left(-\frac{(\sqrt{2\kappa^* - 1} - 1)^2}{4}\right).\end{aligned} \tag{99}$$

By letting $\kappa^* = C_0 \log m$ with C_0 being a sufficiently large constant,

$$\begin{aligned}\Pr\left(\max_{j\in\mathcal{O}^c} \frac{\hat{\gamma}_j^2}{\sigma_{\varepsilon\varepsilon}} \le \kappa^*\right) &\ge 1 - \exp\left(\log m - \frac{2C_0 \log m - 2\sqrt{C_0 \log m - 1}}{4}\right) \\ &\ge 1 - \exp\left(-\frac{(2C_0 - 4)\log m - 2\sqrt{C_0 \log m - 1}}{4}\right) \to 1,\end{aligned} \tag{100}$$

if $m \to \infty$.

On the other hand, for $j \in \mathcal{O}$,

$$\hat{\gamma}_j = \gamma_j + \varepsilon_j, \tag{101}$$

and hence

$$\frac{\hat{\gamma}_j^2}{\sigma_{\varepsilon\varepsilon}} \sim \chi_1^2\left(\frac{\gamma_j^2}{\sigma_{\varepsilon\varepsilon}}\right), \tag{102}$$

where $\chi_1^2(\lambda)$ refers to the noncentral chi-squared distribution with degree of freedom 1 and noncentrality parameter λ. Let $F_{\chi_1^2(\lambda)}(\cdot)$ be the CDF of this noncentral chi-squared distribution, which is indeed equal to

$$F_{\chi_1^2(\lambda)}(x) = 1 - \left(Q(\sqrt{x} - \sqrt{\lambda}) + Q(\sqrt{x} + \sqrt{\lambda})\right), \tag{103}$$

where $F_{\chi_1^2(\lambda)}(\cdot)$ be the CDF of $\chi_1^2(\lambda)$ and $Q(x)$ is the Gaussian Q-function, i.e., $Q(x) = 1 - \Phi(x)$ and $\Phi(x)$ is the CDF of standard normal distribution.

Note that there should exist a constant D_0 such that

$$\frac{\gamma_j^2}{\sigma_{\varepsilon\varepsilon}} \ge D_0 n_{\min} \tag{104}$$

where D_0 is a sufficient large constant. And

$$\begin{aligned}\Pr\left(\min_{j\in\mathcal{O}}\frac{\hat{\gamma}_j^2}{\sigma_{\varepsilon\varepsilon}}\geq\kappa^*\right)&=1-\Pr\left(\min_{j\in\mathcal{O}^c}\frac{\hat{\gamma}_j^2}{\sigma_{\varepsilon\varepsilon}}<\kappa^*\right)\\&\geq 1-\Pr\left(\frac{\hat{\gamma}_j^2}{\sigma_{\varepsilon\varepsilon}}<\kappa^*\right),\quad j\text{ is arbitrary element in }\mathcal{O}.\end{aligned}\tag{105}$$

Hence,

$$\begin{aligned}\Pr\left(\min_{j\in\mathcal{O}}\frac{\hat{\gamma}_j^2}{\sigma_{\varepsilon\varepsilon}}\geq\kappa^*\right)&\geq Q(\sqrt{\kappa^*}-\sqrt{D_0 n_{\min}})+Q(\sqrt{\kappa^*}+\sqrt{D_0 n_{\min}})\\&\geq Q(\sqrt{C_0\log m}-\sqrt{D_0 n_{\min}})+Q(\sqrt{C_0\log m}+\sqrt{D_0 n_{\min}})\to 1\end{aligned}\tag{106}$$

if $m, n_{\min}\to\infty$. Thus, Theorem 1.6 is proved. □

References

Bickel, P.J. and Levina, E. (2008). Regularized estimation of large covariance matrices. The Annals of Statistics. **36**(1), pp. 199-227.

Fisher, R.A. (1919). The correlation between relatives on the supposition of Mendelian inheritance. Earth and Environmental Science Transactions of the Royal Society of Edinburgh. **52**(2), pp. 339-433.

Bulik-Sullivan, B.K., Loh, P.R., Finucane, H.K., Ripke, S., Yang, J., Schizophrenia Working Group of the Psychiatric Genomics Consortium, Patterson, N., Daly, M.J., Price, A.L. and Neale, B.M. (2015). LD Score regression distinguishes confounding from polygenicity in genome-wide association studies. Nature genetics. **47**(3), pp. 291-295.

Fan, J. and Li R. (2001). Variable selection via nonconcave penalized likelihood and its oracle properties. Journal of the American statistical Association. **96**(456), pp. 1348-60.

Fan, J., Liao, Y. and Mincheva, M. (2011). High dimensional covariance matrix estimation in approximate factor models. The Annals of Statistics. **39**(6), pp. 3320–3356.

Huang, J., Breheny, P. and Ma, S. (2012). A selective review of group selection in high-dimensional models. Statistical Science, **27**(4), pp. 481-499.

Muirhead, R.J., (2009). Aspects of multivariate statistical theory. John Wiley & Sons.

Vershynin, R. (2010). Introduction to the non-asymptotic analysis of random matrices. arXiv preprint. arXiv:1011.3027.

Vershynin, R. (2018). High-dimensional probability: An introduction with applications in data science. Cambridge university press.

Jankova, J and Van De Geer, S. (2018). Semiparametric efficiency bounds for high-dimensional models The Annals of Statistics, **46**(5), pp. 2336-2359.

Benjamini, Y. and Hochberg, Y. (1995). Controlling the false discovery rate: a practical and powerful approach to multiple testing. Journal of the Royal statistical society: series B (Methodological), **57**(1), pp.289-300.

Lin, Z., Xue, H. and Pan, W. (2023). Robust multivariable Mendelian randomization based on constrained maximum likelihood. The American Journal of Human Genetics, **110**(4), pp.592-605.